

# WM RECORD COPY

11/10/81 1676

SAND81-1918 • Unlimited Release • UC-70

Printed March 1985

## In Situ Tuff Water Migration/Heater Experiment: Final Report

'85 APR 23 AIO:26

WM DOCKET CONTROL  
CENTER

J. Keith Johnstone, G. Ronald Hadley, David R. Waymire

Prepared by  
Sandia National Laboratories  
Albuquerque, New Mexico 87185 and Livermore, California 94550  
for the United States Department of Energy  
under Contract DE-AC04-76DP00789

HYDROLOGY DOCUMENT NUMBER 181

Issued by Sandia National Laboratories, operated for the United States Department of Energy by Sandia Corporation.

**NOTICE:** This report was prepared as an account of work sponsored by an agency of the United States Government. Neither the United States Government nor any agency thereof, nor any of their employees, nor any of their contractors, subcontractors, or their employees, makes any warranty, express or implied, or assumes any legal liability or responsibility for the accuracy, completeness, or usefulness of any information, apparatus, product, or process disclosed, or represents that its use would not infringe privately owned rights. Reference herein to any specific commercial product, process, or service by trade name, trademark, manufacturer, or otherwise, does not necessarily constitute or imply its endorsement, recommendation, or favoring by the United States Government, any agency thereof or any of their contractors or subcontractors. The views and opinions expressed herein do not necessarily state or reflect those of the United States Government, any agency thereof or any of their contractors or subcontractors.

Printed in the United States of America  
Available from  
National Technical Information Service  
U.S. Department of Commerce  
5285 Port Royal Road  
Springfield, VA 22161

NTIS price codes  
Printed copy: A06  
Microfiche copy: A01

SAND81-1918  
Unlimited Release  
Printed March 1985

Distribution  
Category UC-70

IN SITU TUFF WATER MIGRATION/HEATER EXPERIMENT:  
FINAL REPORT

J. Keith Johnstone  
NNWSI Repository Performance Assessments Division

G. Ronald Hadley  
Fluid Mechanics and Heat Transfer Division

David R. Waymire  
Test Planning and Diagnostics Division

Sandia National Laboratories  
Albuquerque, NM 87185

Abstract

This report summarizes the results of the In Situ Tuff Water Migration/Heater Experiment operated in the welded portion of the Grouse Canyon Member of the Belted Range Tuff in U12g-tunnel (G-Tunnel) on the Nevada Test Site (NTS). The experiment was located approximately 400 m below the surface and 200 m above the water table in nearly saturated rock. The experiment was designed to provide an initial assessment of the thermally induced behavior of the potentially large volumes of water (~25 vol% in this case) available in saturated or nearly saturated tuffaceous rocks. Instruments in the water collection cavities, including water depth gages, pH probes, humidity gages, and pressure transducers measured some properties of the collected water. Other holes in the array were instrumented to measure temperature profiles, thermally induced stress, and one provided a test bed for a continuously operating laser interferometer for measuring thermally induced rock displacements. Initial analysis of the water generation rate data in the heater hole, assuming a one-dimensional evaporation front/vapor diffusion model, provided good qualitative agreement. The results of chemical analyses of water samples supports the notion of mass transport by vapor diffusion in the heater hole but not in the water migration holes. Rock temperatures in the heater hole exceeded 240°C. The stress meters measured maximum radial and circumferential thermal stresses of 8.62 and 4.83 MPa respectively--approximately 40 percent of the pretest predicted values. The experiment with the laser interferometer was a failure. The results of the water migration experiment indicate that the pore water in these rocks was highly mobile, probably by a vapor diffusion/condensation process.

## CONTENTS

	<u>Page</u>
I. INTRODUCTION	1
II. EXPERIMENTAL DESCRIPTION	2
A. Configuration	2
B. Instrumentation	4
C. Heater Package and Packer Design	6
III. FIELD OPERATIONS	7
A. Ambient Conditions	7
B. Heater Operation	9
C. Cool Down	16
IV. RESULTS AND DISCUSSION	16
A. Thermal Behavior	16
B. Water Behavior	20
C. Water Chemistry	26
D. Stress Behavior	29
E. Laser Interferometer	30
F. Permeability Measurements	31
V. CONCLUSIONS	32

TABLES

<u>Table No.</u>	<u>Title</u>	<u>Page</u>
1.	Dimensions of Experimental Holes and Their Position Relative to the Heater Hole at the Depth of the Heater Midplane	2
2.	Instrumentation Fielded in the In Situ Experiment	5
3.	Total Instrumentation and Data Channels	10
4.	Last Background Data Reading Before Heater Turn-On	13
5.	Last Data Reading Before Heater Turn-Off	15
6.	Next to the Last Data Reading Before the Data Acquisition System Shutdown	17
7.	Summary of Total Water Volumes Generated in Each Experimental Cavity	21
8.	Anion Concentrations at Different Times in Water Samples from HH-1, WM-1, WM-2, and Well #8	28
9.	Comparison of Pre and Posttest Water Injection Flow Rates in HH-1	32
10.	Comparison of Pre and Posttest Permeabilities (k) in HH-1 and WM-1, 2, and 3	33

FIGURES

<u>Figure No.</u>	<u>Title</u>	<u>Page</u>
1.	Position of the experimental holes at the depth of the heater midplane. The carat (<) in a hole marks the location of the rock wall thermocouple nearest the heater hole.	38
2.	Plan view of the experimental hole layout.	39
3.	Scale drawing showing the relation of the water collection and instrumentation cavities in the water migration holes to the heater. For this illustration, the water migration holes were rotated into a plane while maintaining the spacing relative to the heater hole.	40
4.	Gas pressurization test carried out in HH-1 during the pretest checkout; test began at 15 psi regulator and went to 30 psi.	41
5.	Comparison of the background pressure variations in HH-1, WM-1, and the alcove.	42
6.	Example of the cyclic displacement measured by the laser interferometer before heater turn-on.	43
7.	Heater power output as a function of time.	44
8.	Comparison of rock wall temperatures with those predicted from pretest modeling. Rock wall thermocouples shown were located at 12 o'clock (vertical) and 4 o'clock positions.	45
9.	Example of the temperature drop registered by the heater hole spring-out, rock wall thermocouples when released from the heater skin (J-Day 36, Channel #27, far-end rock wall, 4 o'clock position).	46
10.	Comparison of the pre and posttest calibration at different temperatures of the heater hole relative humidity gage.	47
11.	Water depth gage readings in HH-1 during the period of heater turn-off.	48
12.	Water depth gage readings in WM-2 during the period of heater turn-off.	49
13.	Temperature profiles in the heater/instrument packer/ assembly. Heater skin temperature - 2 o'clock position; Near-end-Ch#8, Midplane-Ch#11, Far-end-Ch#14. Insulator section; Near-end-Ch#4, Far-end-Ch#3. Water collection cavity; Air-Ch#6, Water-Ch#7.	50

FIGURES (continued)

<u>Figure No.</u>	<u>Title</u>	<u>Page</u>
14.	Rock wall temperature profiles opposite the heater - 12 o'clock position. Near-end-Ch#17, Midplane-Ch#23, Far-end-Ch#26.	53
15.	Comparison of the circumferential and axial heater skin and rock wall temperatures just before heater turn-off. All temperatures in °C. Numbers inside circles are temperature differences.	56
16.	Rock wall temperature profiles in the water migration holes. WM-1, Ch#32. WM-2, Ch#36. WM-3, Ch#42.	57
17.	Representative temperature profiles from the two thermocouple holes and the stress hole. TH-1, Ch#47. TH-2, Ch#57. SH-1, Ch#69.	60
18.	Experimentally determined temperature isotherms surrounding the heater just before turn-off.	63
19.	Comparison of air temperature response to water sample withdrawal from HH-1.	64
20.	Comparison of water temperature response to water sample withdrawal from HH-1.	65
21.	Depth gage data measured in WM-1.	66
22.	Depth gage data measured in WM-2.	69
23.	Depth gage data measured in the heater hole water collection cavity.	72
24.	Depth gage data vs expanded time scale in HH-1 at heater turn-on.	75
25.	Depth gage data vs expanded time scale in HH-1, showing automatic and manual water sampling.	76
26.	Water generation rates in HH-1, WM-1, and WM-2. Rates are not corrected for possible leakage past packer.	77
27.	Relative humidity measured in HH-1 water collection cavity.	78
28.	Comparison of the relative humidity gage response to water sample withdrawal in HH-1.	81
29.	Schematic drawing of the evaporation front model in one-dimensional cylindrical geometry.	82

FIGURES (continued)

<u>Figure No.</u>	<u>Title</u>	<u>Page</u>
30.	Comparison of evaporation front model results and experimental data from HH-1 for high humidity boundary condition and permeability = $10^{-15}m^2$ .	83
31.	Comparison of evaporation front model results and experimental data from HH-1 for high humidity boundary condition and permeability = $10^{-16}m^2$ .	84
32.	Comparison of evaporation front model results and experimental data from HH-1 for high humidity boundary condition and permeability = $10^{-17}m^2$ .	85
33.	Comparison of evaporation front model results and experimental data from HH-1 for dry boundary condition and permeability = $10^{-16}m^2$ .	86
34.	Effect of removing the isothermal boundary condition on the model results. Compare with Figure 31.	87
35.	Evaporation front and isotherm position vs time.	88
36.	pH gage response in WM-2. Circles are pH values measured in the alcove in water samples collected from WM-2. Triangles are pH values measured in water samples collected from WM-1.	89
37.	pH gage response in HH-1. Circles are pH values measured in the alcove in water samples collected from HH-1.	92
38.	pH gage response to manual water sample removal from HH-1 vs expanded time scale. Circles are pH values measured in the alcove in the water samples collected.	95
39.	pH gage response to automatic collection of samples from HH-1 vs expanded time scale.	96
40.	Silicon ion concentration in water samples collected from HH-1, WM-1, and WM-2 at different times.	97
41.	Calcium ion concentration in water samples collected from HH-1, WM-1, and WM-2 at different times.	98
42.	Potassium ion concentration in water samples collected from HH-1, WM-1, and WM-2 at different times.	99

FIGURES (concluded).

<u>Figure No.</u>	<u>Title</u>	<u>Page</u>
43.	Stress meter data SE-28 and SE-7 were oriented to measure thermal stresses radial to the heater. SE-13 was oriented to measure circumferential thermal stresses.	100
44.	Laser interferometer data.	103
45.	Example of the water pressure vs time data obtained during the posttest permeability testing in WM-1.	106

## I. INTRODUCTION

The Nevada Nuclear Waste Storage Investigations (NNWSI) Project is currently evaluating tuff located at Yucca Mountain on and adjacent to the Nevada Test Site (NTS) as a potential medium for placement of a high level commercial nuclear waste repository. At the time that this study was initiated, several different tuff formations were being considered as a potential repository medium. Porosities in these tuffs range from 15 to 35 vol.%. In those units below the water table, the tuffs are fully saturated. Above the water table, the tuffs are often observed to be near fully saturated. The In Situ Tuff Water Migration/Heater Experiment was designed to begin to address and understand the behavior of potentially large amounts of water in saturated or near-saturated rock near a heat source. The experiment was carried out in the welded portion of the Grouse Canyon Member of the Belted Range tuff in the U12g tunnel (G-tunnel) located in Rainier Mesa at NTS. Note that Rainier Mesa is not a potential repository site. The experimental site was about 400 m below surface but more than 200 m above the water table. The welded Grouse Canyon tuff in the vicinity of the experiment contained 22 to 28 vol.% porosity and was >85% saturated. Although the tuff is chemically dissimilar to those at Yucca Mountain, the thermal and mechanical properties are similar to several units in Yucca Mountain that were under consideration for housing a repository.

The objectives of this experiment are listed below:

- 1) Assess water generation/migration behavior in welded tuff.
- 2) Support thermal/thermomechanical code development.
- 3) Support instrumentation development.
- 4) Measure in situ thermal conductivity.

They are described in detail elsewhere.<sup>1</sup> We wish to emphasize that first and foremost, the primary goal of the experiment was to assess the water behavior. No attempt was made to scale the dimensions or the power output of the small diameter heater used in this experiment to a full-sized nuclear waste canister.

The in situ experiment was operated with the heater power on for 63 days. Ambient conditions were monitored up to six weeks before heater turn-on, and cool-down behavior was monitored for approximately seven weeks subsequent to heater turn-off. This is the final report for this experiment and is the last in a series of reports describing all aspects of the in situ experiment which include the Experimental Plan,<sup>1</sup> the Pretest Thermal Analysis,<sup>2</sup> the Hardware Mechanical Design Definition,<sup>3</sup> the Instrumentation Design and Fielding,<sup>4</sup> the Data Acquisition and Playback System,<sup>5</sup> and the Posttest Thermal Analysis.<sup>6</sup> Wherever possible, these reports will be referenced rather than repeat the information. This report, the Final Report, will discuss the operation and results of the in situ experiment concentrating on the water behavior observed.

## II. EXPERIMENTAL DESCRIPTION

### II. A. Configuration

The as-built experimental hole array is shown in Figures 1 and 2. The distances between holes shown in Figure 1 are those at the depth of the midplane of the heater. The laser interferometer hole was drilled at an angle of 66° to the heater hole and aligned with the midplane of the heater. The carat in a hole (<), Figure 1, marks the location of the rock wall thermocouple nearest to the heater hole. Two thermocouples were placed in the stress hole (SH-1), but their exact circumferential position is unknown. Dimensions associated with the experimental hole array are summarized in Table 1. Two thermocouples were fielded in the laser hole, but they were primarily for measuring air and instrument temperatures, not rock wall temperature.

The as-built array varies from the originally proposed array<sup>1</sup> in the position and designation of some of the holes because of an error in rig alignment during drilling of one of the water migration holes (WM#3). However, the error was accommodated by reassigning the function of the errant hole to that of a thermocouple hole (TH-1) and altering the position and function of the holes remaining to be drilled. The result was a minor change in the appearance of the array but no change in the number or function of the holes. The experimental design of the array remained unchanged.

TABLE 1

Dimensions of Experimental Holes and Their Position  
Relative to the Heater Hole at the Depth of  
the Heater Midplane

	Diameter (cm)	Depth (m)	Radial Distance From HH-1 C to Hole C (cm)	Radial Distance From HH-1 C to T Thermocouple max (cm)
<b>Heater Hole</b>				
HH-1	12.7	19.8		6.35
<b>Water Migration Hole</b>				
WM-1	9.6 (HQ) <sup>a</sup>	19.2	62.1	57.9
WM-2	9.6 (HQ)	19.0	39.9	40.2
WM-3	9.6 (HQ)	18.8	34.4	31.8
<b>Thermocouple Hole</b>				
TH-1	7.6 (NQ)	21.3	63.1	58.3
TH-2	9.6 (HQ)	21.3	37.0	33.2
<b>Stress Hole</b>				
SH-1	4.8 (AQ)	19.7	79.9	79.9 ±2.4

(a) Letters correspond to alpha designation of standard diamond core bit size.

Except for the laser hole, the experiment holes were oriented N 60° W so that they ran parallel to one of the major joint sets in the Grouse Canyon Member. The holes were inclined upward at an angle of 20° because, at the time of the experiment, the welded Grouse Canyon tuff overlaid the workings in G-tunnel. The laser hole was oriented S 54° W, +17°. Even though exploratory drilling was carried out to characterize the welded tuff, a considerable amount of "exploration" was associated with the drilling of the actual experimental holes because of our inability to project and correlate fractures between holes separated by no more than 1 m. Even with the application of error bars to the fracture orientations, the correlation success was only about 6%. Better success was achieved in correlating fracture zones from hole to hole, but this did not provide the detail needed to decide on instrument and packer placement. Consequently, each hole was characterized in detail as it was drilled, primarily by the core logs. The interior of the holes was also viewed using a borehole television camera which showed fewer joints than observed in the core. This is typical since the drilling action tends to cause breakage in the core. The main value of the TV scans was to confirm the core data in the vicinity of experiment and to note voids or pullouts in the rock wall that could affect thermocouple placement or packer sealing.

Based on experimental requirements, the precision nature of the drilling, and practical considerations, the experiment holes were drilled in the following order: HH-1, SH-1, WM-1, WM-2, TH-1, WM-3, TH-2, and LH-1. The heater hole (HH-1) was drilled first to ensure that suitably competent rock could be located to contain the heater and provide for leak-free seals around the packers. Also, because of the straightness required (<0.635-cm deviation in 3.05 m), and the multiple drilling and reaming operations required to obtain the final 12.7-cm diameter, the heater hole promised to be one of the more difficult to obtain. After the heater hole was successfully completed, the stress hole was drilled. This second hole was drilled for two reasons. First, it was the parallel hole farthest from the heater hole, and it was the logical choice since we were uncertain of the drillers' ability to maintain alignment parallel to the heater hole while drilling. Second, we wanted to field the stress gages to see if we could detect any perturbations in the stress field caused by the additional drilling and mining. No changes were observed. The water migration holes were drilled next with particular care taken during the last meter of depth to terminate drilling when a suitable region near the proposed center plane of the heater was located. Again, the sequence was selected to minimize the impact of misalignment or drilling difficulties on the experimental area.

The heater pilot hole was initially drilled with an NQ core bit (7.6-cm diameter) and the core examined to select the experimental area. The hole was then reamed with a 12.7-cm-diameter diamond core reamer to a depth of 19.4 m which left 46 cm of the NQ hole remaining. Because the quality of the reamed hole to that point was excellent, and the field personnel and drillers raised serious doubts about the ability to maintain the quality for the final 46 cm to total depth (TD), the reaming was terminated and the heater assembly was modified to minimize the effect of the cavity (see below). Even though the reamed heater hole met the drilling criteria, insertion tests with a heater assembly-sized mandrel indicated there would be difficulty in inserting

the heater assembly to the desired location. The problem was eliminated by reaming the first 10.6 m of the hole to 20.3 cm in diameter.

Within the experimental region, the fracture frequency ranged from 2.6/m in HH-1 to 5.6/m in WM-3. The average for all holes was 3.9/m. Because the impact of fractures on the thermally induced water behavior was unknown, we attempted to minimize the number of fractures in the heater/water collection cavity and to locate the water migration cavities such that one cavity was fracture free (WM-1), one contained a single fracture (WM-2), and one contained multiple fractures (WM-3). Only five fractures were present in the 3.5-m-long heater/water collection cavity.

The relation between the water collection cavities in the water migration holes and the heater is shown in Figure 3. The configuration of the experiment was such that water collected in the heater hole ran downhill, away from the heater, and pooled against the deep packer, thereby preventing the refluxing or short circuiting of the power leads that had been observed in other in situ heater experiments.<sup>7-9</sup> The same pooling occurred in the collection cavities in the water migration holes. Much of the instrumentation in these holes was mounted on the packer face and positioned to measure the water as it was collected.

## II. B. Instrumentation

As much as possible, the experiment was designed to record the response of the rock and the water it contained to the thermal input. Consequently, every attempt was made to position the instruments in the holes surrounding the heater hole at the midplane of the heater or symmetrically distributed above and below it. The instruments fielded in the experiment are listed in Table 2. They are described in detail and their positions in the holes given by Waymire and Duimstra.<sup>4</sup>

In addition, water and gas sampling tubes were placed in the heater/water collection and water migration cavities. Off-the-shelf instruments were used whenever possible; however, due to the nature of the experiment, several were fielded on a developmental basis or had to be built or modified. Among these were the water level sensors, relative humidity sensors, stress meters, and the laser strain meter. The data was collected, stored, displayed, reduced, and graphed according to the experimenter's requirements using an HP3052A Data Acquisition System and an HP9845T calculator/controller.<sup>5</sup> A total of 120 channels of data were recorded during the course of the experiment as frequently as every 5 minutes.

The most thoroughly instrumented of the holes was the heater hole due mainly to the large number of thermocouples required to monitor the heater operation and temperatures at potentially critical areas. One thermocouple was attached to each of the two heating elements, nine were distributed along the heater skin, nine were attached to cantilever springs, which forced them against the rock wall opposite the heater,<sup>4,6,9</sup> two were located at opposite ends of the insulator section, one in the power lead junction section, and two

TABLE 2

Instrumentation Fielded in the In Situ Experiment

---

HEATER HOLE (HH-1)

25 Thermocouples  
2 Pressure Transducers  
1 pH Sensor  
1 Relative Humidity Sensor  
1 Water Level Sensor

WATER MIGRATION HOLES (WM-1, WM-2, WM-3)

4 Thermocouples  
2 Pressure Transducers  
1 pH Sensor  
1 Relative Humidity Sensor  
1 Water Level Sensor

THERMOCOUPLE HOLE (TH-1)

9 Thermocouples  
2 Thermistors

THERMOCOUPLE HOLE (TH-2)

13 Thermocouples  
2 Thermistors

STRESS HOLE (SH-1)

3 Stress Meters  
2 Thermocouples

LASER HOLE (LH-1)

1 Laser Strainmeter  
3 Thermocouples

ALCOVE

3 Thermocouples  
1 Pressure Transducer  
4 Background Standard Ice-Bath Thermocouples  
4 Thermocouple Reference Junctions

---

in the water collection cavity - one in the water pool and one in air. The rest of the heater hole instrumentation was located in the water collection cavity. Similar instruments were installed in each of the water migration holes, except that because of an unlikely malfunction, a pH probe was not fielded in WM-1.<sup>4</sup> The thermocouples in the water migration holes were arranged so that one was in the water pool, one was in air, and one each was sprung against the left and right side rock wall.

## II. C. Heater Package and Packer Design

The final heater package design is described in detail in Reference 3, shown schematically in Figure 3, and described briefly here. The heater package as originally conceived was composed of a heater, insulator section, junction section, water pooling/instrument section, and packers. A later addition to the package was a 46-cm-long snout composed of a thin 304 stainless steel sleeve filled with welded tuff core designed to fill the final length of NQ hole that remained unreamed in the heater hole. The purpose of the snout was to return the unusable hole to as close to undisturbed rock as possible and to reduce convection currents in that region.

The heater was a 304 stainless steel cylinder 10.2 cm in diameter and 1.22 m long and contained two Chromolux hairpin resistive heating elements which extended the length of the can. Six equally spaced axial fins were attached to the heater skin to center it in the hole and help reduce circumferential convection currents in the 1.27-cm air-filled annulus between the heater and the rock wall. The success in reducing convection is discussed in Section VI.A. and Reference 6. The heater skin and spring-out rock wall thermocouples were located at the heater midplane and approximately 19 cm from each end.

The insulator section was a thin 304 stainless steel sleeve filled with bubbled alumina (Alundum 163, Norton Co.). The bubbled alumina was selected for its high insulating capability, ease of handling, and chemical inertness. The insulator section was intended to minimize out-hole heat losses from the heater by conduction or convection. All of the thermocouple and heater element leads passed through the interior of the insulator section.

The junction section is where the power leads were connected to the heater elements. The section was completely encapsulated with RTV to protect the connections from corrosion and potential loss of contact.

The water pooling and instrument cavity has been discussed before. Besides the instrumentation present, the most important feature of this cavity was its dependence on the packer to provide a leak-free seal with rock so that any water that migrated into the hole was collected. Previous experience<sup>8,9</sup> with commercial pneumatic packers indicated that they were not suitable for long-term seals at potentially elevated temperatures. In addition, the need to withdraw water periodically and to attach instruments further limited the usefulness of commercial packers. To meet the needs, engineers designed a motor-driven, wedge-type packer using a flat, molded, RTV O-ring.<sup>3</sup> Laboratory tests confirmed the design.<sup>3</sup> The packers were used

in the three water migration holes and the heater hole and worked according to specification in all but WM-3. In that hole, we were unable to obtain a seal capable of retaining water.

### III. FIELD OPERATIONS

#### III. A. Ambient Conditions

Before heater turn-on, the ambient conditions in the experimental area were monitored as part of the background determination and instrument check-out. As noted earlier, the three stress gages were the first instruments installed in the field, 138 days before heater turn-on. They were monitored periodically to determine their stability as well as to observe any changes in the in situ stress field that may have been brought about by the subsequent field activities. In addition to the drilling, these activities included blasting associated with the excavation of the laser drift. After initial stress relief due to gage preloading in the borehole, no other effects were measured before heater turn-on.

Before the other instrument packages were installed, each of the experimental holes was tested for permeability. The details of the testing are discussed in Section IV.F. We attempted to measure hole-to-hole and single-hole behavior. Equipment constraints (Section IV.F.) as well as approximating fracture flow as Darcy flow seriously limit the usefulness of these data. Nevertheless, the measurements showed that all of the holes were highly permeable except WM-1 which had a permeability factor of 10 to more than 100 less than the other holes in the array, which was consistent with the hole logging results and our cavity selection criteria.

The packer/instrumentation packages in the water migration and heater holes were installed 68 to 63 days before heater turn-on. All of the effort before heater turn-on was spent checking out systems, calibrating instruments, and collecting background data. The packer seals, pH probes, and water depth gages were checked by injecting known amounts of tuff equilibrated water into the collection cavities. The pH readings compared well with those taken in the alcove with a routinely calibrated probe. The depth gages functioned according to design although we had only limited success in establishing a quantitative, in-hole calibration.

Standing water pool tests, lasting up to 4 days, indicated that leak rates around the packers in all holes but WM-3 were 1 ml/hr or less. After installation, the packers were periodically tightened (also during heater operation) to eliminate potential loosening due to relaxation of the O-rings. It is important to note that we did not measure any influx of water into the holes at any time before heater turn-on.

The leak rate in WM-3 was high enough that a standing pool of water could not be maintained in the hole. Attempts to tighten the packer against the rock did not resolve the problem; consequently, we did not expect to collect water in WM-3 during the experiment:

As a safety measure, a gas pressurization test was conducted in the heater hole after all of the packer/instrumentation packages were installed. The test was intended to evaluate the potential for developing high pressures in the heater hole which might create a safety hazard for personnel in the instrumentation alcove but also provided a graphic illustration of the potential communication between the heater and water migration holes. The gas used was nitrogen. The results are shown in Figure 4.<sup>(a)</sup> As indicated by the water permeability tests, WM-2 and WM-3 were connected by fractures to the heater hole while WM-1 was not. Communication with the heater hole was greatest for WM-3. The test indicated that over-pressurization of the heater hole was unlikely due to the gas transmissivity of the fractures.

Observation of the ambient pressure in each of the cavities further confirmed the improbability of hole pressurization for all except WM-1. The background observations showed that the pressure within the cavities varied with the ambient barometric pressure in the drift. The data indicate that even though we had good packer seals in most cases, the frequency of intersecting joints was sufficient to provide good communication through the rock mass with the part of the borehole that was open to the drift (around the packers) or with the drift itself. Since WM-1 was located in unfractured rock, it did not show the detailed behavior of the other holes, but it did record the broad long-period variations (see Figure 5).<sup>(b)</sup>

None of the relative humidity gages provided satisfactory background readings, which was not unexpected since at 100% relative humidity, the gages saturated. By the time the heater was turned on, three of the four gages had failed outright or were highly suspect. The only gage that appeared to still be functional was in the heater hole, the most important of those to be monitored. In general, these gages proved to be unsatisfactory. The problems we encountered are described in detail in Reference 4. Note, however, that they were incorporated into the experiment on a developmental basis. The failure of 75% of the Rh gages was disappointing but not totally unexpected.

The laser interferometer also failed to stabilize during the background period. The instrument recorded cyclic displacement, an example of which is shown in Figure 6. We were unable to determine the cause of the behavior, and since the apparatus was considered to be developmental and not essential to

---

(a) Several of the pressure gages registered negative baseline pressures. This is due to calibrating and sealing them at a lower elevation (Albuquerque) than where they were fielded (G-tunnel).

(b) Throughout this report, data is generally plotted vs J-Day (Julian-Day). That is, days numbered consecutively starting with January 1 as J-Day = 1. This provides an easy means of representing time as well as uniquely identifying each day with its calendar date. Keep in mind, however, 1980 was a leap year so that J-Day = 60 is February 29, not March 1 and correlation of J-Days with calendar dates thereafter must be adjusted accordingly.

monitoring water behavior, we elected to proceed with the experiment in spite of the instability.

By the time the heater was turned on, the temperature throughout the experimental area had fully stabilized. The ambient rock temperature was  $17 \pm 0.5^\circ\text{C}$ . Individual thermocouples fluctuated by  $\pm 0.1$  to  $0.2^\circ\text{C}$ . The variation between thermocouples was well within the experimental error for thermocouples of this type. The data channel identification list is given in Table 3, and the last background data reading before heater turn-on is shown in Table 4.

### III. B. Heater Operation

After a final Quality Assurance audit of the experimental instrumentation and procedures, the power to the heaters was turned on on Tuesday, February 5, 1980 (J-Day = 36), at 1,430 hr. Because the primary objective of the experiment was to initiate assessment of the behavior of the potentially large quantities of water in the rock, no attempt was made to scale the power output of the small diameter heater to a full-sized nuclear waste canister. The main consideration in establishing the operating conditions was to heat the rock to the highest temperature possible with assurance that the rock would not fracture, disintegrate, or respond in some other manner that would interfere with the observation or confuse the interpretation of the water behavior. Based on these constraints, the results of the pretest modeling<sup>1</sup> indicated that rock wall temperatures much in excess of  $220^\circ\text{C}$  could cause failure in the rock surrounding the heater due to thermal stresses in excess of laboratory-determined, room temperature, unconfined, uniaxial compressive strength. Consequently,  $220^\circ\text{C}$  was selected as the maximum allowable rock temperature which corresponded to a heater power output of 1 kW. Because of the limitations in the codes and dependence of the unconfined compressive strength of the welded tuff on variable parameters such as strain rate and degree of saturation, the 1-kW power level was considered only an approximate value until we could observe the actual thermal response during the experiment.

The actual power curve is shown in Figure 7. It was apparent soon after the heater was turned on that the rock was increasing in temperature well in excess of the rate predicted by the pretest thermal calculations, as shown in Figure 8. Therefore, during the course of the experiment (primarily the first 20 days), the power was gradually adjusted downward manually to correspond to the temperature limitation on the rock wall.

A second feature apparent in Figure 7 is the relatively large power fluctuations ( $\pm 4\%$ ) during the course of a single weekday. Over the weekends, the fluctuations were less than  $\pm 1.5\%$ . This behavior comes about because the heater power supply was wired directly into the commercial power grid and was controlled manually with power stats. We would recommend in future experiments of this type that constant DC power supplies be used to eliminate this problem.

TABLE 3

Total Instrumentation and  
Data Channels

CH#	I.D.	Gage Type	Location	Units	Calibration
0	RF-1	REFERENCE JUNC	CARD 1	OHMS	SLA
1	T-1	TYPE E TC #10 TCM	HEATER ELEMENT E-1	DEGREES C	NBS
2	T-2	TYPE E TC #11	HEATER ELEMENT E-2	DEGREES C	NBS
3	T-3	TYPE E TC #12	INSUL SECTION HI	DEGREES C	NBS
4	T-4	TYPE E TC #13	INSUL SECTION LO	DEGREES C	NBS
5	T-5	TYPE E TC #14	JUNCTION SECTION	DEGREES C	NBS
6	T-6	TYPE E TC #15	HEATER INSTR AIR	DEGREES C	NBS
7	T-7	TYPE E TC #16	HEATER INSTR H2O	DEGREES C	NBS
8	T-8	TYPE E TC #6	NEAR HEATER END 2	DEGREES C	NBS
9	T-9	TYPE E TC #3 TCM	NEAR HEATER END 6	DEGREES C	NBS
10	T-10	TYPE E TC #9	NEAR HEATER END 10	DEGREES C	NBS
11	T-11	TYPE E TC #5	HEATER MIDPLANE 2	DEGREES C	NBS
12	T-12	TYPE E TC #2 TCM	HEATER MIDPLANE 6	DEGREES C	NBS
13	T-13	TYPE E TC #8	HEATER MIDPLANE 10	DEGREES C	NBS
14	T-14	TYPE E TC #4	FAR HEATER END 2	DEGREES C	NBS
15	T-15	TYPE E TC #1 TCM	FAR HEATER END 6	DEGREES C	NBS
16	T-16	TYPE E TC #7	FAR HEATER END 10	DEGREES C	NBS
17	T-17	TYPE E TC #22	NEAR HEATER ROCK 12	DEGREES C	NBS
18	T-18	TYPE E TC	BKGD STANDARD-ICE	DEGREES C	NBS
19	CAL V	ANALOGIC	CARD 1 CALIBRATION	VOLTS	SLA
20	RF-2	REFERENCE JUNC	CARD 2	OHMS	SLA
21	T-19	TYPE E TC #19	NEAR HEATER ROCK 4	DEGREES C	NBS
22	T-20	TYPE E TC #25	NEAR HEATER ROCK 8	DEGREES C	NBS
23	T-21	TYPE E TC #21	MID-HEATER ROCK 12	DEGREES C	NBS
24	T-22	TYPE E TC #18 TCM	MID-HEATER ROCK 4	DEGREES C	NBS
25	T-23	TYPE E TC #24	MID-HEATER ROCK 8	DEGREES C	NBS
26	T-24	TYPE E TC #20	FAR HEATER ROCK 12	DEGREES C	NBS
27	T-25	TYPE E TC #17	FAR HEATER ROCK 4	DEGREES C	NBS
28	T-26	TYPE E TC #23	FAR HEATER ROCK 8	DEGREES C	NBS
29	T-27	TYPE E TC #1	WM-1 WATER 62.0 FT	DEGREES C	NBS
30	T-28	TYPE E TC #2	WM-1 AIR 62.17 FT	DEGREES C	NBS
31	T-29	TYPE E TC #3	WM-1 LEFT 62.3 FT	DEGREES C	NBS
32	T-30	TYPE E TC #4	WM-1 RIGHT 62.3 FT	DEGREES C	NBS
33	T-31	TYPE E TC #1	WM-2 WATER 61.5 FT	DEGREES C	NBS
34	T-32	TYPE E TC #2	WM-2 AIR 61.67 FT	DEGREES C	NBS
35	T-33	TYPE E TC #3	WM-2 LEFT 61.8 FT	DEGREES C	NBS
36	T-34	TYPE E TC #4	WM-2 RIGHT 61.8 FT	DEGREES C	NBS
37	T-35	TYPE E TC #1	WM-3 WATER 61.08 FT	DEGREES C	NBS
38	T-36	TYPE E TC	BKGD STANDARD-ICE	DEGREES C	NBS
39	CAL V	ANALOGIC	CARD 2 CALIBRATION	VOLTS	SLA
40	REF-3	REFERENCE JUNC	CARD 3	OHMS	SLA
41	T-37	TYPE E TC #2	WM-3 AIR 61.25 FT	DEGREES C	NBS
42	T-38	TYPE E TC #3	WM-3 LEFT 61.38 FT	DEGREES C	NBS

TABLE 3 (continued)  
Total Instrumentation and  
Data Channels

CH#	I.D.	Gage Type	Location	Units	Calibration
43	T-39	TYPE E TC #4	WM-3 RIGHT 61.38 FT	DEGREES C	NBS
44	T-40	TYPE E TC	TH-1 53.5 FT	DEGREES C	NBS
45	T-41	TYPE E TC	TH-1 56.5 FT	DEGREES C	NBS
46	T-42	TYPE E TC	TH-1 59.5 FT	DEGREES C	NBS
47	T-43	TYPE E TC	TH-1 60.5 FT	DEGREES C	NBS
48	T-44	TYPE E TC	TH-1 61.5 FT	DEGREES C	NBS
49	T-45	TYPE E TC	TH-1 62.5 FT	DEGREES C	NBS
50	T-46	TYPE E TC	TH-1 63.5 FT	DEGREES C	NBS
51	T-47	TYPE E TC	TH-1 64.5 FT	DEGREES C	NBS
52	T-48	TYPE E TC	TH-1 69.5 FT	DEGREES C	NBS
53	T-49	TYPE E TC	TH-2 56.5 FT	DEGREES C	NBS
54	T-50	TYPE E TC	TH-2 58.5 FT	DEGREES C	NBS
55	T-51	TYPE E TC	TH-2 60 FT	DEGREES C	NBS
56	T-52	TYPE E TC	TH-2 60.5 FT	DEGREES C	NBS
57	T-53	TYPE E TC	TH-2 61 FT	DEGREES C	NBS
58	T-54	TYPE E TC	BKGR STANDARD-ICE	DEGREES C	NBS
59	CAL V	ANALOGIC	CARD 3 CALIBRATION	VOLTS	SLA
60	RF-4	REFERENCE JUNC	CARD 4	OHMS	SLA
61	T-55	TYPE E TC	TH-2 61.5 FT	DEGREES C	NBS
62	T-56	TYPE E TC	TH-2 62 FT	DEGREES C	NBS
63	T-57	TYPE E TC	TH-2 62.5 FT	DEGREES C	NBS
64	T-58	TYPE E TC	TH-2 63 FT	DEGREES C	NBS
65	T-59	TYPE E TC	TH-2 63.5 FT	DEGREES C	NBS
66	T-60	TYPE E TC	TH-2 64.5 FT	DEGREES C	NBS
67	T-61	TYPE E TC	TH-2 65.5 FT	DEGREES C	NBS
68	T-62	TYPE E TC	TH-2 67.5 FT	DEGREES C	NBS
69	T-63	TYPE E TC	STRESS 62.3 FT	DEGREES C	NBS
70	T-64	TYPE E TC	STRESS 62.3 FT	DEGREES C	NBS
71	T-65	TYPE E TC	LH-1 29.8 FT	DEGREES C	NBS
72	T-66	TYPE E TC	LH-2 28.7 FT	DEGREES C	NBS
73	T-67	TYPE E TC	INSTR ALCOVE	DEGREES C	NBS
74	T-68	TYPE E TC	LASER 28.7 FT	DEGREES C	NBS
75	T-69	TYPE E TC	ALCOVE ROCK WALL	DEGREES C	NBS
76	T-70	TYPE E TC	INSTR RACK	DEGREES C	NBS
77	T-71	TYPE E TC	LASER ALCOVE	DEGREES C	NBS
78	T-72	TYPE E TC	BKGD STANDARD-ICE	DEGREES C	SLA
79	CAL V	ANALOGIC	CARD 4 CALIBRATION	VOLTS	SLA
80	PR-1	PRESSURE SN 1002	HEATER HOLE	PSI	.0427 V/PSI
81	PR-2	PRESSURE SN 1025	HEATER HOLE	PSI	.048 V/PSI
82	PR-3	PRESSURE SN 1005	HOLE WM-1	PSI	.043 V/PSI
83	PR-4	PRESSURE SN 1017	HOLE WM-1	PSI	.0482 V/PSI
84	PR-5	PRESSURE SN 1004	HOLE WM-2	PSI	.0433 V/PSI
85	PR-6	PRESSURE SN 1018	HOLE WM-2	PSI	.0481 V/PSI

TABLE 3 (concluded)  
Total Instrumentation and  
Data Channels

CH#	I.D.	Gage Type	Location	Units	Calibration
86	PR-7	PRESSURE SN 1006	HOLE WM-3	PSI	.043 V/PSI
87	PR-8	PRESSURE SN 1023	HOLE WM-3	PSI	.049 V/PSI
88	PR-9	PRESSURE SN 1020	ALCOVE	PSI	.0476 V/PS
89	S-1	STRESS SE-28	SH-1 0 DEG 62.75 FT	MV	SLA
90	S-2	STRESS SE-7	SH-1 0 DEG 62.29 FT	MV	SLA
91	S-3	STRESS SE-13	SH-1 90 DEG 61.5 FT	MV	SLA
92	LAS-2	LASER STRAIN	LH-1	MICRON	10V/4096CT
93	PH-1	PH SENSOR R11713	HEATER HOLE	PH	SLA
94	PH-2	PH SENSOR R11714	ALCOVE	PH	SLA
95	PH-3	PH SENSOR R11840	WM-2	PH	SLA
96	PH-4	PH SENSOR R11712	WM-3A	PH	SLA
97	RH-2	REL HUMID SN501	WM-1	%RH	TH SCI
98	RH-1	REL HUMID SN502	HEATER HOLE	%RH	TH SCI
99	CAL V	ANALOGIC	CARD 5 CALIBRATION	VOLTS	SLA
100	RH-4	REL HUMID SN503	WM-3A	%RH	TH SCI
101	RH-3	REL HUMID SN504	WM-2	%RH	TH SCI
102	V-1	ELEMENT VOLTAGE	HEATER HOLE	VOLTS	SLA
103	A-1	ELEMENT CURRENT	HEATER HOLE	AMPS	SLA
104	P-1	HEATER POWER	HEATER HOLE	WATTS	SLA
105	V-2	ELEMENT VOLTAGE	HEATER HOLE	VOLTS	SLA
106	A-2	ELEMENT CURRENT	HEATER HOLE	AMPS	SLA
107	P-2	HEATER POWER	HEATER HOLE	WATTS	SLA
108	WAT-1	WATER LEVEL	HEATER HOLE	VOLT	SLA
109	WAT-2	WATER LEVEL	WM-1	VOLT	SLA
110	WAT-3	WATER LEVEL	WM-2	VOLT	SLA
111	WAT-4	WATER LEVEL	WM-3	VOLT	SLA
112	LAS-1	LASER STRAIN	LH-1	MICRON	20V/4096CT
113	CAL V	ANALOGIC	CARD 6 CALIBRATION	MICRON	SLA
114	TH-1	THERMISTOR	TC-1 58.5 FT	DEGREES C	SLA
115	TH-2	THERMISTOR	TC-1 67.5 FT	DEGREES C	SLA
116	TH-3	THERMISTOR	TC-2 59.5 FT	DEGREES C	SLA
117	TH-4	THERMISTOR	TC-2 69.5 FT	DEGREES C	SLA
118	P-1D	HEATER POWER	HEATER HOLE	WATTS (DIG)	SLA
119	P-2D	HEATER POWER	HEATER HOLE	WATTS (DIG)	SLA
120	P-3D	HEATER POWER	TOTAL POWER	WATTS (DIG)	SLA

TABLE 4

Last Background Data Reading Before Heater Turn-On  
 [Data are in matrix format according to channel number (see Table 3)]

	01	02	03	04	05	06	07	08	09	10
000	17.16	16.98	16.99	17.01	17.03	17.62	17.01	17.01	17.08	16.99
010	16.91	17.03	16.89	16.81	16.96	16.81	16.83	-.06	106.17	28.29
020	16.97	16.97	16.99	17.59	16.99	16.91	16.96	16.92	17.12	17.59
030	17.25	17.20	16.99	17.54	17.15	17.12	16.94	-.02	105.58	28.02
040	17.37	17.23	17.23	16.93	16.90	16.98	17.13	17.27	17.28	17.03
050	16.90	16.64	16.92	16.88	16.93	16.90	16.95	.25	105.35	27.67
060	17.03	16.98	16.93	16.93	16.85	16.82	16.75	16.69	18.03	17.93
070	20.66	19.52	21.42	23.18	19.93	25.21	18.97	.13	105.01	.17
080	.20	.29	.02	-.00	.02	.12	.11	-.08	.01	.01
090	.01	0.00	8.80	7.12	7.54	7.35	150.33	103.15	10.00	132.38
100	15.63	-1.30	.00	-4.91	.05	.07	-1.93	.36	.41	.54
110	.51	161.84	163.62	17.13	16.86	17.23	16.88	0.00	0.00	0.00

The deployment of the spring-out rock wall thermocouples in the heater hole was easily noted by watching their individual temperature profiles. The thermocouples were attached to Inconel 750 cantilever springs and mounted on the outside surface of the heater. To prevent them from dragging against the rock wall during heater insertion, the thermocouple/spring assembly was held against the side of the heater with a low melting (~40°C), eutectic alloy washer. When the heater skin approached 40°C, the washers melted and the thermocouples sprung out against the hole wall. Since the rock was at a lower temperature than the heater skin, the thermocouple registered a temperature drop upon contact with the wall. An example is shown in Figure 9.

Twice during the experiment, the data acquisition system shut off for a period of about 15 hr, the first time on the evening of J-day 64 and again about the same time the next day. The reason was a change incorporated into the TUFF program used to control scan rates and accumulate data. The program change was intended to simplify the automatic withdrawal of water from the water collection cavities, but for reasons never determined, the change shut off the system. Unfortunately, the shutdown occurred after all personnel had left for the day, so it was not discovered until the following morning. After it had occurred on two successive days, we restored the program to its original configuration which eliminated the problem.

Water began accumulating in the heater hole collection cavity within several hours after the heater was turned on and continued to collect until the heater was turned off 63 days later. Water was also collected continuously in WM-1 and WM-2 during the time the heater was on. The water was siphoned from the water collection cavities through small-bore, stainless steel capillary tubing. The drain rate was about 14 ml/min. Although a vacuum system was available to initiate siphoning, with one exception, it was not generally used. The water was withdrawn into a calibrated, graduated cylinder to measure its volume. A cavity was never drained completely. Sufficient water was left in the hole after a withdrawal so that the depth gage remained operating in its most sensitive range. Consequently, water remained in the capillary tube and the siphon was self-starting at each sampling. The exception was WM-3. Periodically, we attempted to withdraw water from the cavity in case the depth gage was malfunctioning. In each attempt, the vacuum was applied to initiate siphoning, but without success. No water was collected in WM-3.

Because of the rate that water was collected in HH-1 and the cost of keeping G-tunnel open around the clock and manning the experiment continuously, an automatic draining system, controlled by the HP9845T controller/calculator, was developed and initiated 22 days into the experiment. Initial programming changes led to the problems discussed above, but were soon resolved. Since the automatic system could not measure volume, manual drains were performed daily (or on Monday following the weekend) to ensure proper water-generation rate calculations.

Seven days after heater turn-on, the gas sampling vent in WM-1 was opened permanently. We did this to provide WM-1 with communication to the alcove similar to that of the other holes. We were concerned that potential pressure buildup in WM-1 could affect the water migration behavior such that it was not comparable with the other holes, and since WM-1 was the most distant water collection hole from the heater, we felt that it was important to simplify the future analysis of the water behavior as much as possible.

The relative humidity gage in the heater hole was the only one to operate during the entire experiment. After the heater was turned on, the humidity dropped below 100%, which brought the gage out of saturation. From then on, the gage was responsive to minute variations in conditions and appeared to operate properly. The gage was exposed to a maximum temperature of 37°C. Comparison of the pre and posttest calibration<sup>4</sup> indicated relatively large changes in gage response (Figure 10); consequently the absolute values registered by the gage probably are not accurate. Nevertheless, we believe the relative behavior is correct, and it provided a qualitative description of the water vapor behavior in the cavity.

During the course of the heated phase of the experiment, it became apparent that the water depth gages provided only a qualitative measure of the water present in the cavity. Attempts to correlate the water removed with the pretest calibration or to quantitatively recalibrate with the gage output voltage were unsuccessful. Consequently, we used the gage output to determine when to remove water from the cavity but used the water volume withdrawn to calculate average rate data.

The pH gages appeared to operate properly throughout the experiment. The pH of each water sample was measured after withdrawal with a calibrated probe and compared with the in situ value.

The laser interferometer was designed to measure the displacement of the approximately 67 cm of rock between the bottom of the laser hole and the wall of the heater hole along the extended axis of the laser hole. The interferometer operated continuously for the entire experiment. From time to time, we experienced difficulties with the fringe counting electronics. A second counter was connected to the circuit in parallel to provide a comparison with the original counter. Both counters operated until the field experiment was terminated.

Throughout the experiment, the pressure gages measured nothing more than barometric variations. Toward the end of the heated phase of the experiment, several of the pressure gages started to behave erratically. These included both gages in WM-2, one gage in WM-1, and the gage in the alcove. The last data reading before heater turn-off is given in Table 5.

TABLE 5

Last Data Reading Before Heater Turn-Off [Data are in Matrix Format According to Channel Number (See Table 3)]

---

04:08:09:20:00

	01	02	03	04	05	06	07	08	09	10
000	429.49	441.26	147.22	54.23	48.15	36.88	33.71	264.57	257.88	262.57
010	301.18	301.10	299.08	278.90	272.09	282.06	184.28	-.03	108.30	30.64
020	182.27	176.38	236.16	225.82	223.13	195.09	188.31	196.43	54.98	56.37
030	53.73	56.88	70.45	72.86	72.28	72.72	74.70	-.02	107.69	30.29
040	76.56	77.16	72.60	24.82	35.21	56.34	60.55	61.05	53.11	46.27
050	43.06	23.46	37.10	60.80	83.89	88.23	87.63	.27	107.40	29.83
060	86.87	82.94	78.52	78.91	69.11	52.51	44.55	29.78	47.83	47.70
070	43.79	34.91	24.01	29.88	22.84	26.97	34.47	.19	106.96	-.22
080	-.62	-2.48	-2.12	-.40	7.95	-1.92	-2.27	-.13	.01	.02
090	.01	244.44	6.47	7.80	7.70	7.53	-117.50	87.23	10.00	15.57
100	.28	8.85	7.27	388.44	53.60	7.27	384.83	.49	.19	.57
110	.55	270.24	163.62	71.45	24.37	48.30	30.56	388.00	385.00	773.00

---

### III. C. Cool Down

Power to the heater was turned off on April 8, 1980 (J-Day = 99), at 0931 hr after 63 days of operation. We continued to monitor all instrumentation during the cool-down period. There were no additional instrument malfunctions. In general, cool down proceeded without incident until near the end of the period when a severe electrical storm eliminated all power to the alcove (late J-Day = 145). An apparent direct lightning strike blew all three 200-amp fuses in the commercial lines and fused two of three relays in the transfer panel, which prevented the backup autostart diesel power supply from activating. In addition, the strike apparently tripped the breaker in the uninterruptible power supply, and lastly, the automatic callback/alarm system failed to operate. Nevertheless, all systems operated properly when restarted (J-Day = 148), and we have no reason to believe that any important data was lost.

The most noteworthy occurrence during the cool-down period was that within a matter of hours after heater turn-off, all water generation and collection in HH-1, WM-1, and WM-2 ceased. Water samples were collected from each of the holes just before heater turn-off. The next sample removed from HH-1 was about 23.5 hr later and amounted to only 60 ml. Based on the generation rate just before heater turn-off, the sample volume would have been 590 ml. Examination of the HH-1 depth gage data for this period, shown in Figure 11, suggests that water influx into HH-1 had declined significantly within approximately 10 hours of heater turn-off. The 60-ml sample was the last obtained during the experiment. The water influx into the holes quickly dropped below the leak rate around the packers, making any further collection impossible, as shown in Figure 11 for HH-1, and even better illustrated in Figure 12 for WM-2.

The cool down was monitored for 50 days after heater turn-off. The data acquisition system (DAS) was shut down on May 28, 1980 (J-Day = 149). The next to the last data recorded (0640 hr) before DAS shutdown are given in Table 6. Note that rock temperatures were within a few degrees of the pretest, ambient values (17°C). Virtually all of the other instruments had stabilized or were changing at such a slow rate that continued observation was not required.

## IV. RESULTS AND DISCUSSION

### IV. A. Thermal Behavior

Representative thermal profiles associated with the heater/instrument/packer assembly from the time of heater turn-on to the shutdown of the DAS are given in Figure 13. None of the temperatures associated with the assembly were excessive. The individual thermocouples are identified by channel number (Ch#) (see Table 3) and include the heater skin temperature at the midplane (Ch#11), far (deep) end (Ch#14) and near-end (Ch#8), the far-end (Ch#3) and near-end (Ch#4) temperatures in the insulator section, and the air (Ch#6) and water (Ch#7) temperatures in the instrument section. The temperatures of the two heating elements are not included, but their profiles are identical to

TABLE 6

Next to the Last Data Reading Before the Data Acquisition System Shutdown  
[Data are in a matrix format according to channel number (See Table 3)]

---

05:28:06:40:00

	01	02	03	04	05	06	07	08	09	10
000	22.01	21.83	21.71	21.51	21.38	21.74	21.10	21.81	21.84	21.78
010	21.74	21.83	21.73	21.66	21.78	21.68	21.69	-.01	108.86	31.22
020	21.80	21.78	21.88	22.46	21.88	21.78	21.80	21.75	21.73	22.11
030	21.78	21.81	21.68	21.75	21.66	21.68	21.90	.05	108.26	30.88
040	22.36	22.20	22.21	20.45	21.16	21.67	21.82	21.87	21.88	21.59
050	21.39	19.95	21.24	21.57	21.80	21.77	21.85	.37	107.94	30.41
060	21.96	21.86	21.86	21.83	21.67	21.55	21.35	20.79	22.49	22.39
070	23.61	23.36	23.79	29.11	22.32	27.13	22.85	.23	107.51	-.31
080	-1.01	-7.04	-.73	-4.92	-4.79	-1.15	-1.14	-.63	.01	.01
090	.01	313.22	7.38	7.07	6.35	9.68	-117.39	97.45	10.00	-18.37
100	70.75	1.78	.00	-5.66	.08	.10	-1.61	.31	.18	.53
110	.53	157.27	163.62	21.71	20.28	21.50	20.63	0.00	0.00	0.00

---

those for the heater skin although much hotter, reaching a maximum value of 473°C. The maximum temperature recorded in the heater/power lead junction box was 48°C, which eliminated previous concerns about the terminals loosening due to excessive heating.

The maximum temperature recorded in the instrument section was 37°C in the air, well within the temperature operating range for all the instruments located there. During the entire heated phase of the experiment, except for a short period just after heater turn-on, the air and water temperatures in the instrumentation section differed by about 3°C with the air temperature hottest. They differed by 0.5°C in the same order before heater turn-on.

The rock wall thermal profiles at the 12 o'clock orientation opposite the heater are given in Figure 14. As mentioned, the curves are for locations opposite the midplane (Ch#23), far end (Ch#26) and near end (Ch#17) of the heater. All of the spring-out rock wall thermocouples deployed properly and operated for the entire experiment. However, calculations indicated that because the cantilever springs and the thermocouple leads, themselves, were attached to the heater skin, they could record temperatures up to 20°C above the true rock temperature.<sup>9</sup> Laboratory experiments confirmed that the error could range between 10° and 20°C above the true temperature during steady-state conditions.<sup>6</sup>

Another concern raised during the experiment design was the potential for relatively large convective contributions to the effective circumferential and axial thermal conductivities in the 1.27-cm annular air gap between the heater and rock wall. Calculations suggested increases up to 30% were possible.<sup>10</sup> Practical limitations prevented the annulus from being reduced; however, six axial, equally spaced fins were added to the heater to reduce circumferential convection. A comparison of the circumferential and axial heater-skin and rock wall temperatures just before heater turn-off is given in Figure 15. The data show that some temperature anisotropy was present, but, in all cases, the deviation from uniform distribution was less than 10%. The maximum circumferential variation was less than 6%. These data indicate that the steps taken to reduce convection were largely successful, but that the convective component remaining leads to a small asymmetry in the transport of the heat from the heater to the rock.

The rock wall temperature profiles in the water migration holes WM-1 (Ch#32), WM-2 (Ch#36), and WM-3 (Ch#42), at the locations closest to the heater hole (Figure 1), are given in Figure 16. Each of these thermocouples was located as close to the heater midplane as the cavity selection criteria and rock quality would permit. The thermocouples were placed on the rock wall on the right and left sides, in the air, and in the water pool for each of these holes. Because of the orientation of WM-1 and WM-3 to the heater, the two rock wall temperatures established the maximum and minimum temperature in each hole, differing by 3 and 4°C, respectively. The air and water temperatures fall between, with the air temperature 1 or 2°C hotter. The orientation of WM-2 was such that the rock wall temperatures were nearly the same, and the lowest temperature was recorded by the water thermocouple. Before heater turn-on, none of the background temperatures in any of the water migration holes varied from each other by more than 0.5°C.

Representative temperature profiles for the two thermocouple holes TH-1 (Ch#47) and TH-2 (Ch#57) and the stress hole (Ch#69) are shown in Figure 17. Only data from the hottest location in each of the thermocouple holes are included in the figure. Correlating these temperatures with the others measured in the thermocouple holes, as well as those discussed above (Figure 16), allowed calculation of temperature isotherms axially symmetric around the heater. An example is given in Figure 18 just before heater turn-off.

In general, all of the temperature profiles were well behaved with little or no unexpected or unexplained responses. Temperatures at locations close to the heater varied directly as the power fluctuated (as described earlier) as shown by the heater-skin temperature (Ch#8, 11, 14) in Figure 13, and the heater-hole, rock wall temperatures in Figure 14. The cyclic temperature fluctuation is completely absent in all locations radially removed from the heater hole due to the damping effect of the thermal inertia in the intervening rock mass (Figures 16 and 17).

None of the experimental holes surrounding the heater hole reached temperatures as high as the boiling point of water (94°C at the experiment elevation) which was predicted by the pretest modeling. The behavior of the water evaporation front and its effect on the effective rock thermal properties is of particular interest when trying to model the thermal and water behavior in

a heated environment.<sup>6</sup> We had located several of the water migration holes as close to the heater hole as possible in hopes of intersecting the boiling isotherm, but without success.

A large temperature gradient existed along the axis of the heater hole from a maximum temperature of about 320°C on the heater skin at the midplane to approximately 37°C in the instrumentation/water collection section. The conditions appear to have been near ideal for observing water migration if transport is by vapor diffusion as discussed later. In any case, the conditions were similar to those in other in situ experiments in which vapor transport and condensation were observed,<sup>7,9</sup> but not quantitatively measured.

The air and water temperatures in the water collection cavities were sensitive to changes in the quantities of water present. The response of the collection cavity air temperature to withdrawal of water samples in HH-1 is shown in Figure 19. The air temperature rises sharply about 0.3°C as the water sample is withdrawn. After sampling, the air temperature gradually decreases as the cavity begins to accumulate water again. Note in the figure that the magnitude of the temperature fluctuation is related to the amount of water withdrawn as shown by comparison of the large manual withdrawal at mid J-Day = 80 to the regular automatic sampling between J-Day = 78 and 80. It appears that evaporation from the water surface tends to cool the surrounding air temperature. The closer the surface of the water pool to the thermocouple, the greater the effect.

The response of the temperature of the water pool to sample withdrawal in HH-1 is shown in Figure 20. While the magnitude of the water temperature change was about the same, the duration of the effect was much shorter, probably because of the much larger thermal capacitance of the water.

The posttest analysis of the thermal results are discussed in detail by Eaton et al.<sup>6</sup> and will only be briefly summarized here. The posttest calculations used the finite element thermal conduction code COYOTE,<sup>11</sup> the same code used in the pretest calculations.<sup>1,2</sup> The posttest calculations differ from the pretest study in four areas:

- 1) thermal properties of welded tuff,
- 2) heater output as a function of time,
- 3) manner in which the influence of water vaporization is considered, and
- 4) magnitude of assumed emissivities of rock wall and heater surface.

During the first five days of heater operation, the calculated temperatures were slightly less than the experimental values. After 40 days of heater operation, the calculated temperatures exceeded the experimental values by an average of 12%. The calculated and experimental values were almost identical during cool down.

The results of the posttest analysis imply that the accuracy of the calculations were highly influenced by the manner in which the heat source and water transport were modeled, since during cooling, when there was no heat source and presumably little or no water movement, the agreement between computed values and experimental results was very good. In addition, the model does not consider convection effects.

#### IV. B. Water Behavior

Before turning the heater on, enough tuff equilibrated water was added to each of the water collection cavities to fill the "dead space" below the depth gages and activate the first pin of the gage. This was done so the gages would be the most sensitive to the influx of water if it occurred. By the time the heater was turned on, the water ballast had leaked out of WM-3. The depth gage responses in WM-1, WM-2, and HH-1 are shown in Figures 21, 22, and 23, respectively. Because of the rate that water was collected in HH-1, the details of the gage response are not apparent in Figure 23. Figures 24 and 25 provide expanded time views of the gage response. Increasing voltage corresponds to increased water accumulation in the collection cavities. The step-like nature of the voltage increases reflects the discrete pin design of the gage. The sharp decline in the voltage readings occurred when a water sample was withdrawn from the cavity. Each gage was individually built; consequently, each delivers a unique output.

It is apparent from these figures that water began to collect in each of the cavities soon after the heater was turned on. The first water sample was removed from the heater hole 7 hr 20 min after turn-on. As discussed earlier, we were unable to quantitatively calibrate the depth gages either pretest or while the experiment was in progress. Considerable posttest effort was expended to again try to quantitatively calibrate the gages in light of knowing the water collection rates in each of the holes and the individual stabilized gage characteristics, but without success. Consequently, the water generation rate in each of the holes was quantitatively determined by dividing the amount of water removed from the cavity by the time interval since the last withdrawal. The results are shown in Figure 26. The data points are positioned at the midpoint of the time interval.

Initially, the water accumulated so rapidly in HH-1 and WM-2 that they required around-the-clock attention. The water generation rate in WM-2 eventually slowed to the point that it only required servicing on a daily basis, but such was never the case in HH-1. As mentioned earlier, HH-1 was fitted with an automatic sampling system combined with periodic manual sampling, which accounts for the depth gage response in Figure 23 after about J-Day = 58 and the increased intervals in Figure 26.

Examination of the depth gage responses during cool down in Figures 21-23 reveals a gradual increase in voltage for HH-1 and WM-2 while WM-1 remained level. We attempted to remove water from the HH-1 and WM-2 cavities several times during cool down, but without success. The same behavior was noticed during the pretest background determinations with the same results, no water. The behavior was apparently a gage characteristic or a minor response to atmospheric conditions in the cavities.

After the experiment was completed, the leak rate for each of the water collection cavities was carefully measured. The values were 0.97 ml/hr, 0.49 ml/hr, and 0.26 ml/hr for HH-1, WM-2, and WM-1, respectively. The cavity in WM-3 leaked too rapidly for a unique value to be measured. The total amount of water collected during the experiment is listed in Table 7. The quantities corrected for the cavity leakage are also in Table 7, assuming that

the leak rates were constant throughout the experiment. Any water generated after heater turn-off at a rate less than the measured leak rate would not be detected.

TABLE 7  
Summary of Total Water Volumes Generated  
in Each Experimental Cavity

	Total Water Removed From Cavity <u>(L)</u>	Cavity Leak Rate <u>(ml/hr)</u>	Quantity of Water Leaked <sup>(a)</sup> <u>(L)</u>	Total Water Generated <u>(L)</u>
HH-1	60.2	0.97	1.5	61.7
WM-2	3.61	0.49	0.74	4.35
WM-1	1.50	0.26	0.39	1.89

(a) Assumes the leak rate was constant for 1,517 hr duration of the experiment.

Several causes of leakage from the cavities were possible. One could have been an incomplete seal between the packers and the rock wall. The higher leak rate for the larger diameter heater hole and posttest evidence of water trapped between the near and far packers in the heater hole suggest such a mechanism. Subsurface defects in the rock, not apparent in the core and hidden from view with the borehole TV camera, could also be a source of leaks.

Posttest examination of the packer RTV "O-rings" showed that they acted like impression packers in that defects in the hole wall, such as voids and fractures, were recorded as permanent deformations in the surface of the "O-rings." The frequency of defects was highest for WM-3 and lowest in WM-1. Nevertheless, upon careful examination, we could not identify an unambiguous, continuous defect or chain of defects across the "O-ring" that would explain the high leak rate in WM-3.

An estimate of the potential water volume available to the heater hole based on the boiling point of water at the elevation of the experiment,  $T_B = 94^\circ\text{C}$ , was obtained by approximating the axially symmetric  $94^\circ\text{C}$  isotherm (like those in Figure 18) with paraboloids and calculating the volume of rock hotter than  $94^\circ\text{C}$ . Two paraboloids joined at the heater midplane were required because the isotherms are not longitudinally symmetric. Assuming that the rock contains 25 vol.% porosity that is fully saturated, and that all of the pore water vaporized and migrated into the heater hole where it was collected, the estimated volume of water available is 59.8 L compared with the collected volume of 60.2 to 61.7 L; the agreement is remarkable. Note, however, if the rock is only 95% saturated, the available volume is 56.8 L, or if boiling were to occur at  $95^\circ\text{C}$  (100% saturated), the available volume is 54.5 L. On the other hand, as discussed below, the evaporation front need not be fixed by the

boiling point of water, in which case the available volume of water is greater than estimated above. The real value of such a calculation is as a check to be sure that the experimental observations are within the realm of possibility, which, in this case, it appears they are. These calculations also suggest that fractures did not play a major role in water behavior other than as potential sources of leakage in the water collection cavities.

The relative humidity gage in the heater hole was the only one of four such gages to operate during the experiment. The relative humidity history recorded by the gage is shown in Figure 27. Although the accuracy of the gage is questionable, the general qualitative behavior appears correct. The gage dropped out of saturation very quickly after the heater was turned on and in less than 3 days had dropped to 90%. For the next 20 days, the data oscillated between 89 and 92%. We could not determine an external cause for the oscillations, but beginning about J-Day = 58, the gage appeared to stabilize and the magnitude of the oscillations decreased markedly, except for a periodic, but unpredictable drop in the reading. In a matter of hours following an anomalous decline, the gage would recover to its original line of response and continue until the next drop. This behavior continued until heater turn-off on J-Day = 99.4 after which the relative humidity gradually increased monotonically for the entire cool-down period.

As with the thermocouples, the relative humidity gage appeared sensitive to withdrawal of water samples as shown in Figure 28. The figure includes one of the unexplained periodic decreases in the readings. It is clear that these decreases were not due to water sampling. The gage registered a small, short-lived increase in relative humidity when a water sample was collected, the opposite that would be expected. Note that the perturbation is also superimposed on the data during the anomalous decline in value. It may be that the change in the reading was due to the effect of temperature on the gage.

The important information gained from this instrument was that once the heater was turned on, the air in the heater hole cavity was less than saturated, and if the gage was accurate, the relative humidity was about 88% at the end of the experiment. Such a condition (<100%) must be met if water transport into the heater hole was by vapor diffusion as discussed below.

Coincident with the in situ experiment, Hadley and Turner<sup>12</sup> were conducting laboratory studies to measure the water loss rate from cores of welded tuff at high temperature. The studies were intended as a start toward identifying specific mass transport mechanisms, such as evaporative drying, two-phase water flow due to pressure gradients, and capillary movement, to name a few, in partially saturated rocks. They found that all of the water loss data, from room temperature up through 150°C, were explained to within a factor of two by a simple evaporation front model. The model assumed the water was lost by the molecular diffusion of water from a receding evaporation front.<sup>12</sup>

Based on the preceding results, one of us, G. Ronald Hadley, developed a more sophisticated evaporation front model to apply to the results of this

experiment. A sketch of the model in one-dimensional cylindrical geometry is shown in Figure 29. The motion of the front is governed by mass balance. The temperature in the rock is calculated in a time-dependent manner including the effects of latent heat at the front. All the heater power was assumed to conduct into the rock with no allowance made for any convection in the air gap between heater and rock.

The vapor region was treated more fully in this case than for the drying experiments described above, including the effects of any air present. Equations have been derived<sup>13</sup> for the combined diffusion and flow of a binary gas mixture through a porous medium and are given below:

$$J_a = -\frac{16}{3\pi} \frac{R\phi}{m_a v_a^{th}} \frac{\partial p_a}{\partial x} - n_a \frac{k}{\mu} \frac{\partial p}{\partial x} + \frac{2}{3} \frac{Rv_a^{th}}{nD_{ab}} (n_b J_a - n_a J_b) \quad (1)$$

$$J_b = -\frac{16}{3\pi} \frac{R\phi}{m_b v_b^{th}} \frac{\partial p_b}{\partial x} - n_b \frac{k}{\mu} \frac{\partial p}{\partial x} + \frac{2}{3} \frac{Rv_b^{th}}{nD_{ab}} (n_a J_b - n_b J_a) \quad (2)$$

With  $n = n_a + n_b$  = Number Density  
 $p = p_a + p_b$  = Pressure  
 $m_{a,b}$  = Mass of a Molecule

$$v^{th} = \text{Thermal Velocity} = \left( \frac{8kT}{\pi m_{a,b}} \right)^{1/2}$$

$k$  = Permeability  
 $\mu$  = Mixture Viscosity  
 $R$  = Average Pore Radius  
 $\phi$  = Porosity

$D_{a,b}$  = Binary Gas Diffusion Coefficient  
 $J_{a,b}$  = Volume Averaged Number Flux

The first term on the right hand side represents Knudsen diffusion, the second Darcy flow, and the last binary diffusion. The latter effect is not strictly additive since it involves both fluxes. Choosing subscripts a,b to refer to water vapor and air respectively, and assuming "air" to consist entirely of nitrogen, we further specialize (1) and (2) by setting  $J_b = 0$ . This is correct since the air has no place to go (cannot penetrate the evaporation front). The resulting two first-order differential equations in three unknowns ( $n_v$ ,  $P$ ,  $J_v$ ) are solved numerically as a two-point boundary value problem. The three boundary conditions

$n_v = n_{v0}$   
 $P = P_{atm}$   
 $n_v = n_{sat}$  at evaporation front,

together with the mass continuity equation in cylindrical coordinates,

$$J_{v0} = 2\pi r J_v,$$

were sufficient to effect a solution at each time step for the tuff heater experiment simulation. Since exact boundary conditions for  $n_v$  at the rock wall were not known, several were tried with the results from two extremes presented here. The first is a dry boundary,  $n_{v0} = 0$ . Simple estimates of water vapor transport down the annulus between heater and rock wall to the cooler region where condensation takes place make this boundary condition very implausible. Due to the high temperature near the heater surface, it is likely that the gas in this region was mostly water vapor. Consequently, a "high humidity" boundary condition was constructed using the algorithm

$$n_{v0} = 0.9(P_{\min})/kT(\text{rock wall}), \quad (3)$$

where  $P_{\min}$  is the lesser of  $P_{\text{atm}}$  or  $P_{\text{vap}}$ ,  $P_{\text{atm}}$  is local atmospheric pressure,  $P_{\text{vap}}$  is the vapor pressure at the evaporation front and  $k$  is Boltzmann's constant. Thus, when the rock wall temperature was below 94°C, the vapor density was determined by conditions at the front. Above 94°C, the vapor density was 90% of the total density in the heater annulus region. Results using both boundary conditions are discussed later.

Since the primary thrust of the modeling was not temperature prediction but rather to describe water motion, some artificialities were used to try and better approximate the actual temperatures encountered during the experiment. First, a power of 650 W was used in the simulation as compared to an average 750 W in the experiment. Secondly, an artificial temperature boundary condition of  $T = 20^\circ\text{C}$  was employed at a radius of 10 x the actual hole radius. Both of these conditions acted to compensate for ignoring end effects in the calculation. The first helped keep temperatures in the right regime and the second caused a flattening of the temperature vs time graph. As will be seen later, the results are temperature sensitive, and a true two-dimensional calculation is needed to provide a more accurate prediction.

Figures 30 through 34 compare the calculated water generation rates in the heater hole with the experimental values (from Figure 26) using different boundary conditions or permeabilities. In all cases, the parameter  $R$  in Equations (1) and (2) (average pore radius) were estimated from the expression

$$R = \left( \frac{8K}{\phi} \right)^{1/2}, \quad (4)$$

which may be derived assuming a straight capillary model. The permeabilities used in these calculations ranged from  $10^{-15}$  to  $10^{-17} \text{m}^2$ , which compare favorably with experimentally determined values for water of  $5 \times 10^{-16}$  to  $2 \times 10^{-17} \text{m}^2$ . The values of  $R$  calculated from Equation (4) ( $\phi = 0.25$ ) range from  $0.18 \mu\text{m}$  to  $0.018 \mu\text{m}$  with a value of  $0.057 \mu\text{m}$  for a permeability of  $10^{-16} \text{m}^2$ . These values also compare favorably with the values of  $0.043$  to  $0.057 \mu\text{m}$  obtained by mercury intrusion porosimetry assuming equivalent cylindrical pores. The determinations were made on samples of welded tuff core removed from the heater cavity during the pretest drilling.

Figures 30-32 show results for the "high humidity" boundary condition and three different permeabilities. The water loss rate is considerably less sensitive to permeability than one might expect, varying only a factor of two over a two-decade range of permeability. In each case, the basic features of the data, the immediate peak and slow tail-off, are present. If instead we use a dry boundary condition (Figure 33), the early peak disappears. It is thus logical to suppose that the peak is a result of changing conditions in the annulus between the heater and rock wall. The slow tail-off in the water generation rate can be shown to be due to geometric effects. For drying occurring from a cavity, the rate drops off slowly for cylindrical geometry, and for spherical geometry it approaches a constant. That is significant because it implies that eventually the water influx rate will remain constant indefinitely.<sup>13</sup>

Figure 34 shows the results of removing the artificial temperature boundary condition mentioned earlier. The poor agreement with the experiment demonstrates the sensitivity to temperature of the water loss rate and the consequent need of a two-dimensional calculation. It should be noted that the scatter in theoretical values in Figures 30 through 34 is numerical in origin and would disappear if the mesh size were decreased sufficiently.

Figure 35 is a plot of isotherm position vs time together with the position of the evaporation front. Contrary to popular belief, the evaporation front does not track a given isotherm but crosses from  $\sim 110^\circ$  to  $\sim 85^\circ\text{C}$ . This is due to the presence of the porous medium, which allows pressures at the evaporation front to exceed one atmosphere. Consequently, that temperature at which the vapor pressure is one atmosphere (normally called the boiling point) is no longer of any significance.

These studies, albeit crude, suggest that vapor-phase drying is the dominant mechanism for water loss in the in situ experiment. They show that Knudsen diffusion was significant in the high permeability regime ( $10^{-15} \text{ m}^2$ ) and dominant in the mid to low regime ( $10^{-16} \text{ m}^2$  to  $10^{-17} \text{ m}^2$ ).

A laboratory program designed to evaluate this model--in particular, the existence of a sharp evaporation front in heated rock--is ongoing.<sup>14,15</sup> Initial results on 4.8-cm-diameter core showed nearly uniform drying of the samples with virtually no evidence of a sharp evaporation front. More recent results from tests that more closely simulate the thermal conditions in the in situ experiment have been moderately encouraging. While a well defined evaporation front does not appear to exist, a noticeably steep transition from nearly dry to nearly saturated regions was observed to propagate into the sample. While we obtained reasonable success in explaining the experimental results with the above model, we do not, at this point, expect evaporation front models to work well in most situations. We do believe, however, that future models must fully incorporate two-phase fluid transport in all problem regions.

We did not attempt to model the water generation rates in WM-2 and WM-1 for several reasons. First, while the present attempt to model the water generation rates in the heater hole provides reasonable agreement with the experimental results and some insight into the problem, the approach still

appears to be oversimplified even for this simple, symmetric configuration. Second, the location of the water migration holes relative to the heat source (heater hole) removes all symmetry from the problem, which makes any attempt to quantitatively estimate the water generation rates extremely difficult. At this point, it is sufficient to note that 1) the hole responses were qualitatively correct--that is, the closer, hotter hole, WM-2, collected more water than the farther, cooler hole, WM-1; and 2) in spite of the pervasive fracturing, reasonable quantities of water moved through intact rock to enter WM-1.

We believe it is likely that transport to the water migration holes was by simple Darcy flow of liquid water. The pressure gradient would be due to the pressure difference between the evaporation front and the ambient pressure in the holes or simply to the thermally induced density gradient in the pore water. Although unlikely, a minor contribution to the water influx rate could be due to evaporation/condensation caused by the thermal gradients in the water migration cavities, aided by the fact that the pooled water was periodically removed from the cavities. Additional insight into the water behavior in the water migration cavities may have been obtained from the relative humidity gages if they had functioned properly.

#### IV. C. Water Chemistry

The responses of the pH gages in WM-2 and HH-1 are shown in Figures 36 and 37. The gage response in WM-3 is not included because no water was collected in that hole, and as noted earlier, no pH gage was installed in WM-1. Expanded pH vs time plots for the gage in HH-1 are given in Figures 38 and 39, showing, as observed for other phenomena, the cyclic response of pH when a water sample was removed from the cavity. In the case of pH, the value decreased when the water sample was removed.

As a check on the in situ gages, the pH of most water samples collected from the cavities was measured manually in the instrument alcove with a pH probe which was routinely calibrated with standard solutions. Immediately upon completion of the sampling, the sample was transferred to a plastic bottle, capped, and vigorously shaken briefly. The cap was removed and the pH measured. When the measurement was completed, the bottle was again tightly capped, the lid taped, and the sample stored for future use. The manually measured pH values are included for comparison in Figures 36 through 38. The values measured for water samples from WM-1 are also included in Figure 36 (triangle symbols). The majority of the manually measured values fall below the comparable values measured with the in situ gages. The manual values also exhibit greater scatter. These values were highly dependent on the length of time that passed from the time that water sampling was initiated to when the measurement was made. Values varied as much as 1-pH unit for time periods of 1 to 2 hr after withdrawal as the samples equilibrated with the surroundings. While we standardized the procedure as much as possible, considerable variation between technicians remained. Nevertheless, the manually measured values reflect the general behavior, if not always the exact values, of the in situ measurements.

After heater turn-on, the heater-hole pH readings initially decreased for a short time before exhibiting a rapid increase to values greater than 10 with particularly large declines when water samples were removed from the cavity. After 7 days, the readings began a steady decline to a value of about 6.2 where they remained for the rest of the experiment. The high pH values measured by the in situ gages were confirmed with the manual gage (Figure 38) as were the large declines when the water samples were removed. While the values measured appear correct, we do not believe this to be the correct rock/water response. The behavior may be due to bake-out of various components (potting compounds) of the heater assembly although laboratory experiments attempting to reproduce the observations were unsuccessful. A more likely possibility is contamination due to decomposition of dyes accidentally introduced into the hole from the hydrofrac pumping equipment used for the pretest permeability studies. While care was taken to clean the equipment before use, posttest core-back studies through the heater hole revealed the presence of the dye on the rock wall surface. We don't know if the contamination occurred during the pre or posttest permeability testing.

Similar behavior was not observed in WM-2. Figure 36 shows that after heater turn-on, the pH dropped to 7.0 to 7.2 where it remained until J-Day 70, after which it increased slowly to about 8 when the heater was turned off. The same trend was observed in the manual readings and was even more apparent for WM-1. The reason for this behavior is unknown. It is unlikely to be a temperature effect since the temperature in either hole (54°C in WM-1 and 70°C in WM-2) increased only about 4°C for that time interval. Note that the in situ gage in WM-2 malfunctioned about J-Day = 69 but appeared to recover by the end of the day. It is not likely that the increasing trend was caused by the gage malfunction since the trend was confirmed by the manual determinations and there was no pH gage in WM-1.

The WM-2 gage behaved erratically during cool down. The cyclic readings between J-Day = 123 to 130 suggested the presence of water even though none was collected on several attempts. Examination of the cavity temperature curves, which had previously exhibited cyclic behavior associated with water level variation, showed only smoothly decreasing values. Consequently, the erratic pH readings appear to be meaningless.

Selected water samples were chemically analyzed to determine what changes, if any, occurred in various ion concentrations during the course of the experiment. Analyses included flame atomic absorption, induction coupled plasma emission spectroscopy, semiquantitative spark emission spectroscopy, and ion chromatography. The study included blind duplicates (unknown to the analyst), and a number of samples were analyzed at Los Alamos National Laboratory to check accuracy and precision. We were particularly interested to see if ion concentrations would decrease in the heater hole samples, which, if they did, would provide support for the notion of water transport by vapor diffusion.

The results for representative ions are shown in Figures 40 through 42 and Table 8. The vertical arrow bar located at J-Day = 65 in each of the figures represents the range in values determined for Camp 12 water (obtained from Well #8 and used during drilling the experiment holes) and a natural seep

TABLE 8

Anion Concentrations at Different Times in  
Water Samples from HH-1, WM-1, WM-2 and Well #8

<u>Sample #</u>	<u>J-Day</u>	<u>F</u> <u>ppm</u>	<u>Cl-</u> <u>ppm</u>	<u>PO<sub>4</sub><sup>3-</sup></u> <u>ppm</u>
HH-1				
HH-3	37.05	1.5	2.1	
HH-12	38.2	1.9	1.2	
HH-19	39.23	0.3	ND	
HH-136	80.4	0.1	0.9	ND
HH-158	98.36	0.3	0.6	ND
WM-1				
WM-129	73.4	2.7	1.4	4.1
WM-160	99.36	0.8	5.6	
WM-2				
WM-28	38.4	9.2	10	15
WM-124	70.4	2.1	8.4	4.6
WM-161	99.38	1.8	5.0	
WELL #8	1.5	8.3	2.5	

occurring in G-tunnel near the in situ experiment. The figures illustrate a noticeable contrast in the time-dependent ion concentrations between the heater hole and the water migration holes. In most cases, the ion concentration in the heater hole water samples decreased, initially followed by a gradual increase, though not above the original values, toward the end of the experiment. The late-time concentration increase could be due to increased reaction rates and solubilities caused by higher temperatures in the condensed water pool, or longer residence time caused by the slower generation rate in the collection cavity. In any case, the effect was generally minor. The overall behavior was completely consistent with water mass transport by vapor diffusion followed by condensation in the cooler transport by vapor diffusion followed by condensation in the cooler regions of the cavity.

The ion concentrations in the water migration holes generally increased initially with time and then gradually decreased, or they remained relatively unchanged throughout the experiment. Initially increasing ion concentration is qualitatively consistent with the increasing temperature in the holes. The decreasing concentrations at later times could be due to depletion of the easily reactable surface ions in the rock adjacent to the cavity. The ion concentration profiles in the water migration holes indicate that water transport is by simple liquid water flow as discussed in the previous section.

#### IV. D. Stress Behavior

Upon emplacement, the stressmeters were prestressed to anchor them in place. They were designed and fielded to measure the thermally induced stresses and do not include pre-existing in situ stresses. The responses of the three stressmeters are shown in Figure 43. The duplicate horizontal stressmeters, SE-7 and SE-28 (Ch#90 and 89), began to measure a stress increase as soon as the heater was turned on. Their response was virtually identical until about 7 days into the experiment when the readings from SE7 began to decline. After approximately 16 days of steady decline, the meter output reversed again and increased steadily during the last 40 days of heater operation.

The other horizontal meter, SE-28, appeared to perform best, increasing continuously to a maximum stress of 8.27 MPa. Then the readings decreased slowly to 7.93 MPa over a 24-day period after which, in 7 days, they increased to about 8.62 MPa at heater turn-off. At the time of heater turn-off, the horizontal meters differed by only 1.38 MPa after, at one time, differing by more than 2.76 MPa.

The meter measuring the vertical (circumferential) stress, SE-13 (Ch#91), appeared to operate properly until the last 10 days of the experiment when the readings dropped nearly 1.38 MPa. The maximum stress measured by the meter was approximately 4.83 MPa.

All the meters' behavior during cool down appeared normal. Each of the meters' readings declined to values below its pre-stressed level indicating that either the platens had adjusted their seating on the borehole wall, or that the rock mass underwent a negative hysteresis during cooling. Note that laboratory studies of the unconfined thermal expansion of this rock matrix do not observe such behavior while the confined thermal expansion does show a negative hysteresis,<sup>16</sup> and the response for the complex highly fractured rock mass remains unknown.

The declines in readings during heater operation may be due to creep relaxation under the meter platens or to slight adjustments in the blocks making up the rock mass between the meter and the heater. Speculation on the subsequent increases in some readings is not as easy. However, assuming that the gage was calibrated correctly and operated properly, increases should, in virtually all cases, be related to true rock-mass responses.

No corrections were made for thermal effects on the stress gages. Note, however, that for the last 46 days of heated operation the temperature in the stress hole increased only 8°C, from 40 to 48°C at heater turn-off, in a nearly linear fashion corresponding to an average increase of about 0.17°C per day. It seems very unlikely that any of the observed variations in the data are due to thermal effects on the gage.

An interesting observation is that both the maximum horizontal and circumferential stresses were approximately 40% of those predicted during the pretest modeling.<sup>1</sup> The pretest calculations relied on linear thermo-elastic models using constant, matrix material properties. The discrepancy is

apparently due to the nonlinear, nonelastic, complex rock-mass properties caused, in part, by the presence of joints, which play an important role in the thermomechanical response. To date, we have not attempted to improve on the pretest calculations for two reasons. First, in spite of the large amount of field work that has been carried out and is presently ongoing, it is still difficult to adequately describe the rock mass properties, or even the appropriate geologic properties such as fracture orientation, frequency, extent, aperture, etc. Second, sufficiently complex models do not exist.

#### IV. E. Laser Interferometer

The response of the laser interferometer intended to measure rock displacement is shown in Figure 44. For the most part, the data is uninterpretable and is probably meaningless. It was apparent even during the pretest background determinations that the interferometer data was likely to be marginal at best. Problems with the electronic fringe counter skipping counts were noted early in the experiment and a second counter was added for comparison during J-Day = 49. The variation in the two readings soon became apparent. By heater turn-off, the readings differed by as much as  $25\mu$ , a rather minor discrepancy considering some of the fluctuations in the data. By the end of data acquisition, readings differed by more than  $150\mu$ .

From time to time, the system would appear to settle down and record, on the average, reasonable appearing data such as between J-Day = 39 and 44, or 51 and 67, only to follow it with periods of wild, unexplainable readings. We found out early in the experiment that the response would be affected by seemingly minor changes in the alcove (laser) ambient environment when a small change in the angle of the ventilation pipe caused the sharp spike just at the end of J-Day = 37. Returning the pipe to its original position brought readings back down to their original values. The response was still baffling, however, because no change in the ambient conditions could be detected. For instance, all the temperatures remained unperturbed. We also found that leaning against the drift rib within a meter of the laser could cause a fluctuation of a few microns.

Posttest evaluation of the laser focused on temperature effects and long-term stability of the laser, both of which resulted in dead ends. A final, low priority study to see if the saturated rock changed dimension during isothermal drying at room temperature may have provided the best answer. Mirrors were attached to each end of a saturated, 10-cm-long piece of core from the experimental area. The core was placed in a laboratory interferometer set to monitor potential distortions upon drying. The response was so rapid that no data could be recorded. Within a few minutes, the mirrors were completely out of alignment. The interferometer would tolerate many minutes of mirror rotation and still it was not enough. Attempts to reorient the sample failed because the response was completely nonuniform from one run to another. These results (or lack of them) suggest that part of the problem with the in situ experiment may be that the laser was mounted in the drift wall. The continuous drying of the rock wall and its heterogeneous dimensional variation may have been continuously altering the interferometer characteristic length. That would also explain why a change in the ventilation pattern could cause an apparent displacement without affecting the temperature.

#### IV. F. Permeability Measurements

Fluid-flow measurements were performed both pre and posttest in most of the experimental holes in an effort to characterize the "permeability." A hydrofracture pump machine was used to inject water into the hole.

Packer locations in each hole were selected, when appropriate, to match the corresponding location of the heater test packer. Pre and posttest locations were generally the same. In the heater hole, injection was performed beyond a packer located at 19.2, 18.1, and 17.0 m. In the posttest studies, the packer was placed at 16.3 instead of 17.0 m. Injections into WM-1, 2, and 3 were done at TD minus 48.3 cm. Packer inflation pressures were 1.4 MPa, and in general, fluid injection pressures were maintained at 690 KPa until the injection flow approached an asymptotic value, after which flow was shut off. Clean water was used, and injection pressure, injection flow, shut-in pressure, discharge flow, and time were measured. Data from the posttest studies were recorded at 5-sec intervals using the DAS. The DAS was not available for the pretest measurements. Pretest data, i.e., before heater turn-on, was recorded manually and on magnetic tape. However, an incorrectly wound tape (new from the vendor) prevented tape data from being available from much of the pretest series.

During the pretest measurements, we attempted to measure both hole-to-hole as well as single-hole parameters. In discharge holes, packers with drain pipes were set in the hope of collecting water from the discharge holes. In many cases, no discharge water was collected. When water was collected, the results always provided values for the permeability which were significantly smaller than single-hole values. Thus, because of water loss through fractures, the two-hole technique only gives a lower bound.

We assumed Darcy flow through a homogeneous, porous, medium for this analysis. We knew this to be a poor assumption because the rock in the vicinity of the heater array was highly fractured while the matrix permeability was low. Consequently, at best, the data and analysis provide an "effective" permeability or conductivity for the given location. Permeabilities were determined by three methods: 1) from the slope of the inverse flow rate vs logtime curve, 2) a numerical fit to the flow rate data, and 3) from the slope of the shut-in pressure decay vs log-time curve. In general, the data was marginal due to the pulsing nature of the pressure and flow rate caused by the injection pump and the short shut-in times.

Shut-in pressure decay data for posttest injection into WM-1 is shown in Figure 45. This is about the best data available from the whole series of fluid flow measurements. WM-1 was the tightest hole and thus the shut-in time is much longer than for any other case. This data is also the closest to meeting the criteria for Darcy flow.

Data in HH-1 at 16.3 m can be compared with pretest data at 17.0 m even though the depth difference may result in inclusion of different fractures. This is true because even though the posttest packer location was further from the end of the hole, the flow at similar pressures is less than for pretest. This is shown in the data in Table 9.

TABLE 9

Comparison of Pre and Posttest Water Injection  
Flow Rates in HH-1

<u>Pretest HH-1 (17.0 m)</u>		<u>Posttest HH-1 (16.3 m)</u>	
<u>P(KPa)</u>	<u>Q(L/sec)</u>	<u>P(KPa)</u>	<u>Q(L/sec)</u>
710	.161	738	.102
723	.161	703	.102
690	.139	758	.110
669	.129		
731	.11		
703	.110		
690	.11		

Posttest data for the heater and water migration holes are listed in Table 10 with the results of the pretest measurements included for comparison. The actual values for the permeabilities are probably not meaningful, but comparison of values in individual holes provides information about the behavior of the fractures after heating. The data show that the effective permeability in all the water migration holes increases in the posttest measurements by a factor of 10 or more over the pretest values. The effective permeability in the heater hole decreased by about 1/2 relative to pretest values. We do not believe, however, that these changes affected the water behavior in the experiment. We never observed any changes in the water generation rate that could be related to the fracture controlled permeability.

The permeability data is particularly interesting when compared to the stress behavior discussed above. The negative hysteresis observed in the stress fields during cool down suggests that in situ fractures could open beyond the preheated values resulting in increased permeability. These results seem to bear that out although considerable additional studies with improved equipment should be carried out.

#### V. CONCLUSIONS

With regard to stimulating water migration, the in situ experiment must be considered an unqualified success. The experiment showed that in a nearly

TABLE 10

Comparison of Pre and Posttest Permeabilities (k)  
in HH-1 and WM-1, 2, and 3

Test	Inject. Hole	<sup>k</sup> Packer Depth (m)	<sup>k</sup> Inject. Flow (/sec)	<sup>k</sup> Inject. Press (KPa)	[1/q] (md)	<sup>k</sup> [check] (md)	[shut-in] (md)	<sup>k</sup> k (md)	Pretest (md)
1	HH-1	18.14	.043	648	16.5	48	24.1	45	75
2	HH-1	16.31	.102	738	248	42	43	42	
3	HH-1	16.31	.102	703	104	45	42.7	45	80
4	HH-1	16.31	.110	758	96.5	45	46.2	45	
5	WM-1	18.64	.011	786	24.4	24	14.5	15	
6	WM-1	18.64	.008	752	8.3	20	10.8	12	0.5
7	WM-1	18.64	.007	710	46.3	20	11.0	15	
8	WM-2	18.49	.008	703	10.2	20	15.1	18	
9	WM-2	18.49	.013	676	50	37	21.5	30	~10
10	WM-2	18.49	.013	717	35.6	35.6	11.1	30	
11	WM-3	18.34	.057	758	190	167	194	170	~15

All values for k ~ ±50%

saturated, porous welded tuff above the water table, water movement is highly dependent on the thermal field and is potentially significant. Preliminary modeling strongly suggests that the mass transport into the heater hole was by a vapor diffusion/condensation mechanism although the details of that process are far from fully understood. The results of the chemical analysis of the water samples recovered from the experiment holes, the relative humidity measurements in the heater hole, and the in situ pH measurements are all consistent with a vapor diffusion/condensation process into the heater hole. The results also suggest, but not as strongly, that mass transport into the water migration holes is by simple Darcy flow of water.

We found that the manner in which the water mass transport is treated in the thermal codes can have a reasonable impact on the calculated temperature profiles.

We should point out that the configuration of the experiment was ideal for encouraging vapor diffusion/condensation processes in that the holes were inclined upward so that the water would run away from the heater into cooler regions and that an air-filled annulus existed between the heater and the rock wall. This type of experiment should be run again in a vertical orientation followed by an identical experiment with the annulus backfilled. In fact, these experiments are currently underway.

The stress measurements indicated a negative hysteresis in thermal expansion. Such behavior had not been observed for this rock in unconfined laboratory measurements. It has only been relatively recently that this effect was observed in laboratory measurements on confined samples, which now makes the laboratory and in situ results consistent with each other. The effect may cause a slight increase in fracture aperture during cooling resulting in an increase in permeability. The pre and posttest permeability results qualitatively support that notion.

Finally, most of the instrumentation performed satisfactorily. We did not lose a single thermocouple, and at least a portion, in most cases a large portion, of all the other instruments worked at one time or another except the laser interferometer, which was a failure. Of the developmental instruments, the stressmeters and the water depth gages worked very well. Although not strictly an instrument, the packers worked very well also.

## REFERENCES

1. J. K. Johnstone, "In Situ Tuff Water Migration/Heater Experiment: Experimental Plan," SAND79-1276 (Albuquerque, NM: Sandia National Laboratories, August 1980).
2. B. M. Bulmer, "Pretest Thermal Analysis of the Tuff Water Migration In-Situ Heater Experiment," SAND79-1278 (Albuquerque, NM: Sandia National Laboratories, February 1980).
3. C. O. Duimstra, "In Situ Tuff Water Migration/Heater Experiment: Hardware Mechanical Design Definition," SAND81-1048 (Albuquerque, NM: Sandia National Laboratories, November 1981).
4. D. R. Waymire and C. O. Duimstra, "In Situ Tuff Water Migration/Heater Experiment: Instrumentation Design and Fielding," SAND81-1058 (Albuquerque, NM: Sandia National Laboratories, April 1982).
5. D. R. Waymire and C. O. Duimstra, "In Situ Tuff Water Migration/Heater Experiment: The Data Acquisition and Playback System," SAND81-1059 (Albuquerque, NM: Sandia National Laboratories, October 1981).
6. R. R. Eaton, J. K. Johnstone, J. W. Nunziato, and C. M. Korbin, "In Situ Tuff Water Migration/Heater Experiment: Posttest Thermal Analysis," SAND81-0912 (Albuquerque, NM: Sandia National Laboratories, October 1983).
7. L. D. Ramspott and L. B. Ballou, "Experimental Design for the First Heater Test at the Climax Stock, Nevada Test Site, Appendix A in NTS Terminal Waste Storage Program Plan for FY 1978," (Las Vegas, NM: U.S. Department of Energy, March 1978).
8. J. L. Krumhansl, "Final Report: Conasauga Near-Surface Heater Experiment," SAND79-1855 (Albuquerque, NM: Sandia National Laboratories, November 1979).
9. A. R. Lappin, R. K. Thomas, and D. F. McVey, "Eleana Near-Surface Heater Experiment Final Report," SAND80-2137 (Albuquerque, NM: Sandia National Laboratories, April 1981).
10. Memo from D. F. McVey to D. R. Waymire, SNL, "Allowable Gap Between Heater and Bore Hole for NTS Tuff Experiment," November 21, 1978.
11. D. K. Garling, "COYOTE, A Finite Element Computer Program for Nonlinear Heat Conduction Problems," SAND77-1332 (Albuquerque, NM: Sandia National Laboratories, June 1978).
12. G. R. Hadley and J. R. E. Turner, Jr., "Evaporative Water Loss From Welded Tuff," SAND80-0201 (Albuquerque, NM: Sandia National Laboratories, April 1980).

REFERENCES (Continued)

13. G. R. Hadley, "Theoretical Treatment of Evaporation Front Drying," Intl. J. Heat Mass Transfer, 25, pp 1511-1522 (1982).
14. D. C. Reda, G. R. Hadley, and J. E. R. Turner, "Application of the Gamma-Beam Attenuation Technique to the Measurement of Liquid Saturation of Two-Phase Flows in Porous Media," SAND80-2433(C), Presented at the 27th International Instrumentation Symposium, Instrument Society of America, Indianapolis, IN, April 27-30, 1981.
15. D. C. Reda and R. R. Eaton, "Definition of a Facility for Experimental Studies of Two-Phase Flows and Heat Transfer in Porous Materials," SAND80-2634(C), Presented at the 20th ASME/AICHE National Heat Transfer Conference, Milwaukee, WI, August 2-5, 1981.
16. A. R. Lappin, Private Communication.

**Appendix**  
**Supporting Graphics**

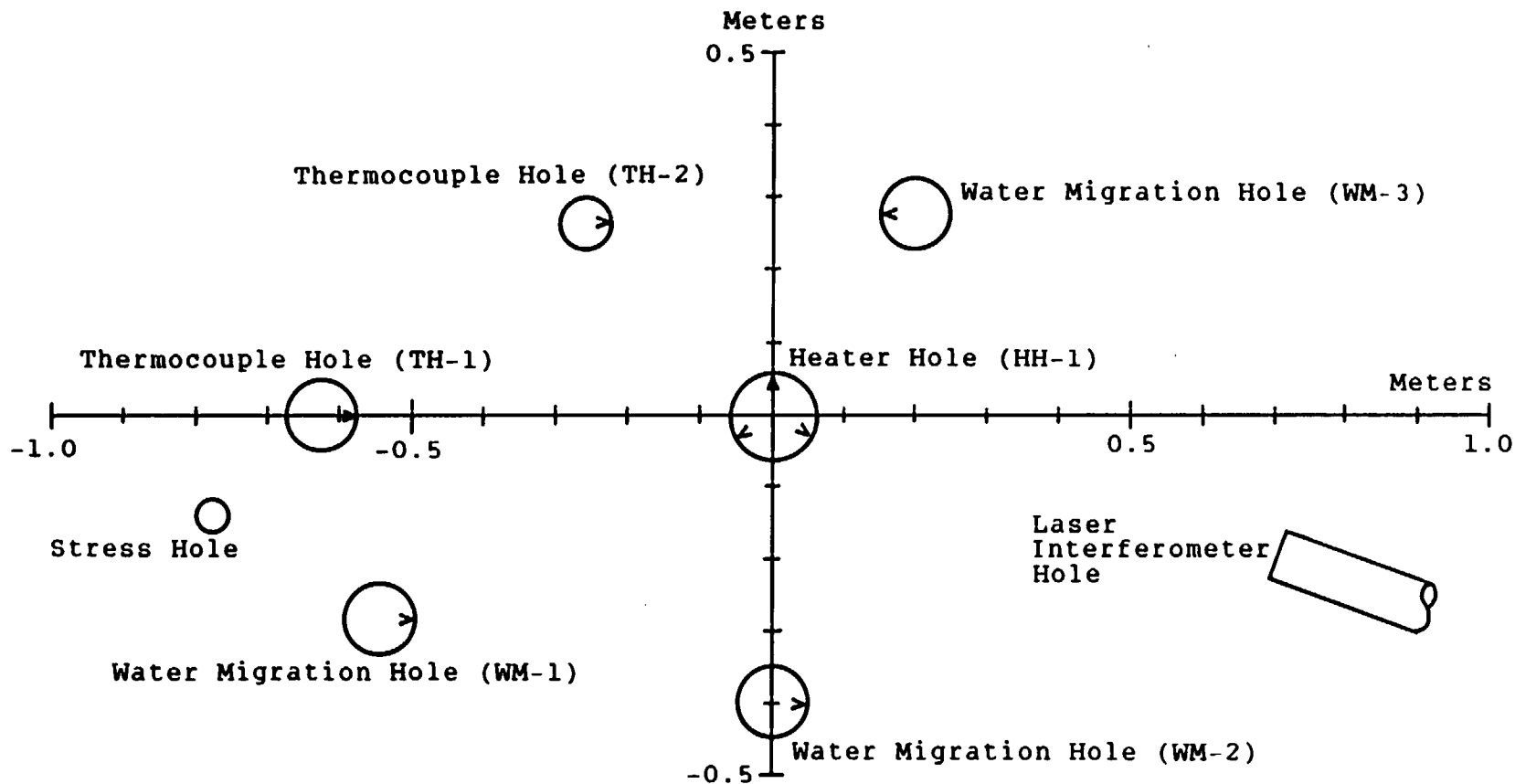


Figure 1. Position of the experimental holes at the depth of the heater midplane. The carat (<) in a hole marks the location of the rock wall thermocouple nearest the heater hole.

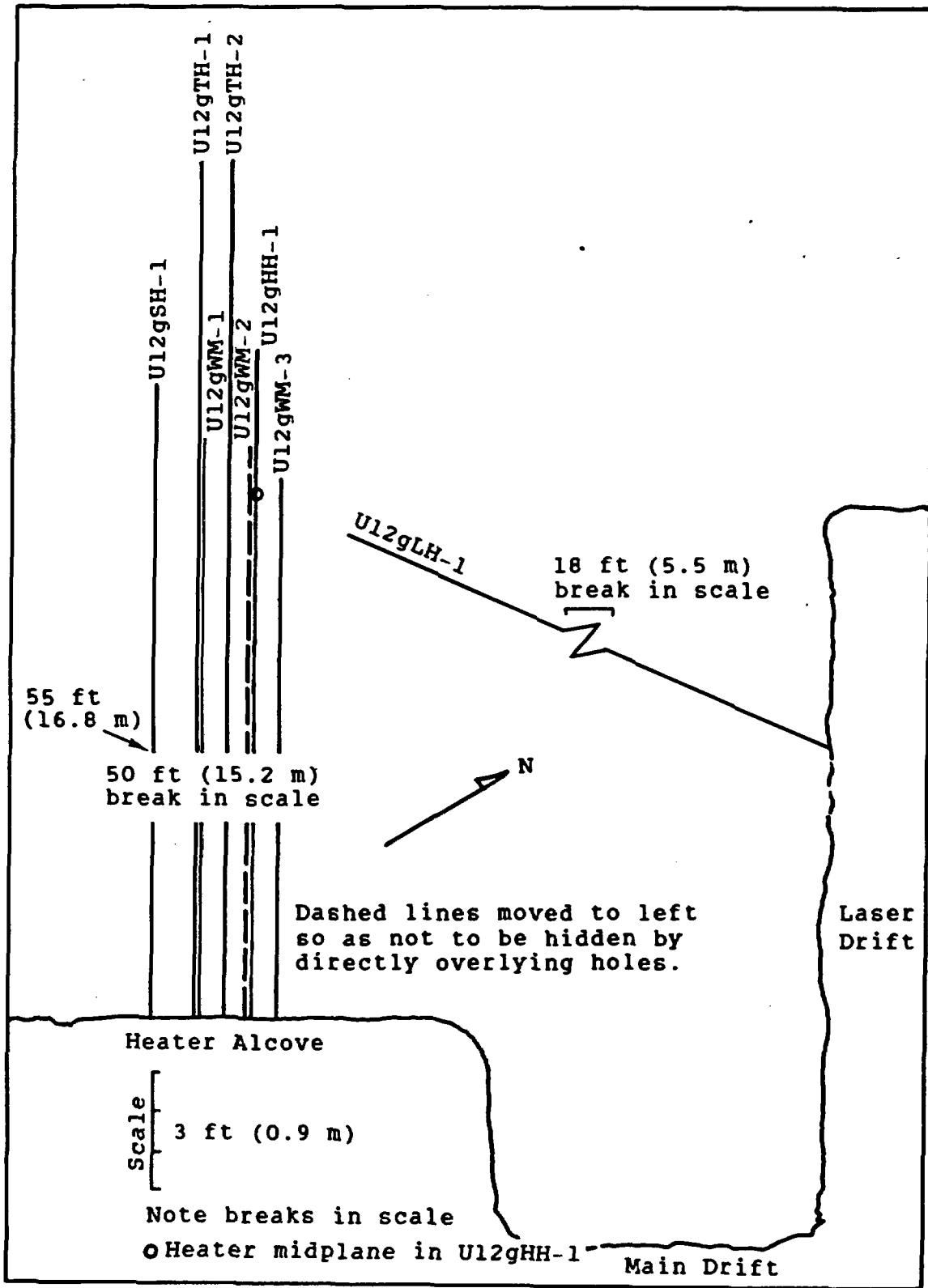


Figure 2. Plan view of the experimental hole layout.

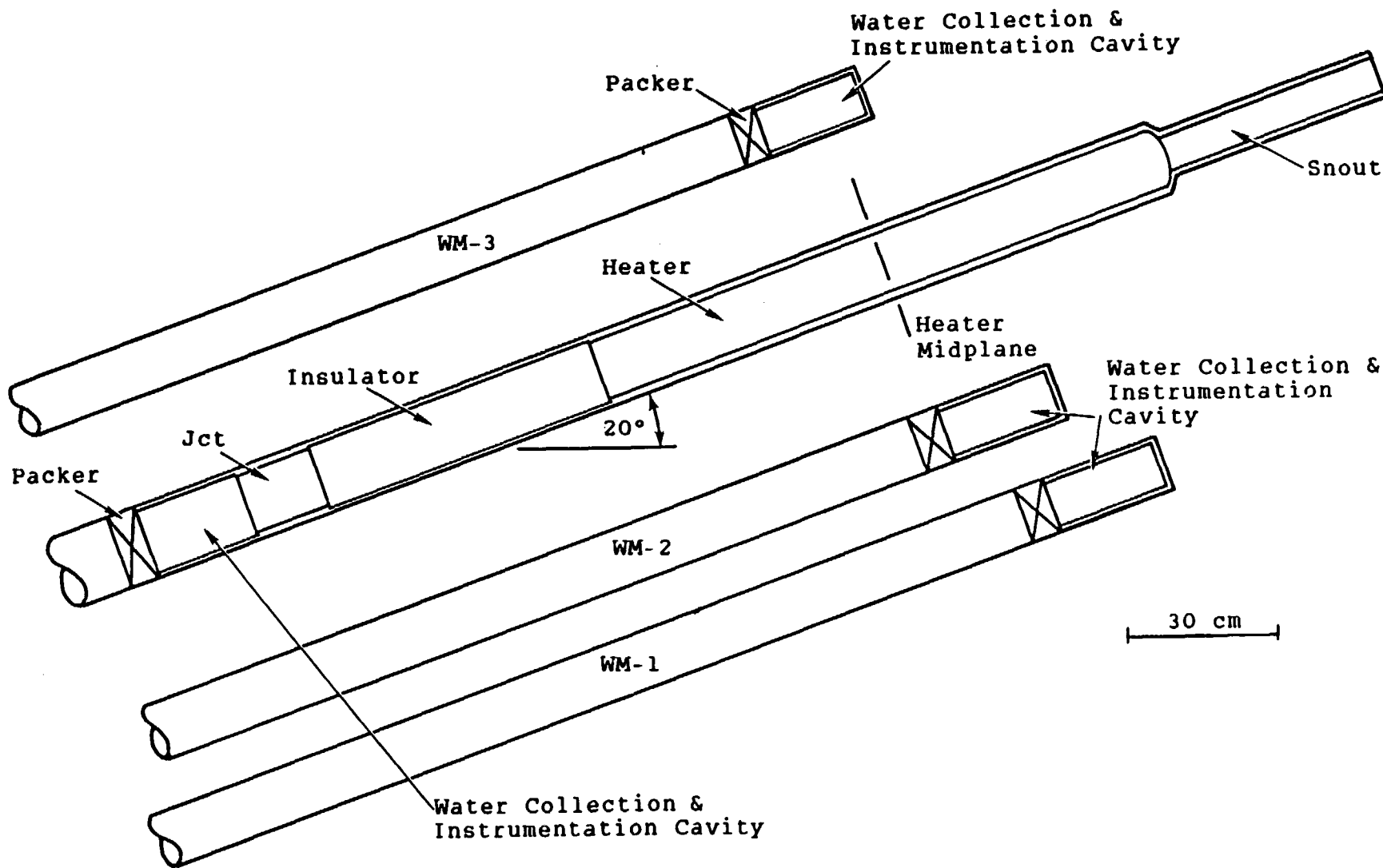


Figure 3. Scale drawing showing the relation of the water collection and instrumentation cavities in the water migration holes to the heater. For this illustration, the water migration holes were rotated into a plane while maintaining the spacing relative to the heater hole.

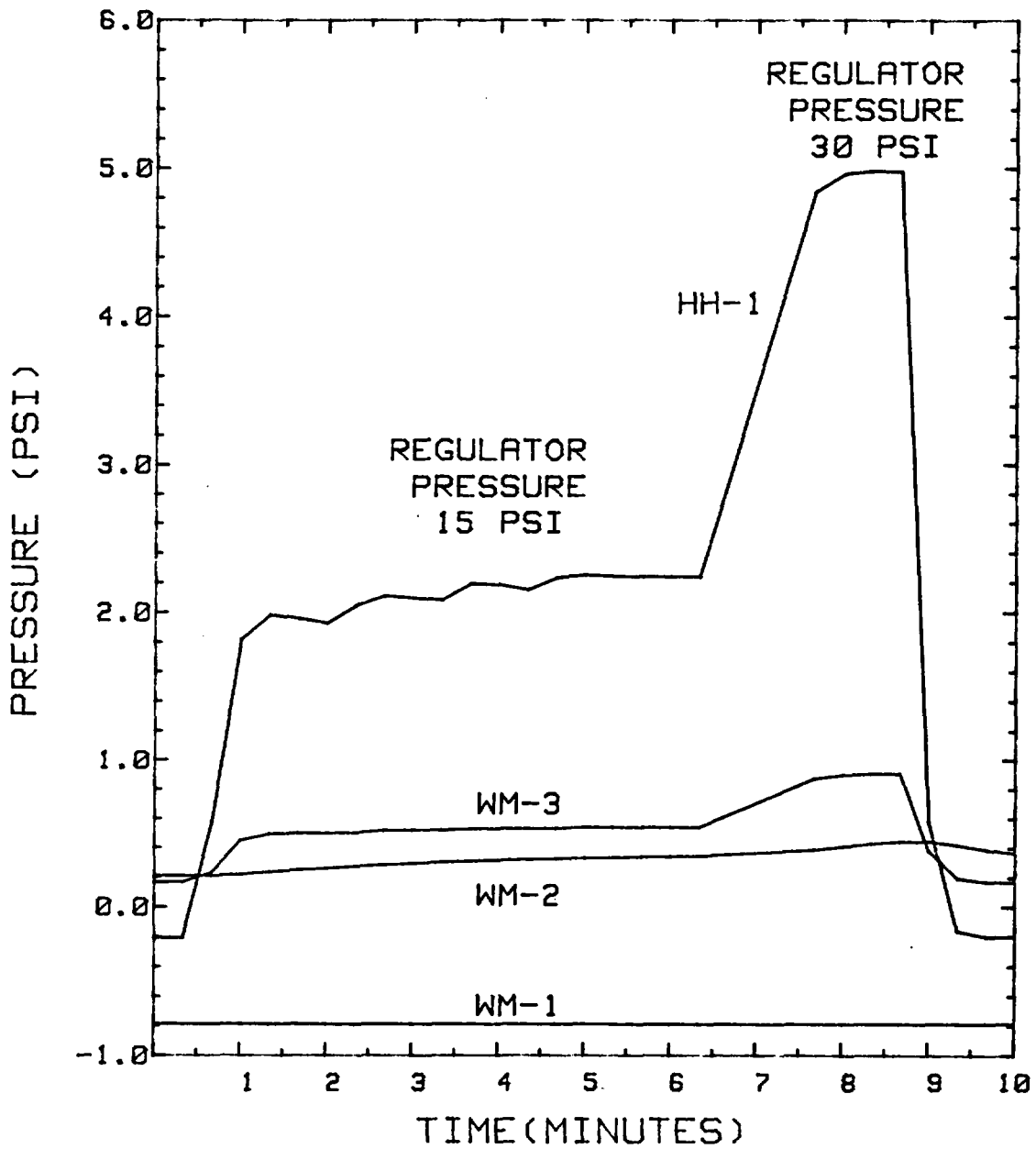


Figure 4. Gas pressurization test carried out in HH-1 during the pretest checkout; test began at 15 psi regulator and went to 30 psi.

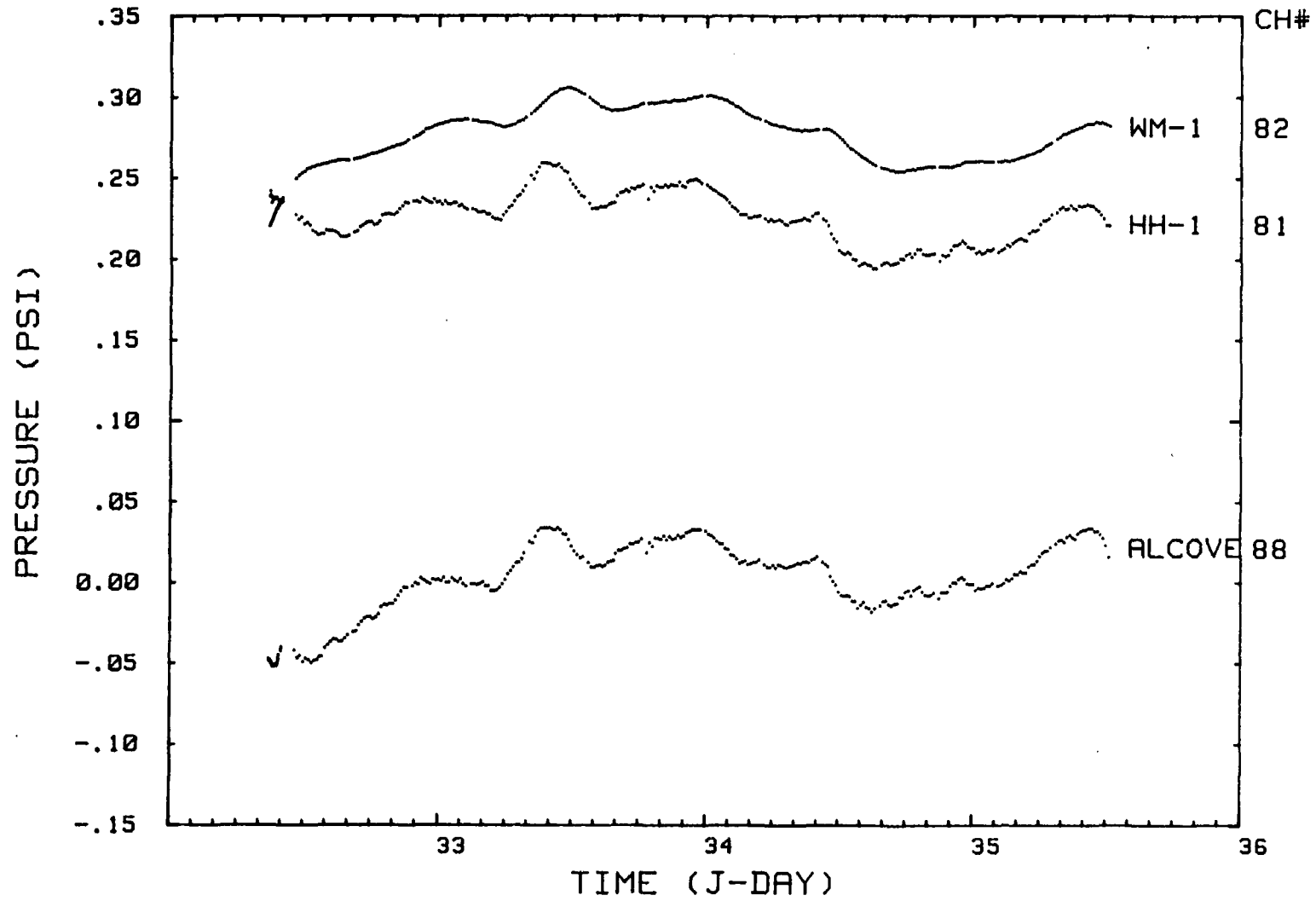


Figure 5. Comparison of the background pressure variations in HH-1, WM-1 and the alcove.

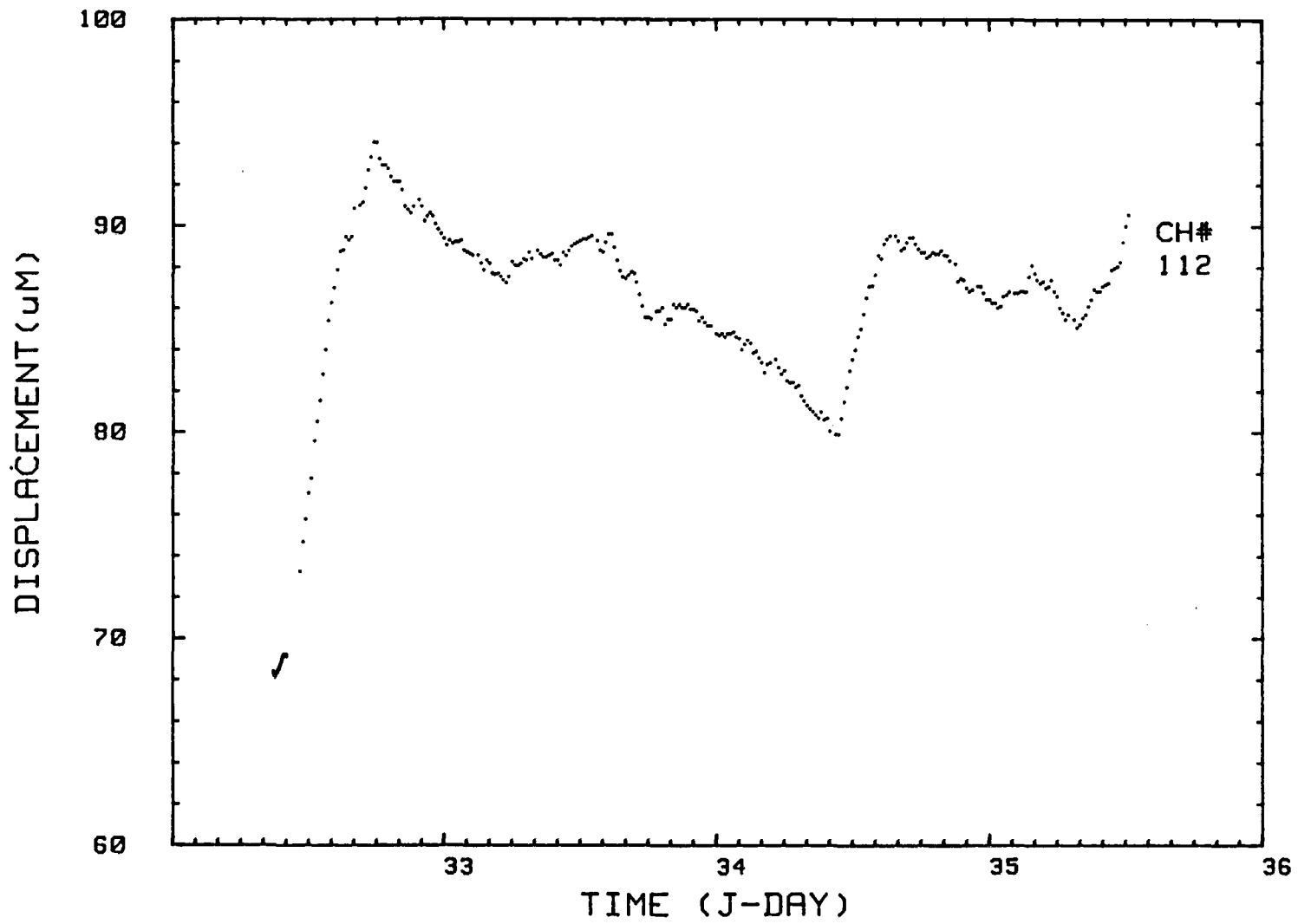


Figure 6. Example of the cyclic displacement measured by the laser interferometer before heater turn-on.

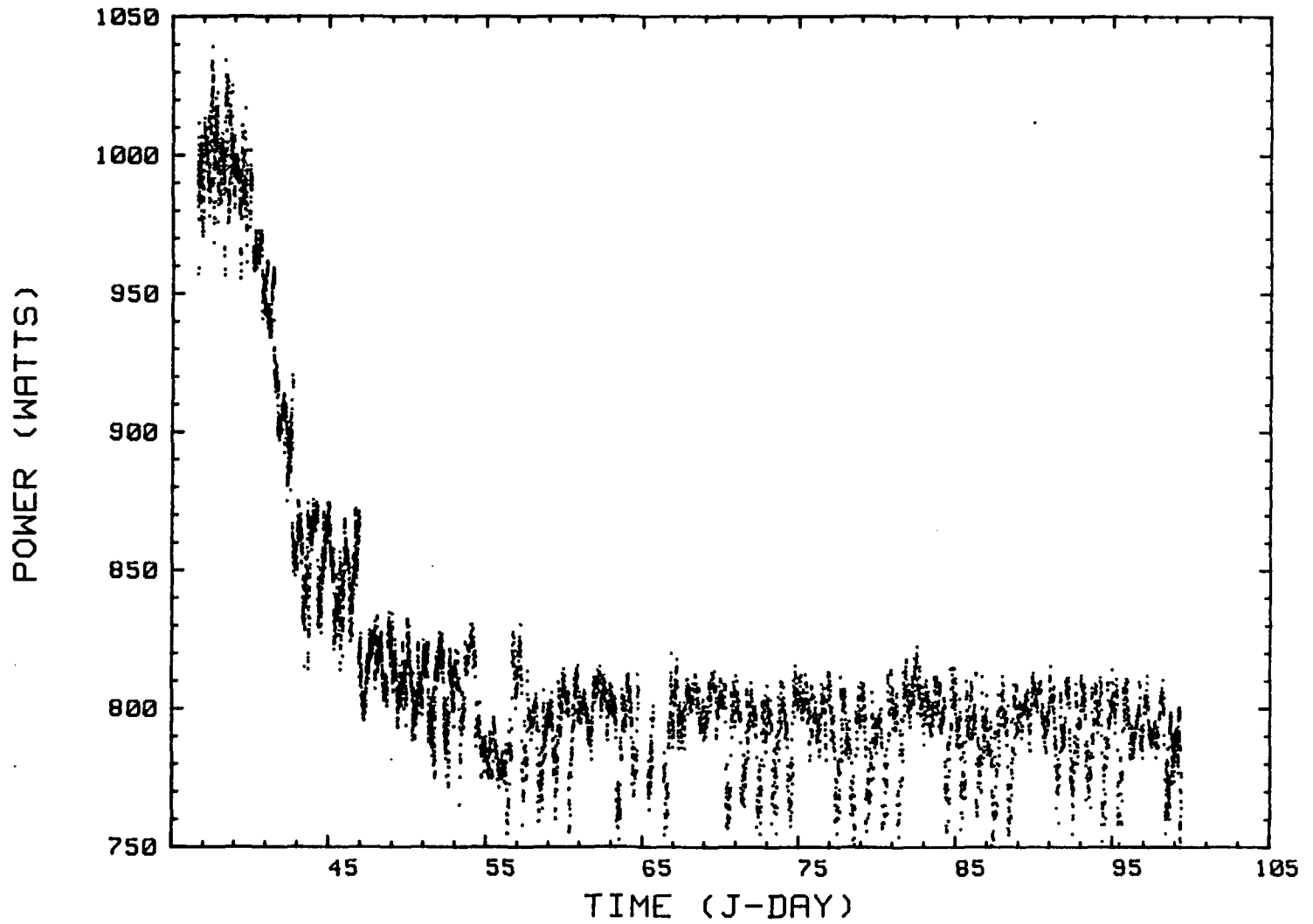


Figure 7. Heater power output as a function of time.

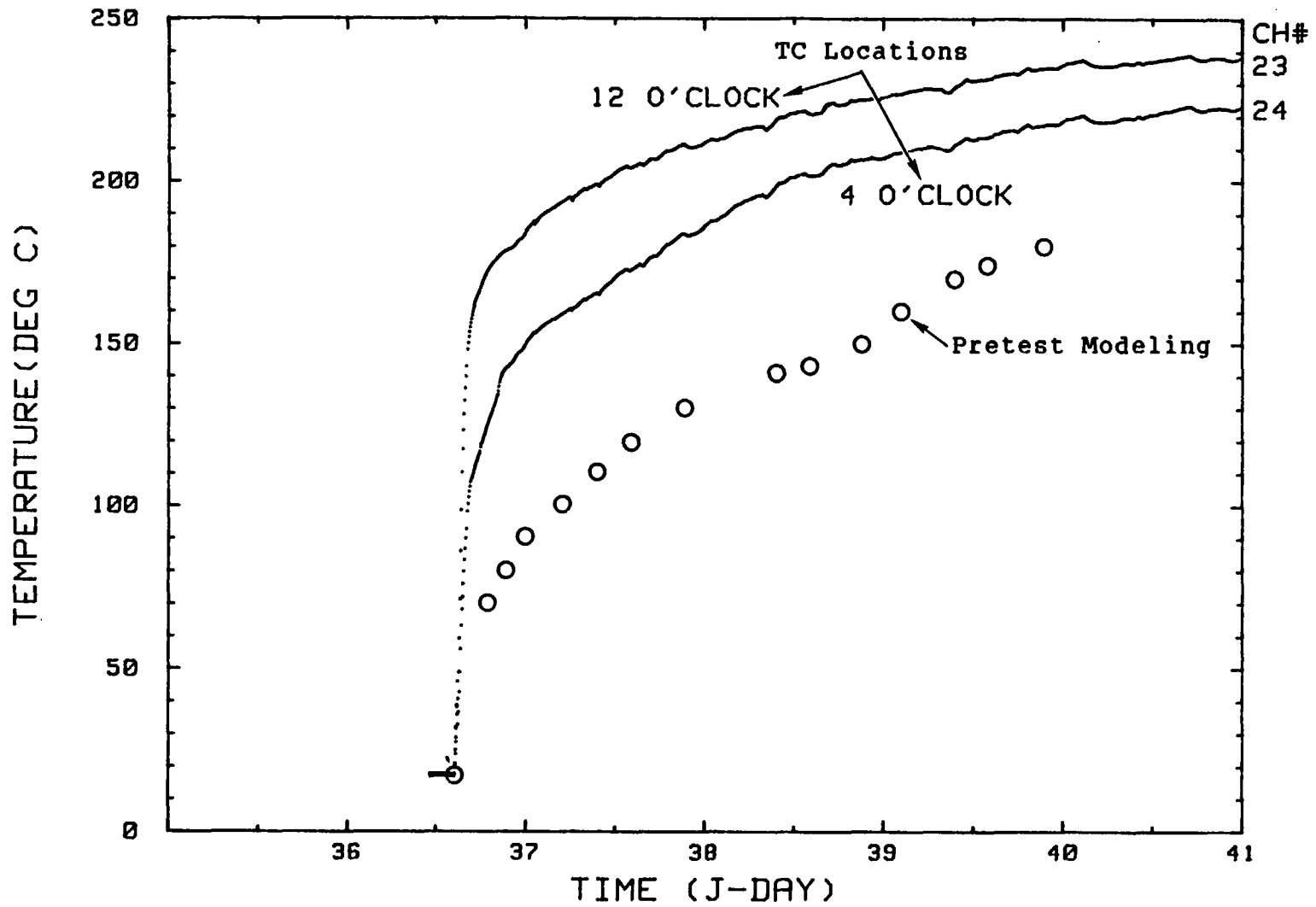


Figure 8. Comparison of rock wall temperatures with those predicted from pretest modeling. Rock wall thermocouples shown were located at 12 o'clock (vertical) and 4 o'clock positions.

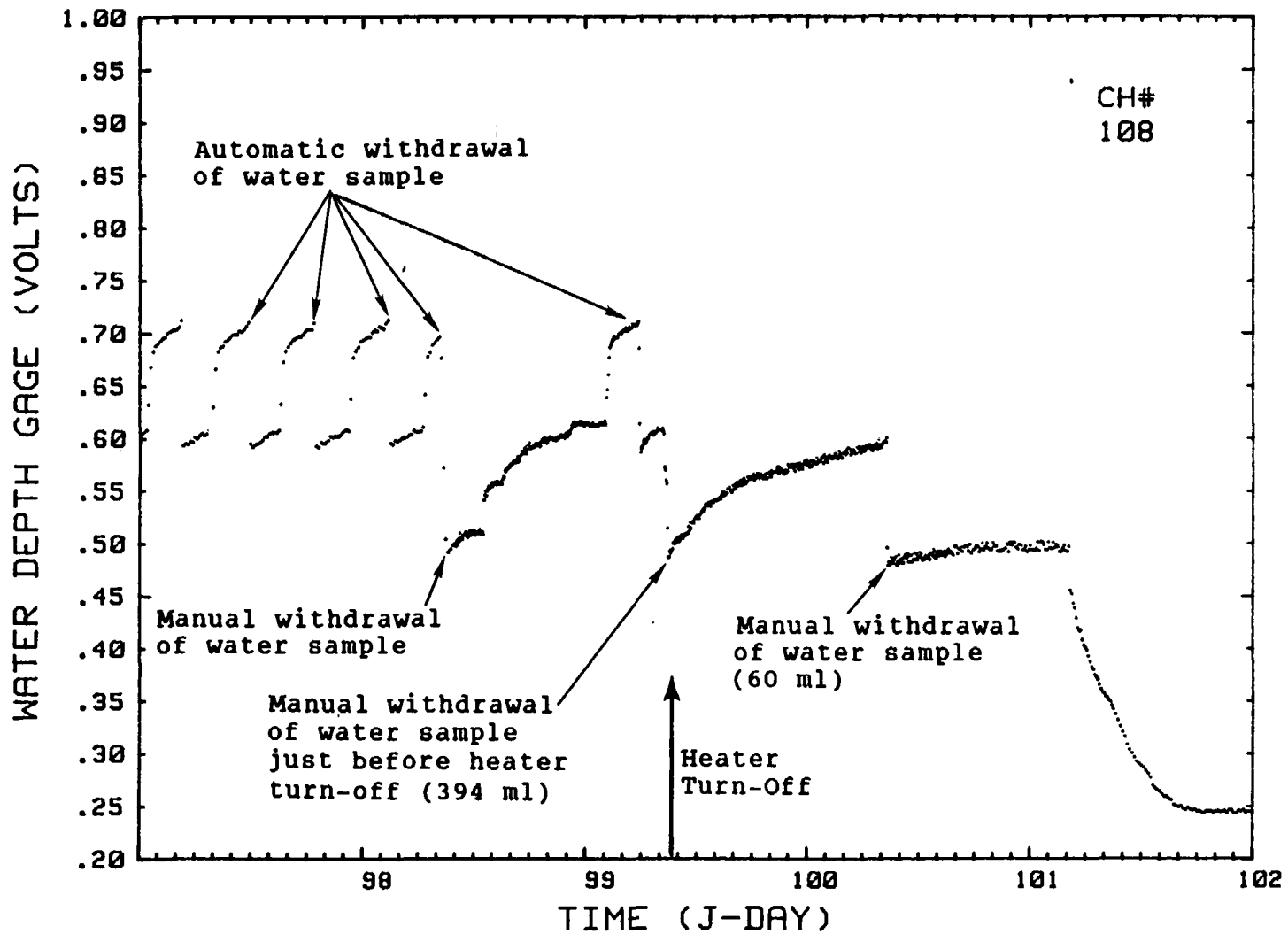


Figure 11. Water depth gage readings in HH-1 during the period of heater turn-off.

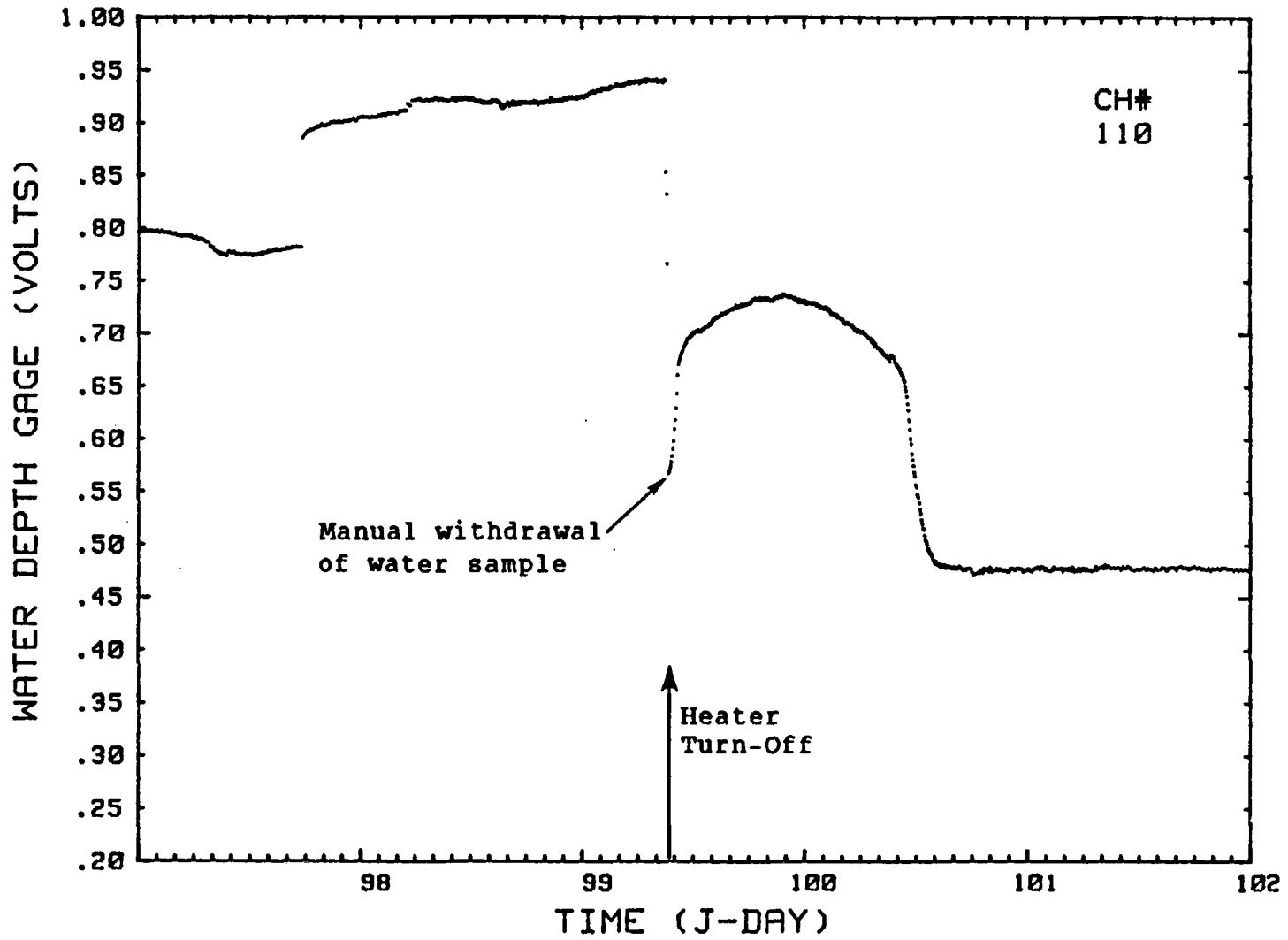


Figure 12. Water depth gage readings in WM-2 during the period of heater turn-off.

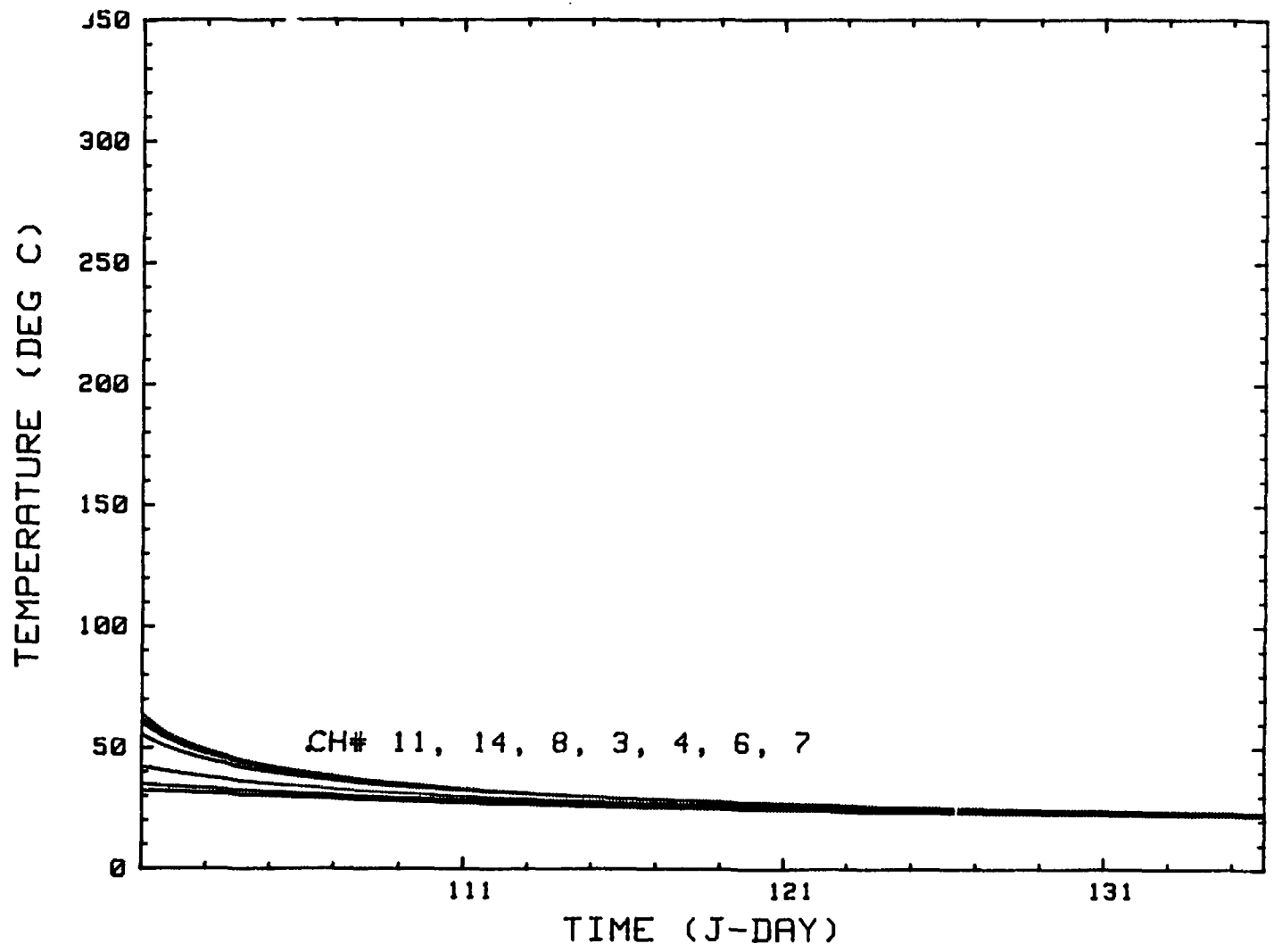


Figure 13 (Continued). Temperature profiles in the heater/instrument packer/ assembly. Heater skin temperature ~ 2 o'clock position; Near-end-Ch#8, Midplane-Ch#11, Far-end-Ch#14. Insulator section; Near-end-Ch#4, Far-end-Ch#3. Water collection cavity; Air-Ch#6, Water-Ch#7.

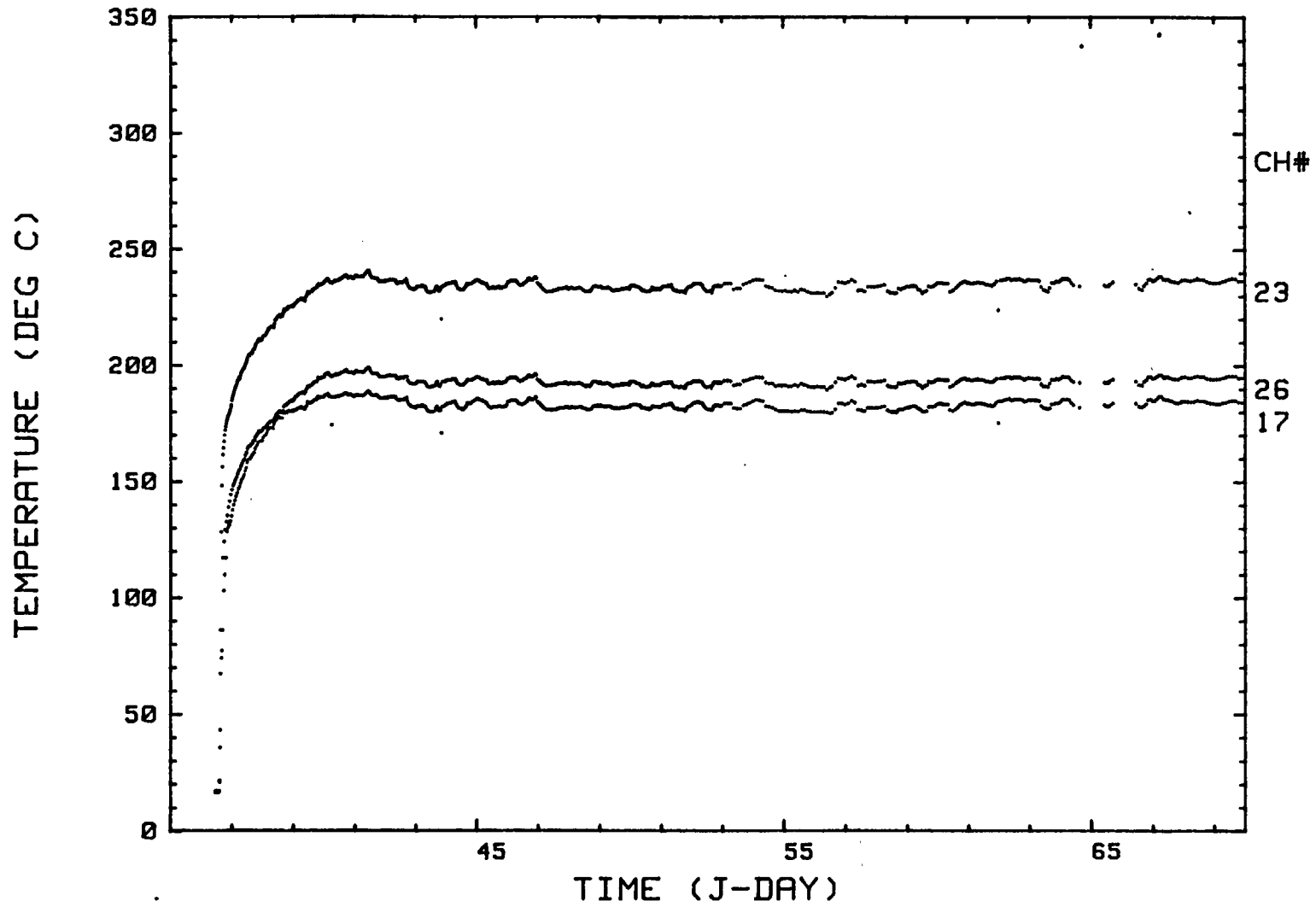


Figure 14. Rock wall temperature profiles opposite the heater - 12 o'clock position. Near-end-Ch#17, Midplane-Ch#23, Far-end-Ch#26.

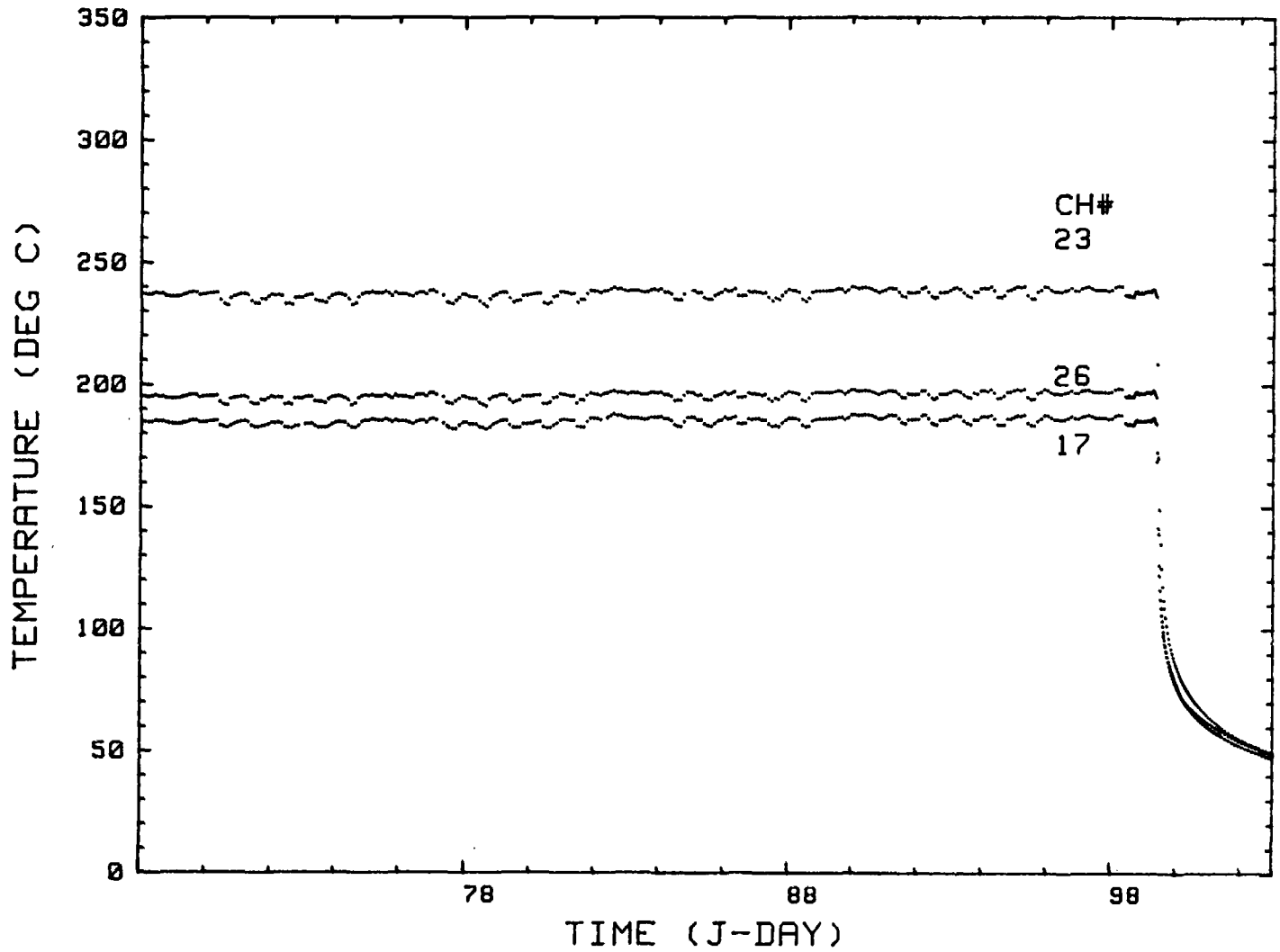


Figure 14 (Continued). Rock wall temperature profiles opposite the heater - 12 o'clock position. Near-end-Ch#17, Midplane-Ch#23, Far-end-Ch#26.

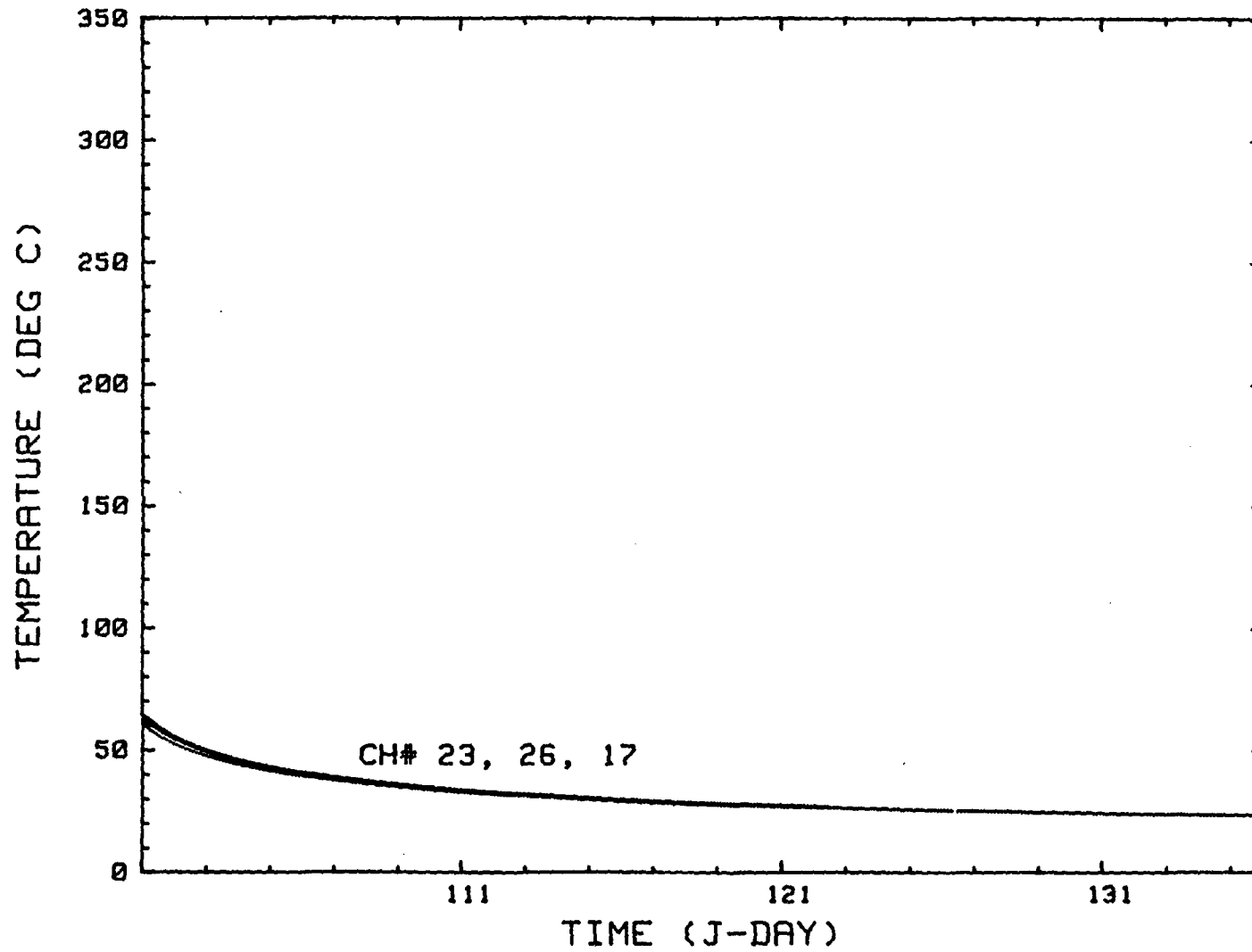


Figure 14 (Continued). Rock wall temperature profiles opposite the heater - 12 o'clock position. Near-end-Ch#17, Midplane-Ch#23, Far-end-Ch#26.

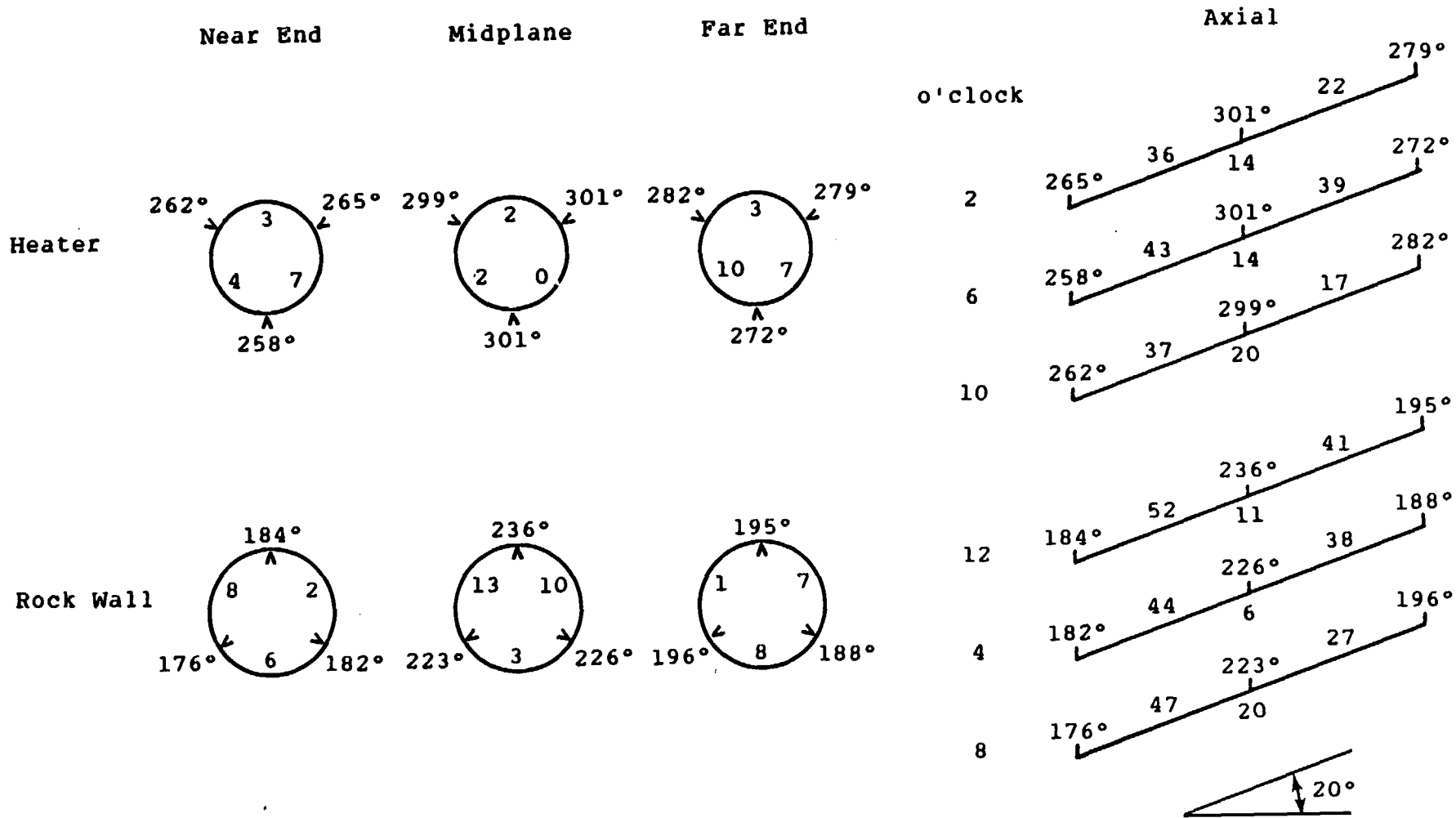


Figure 15. Comparison of the circumferential and axial heater skin and rock wall temperatures just before heater turn-off. All temperatures in °C. Numbers inside circles are temperature differences.

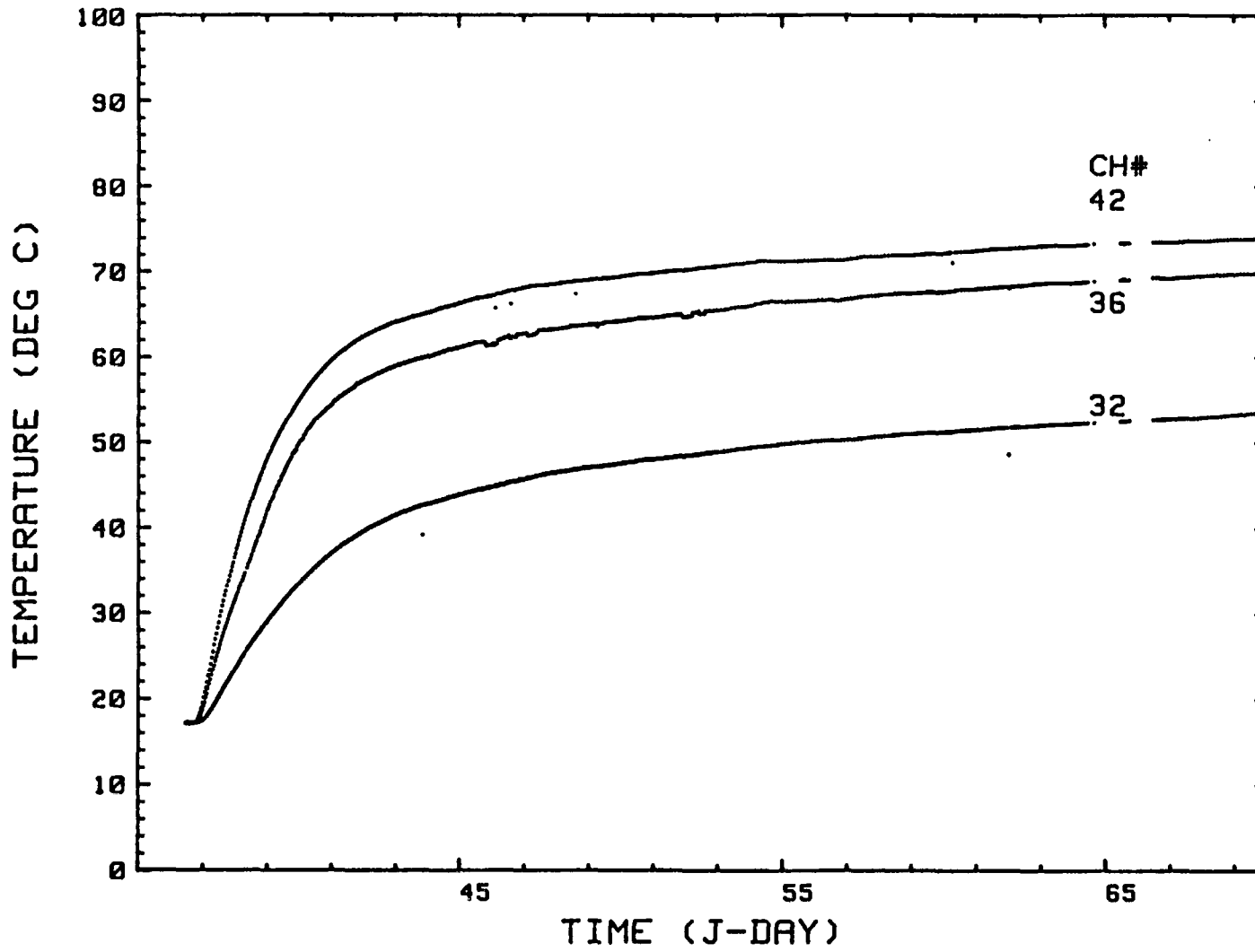


Figure 16. Rock wall temperature profiles in the water migration holes. WM-1, Ch#32. WM-2, Ch#36. WM-3, Ch#42.

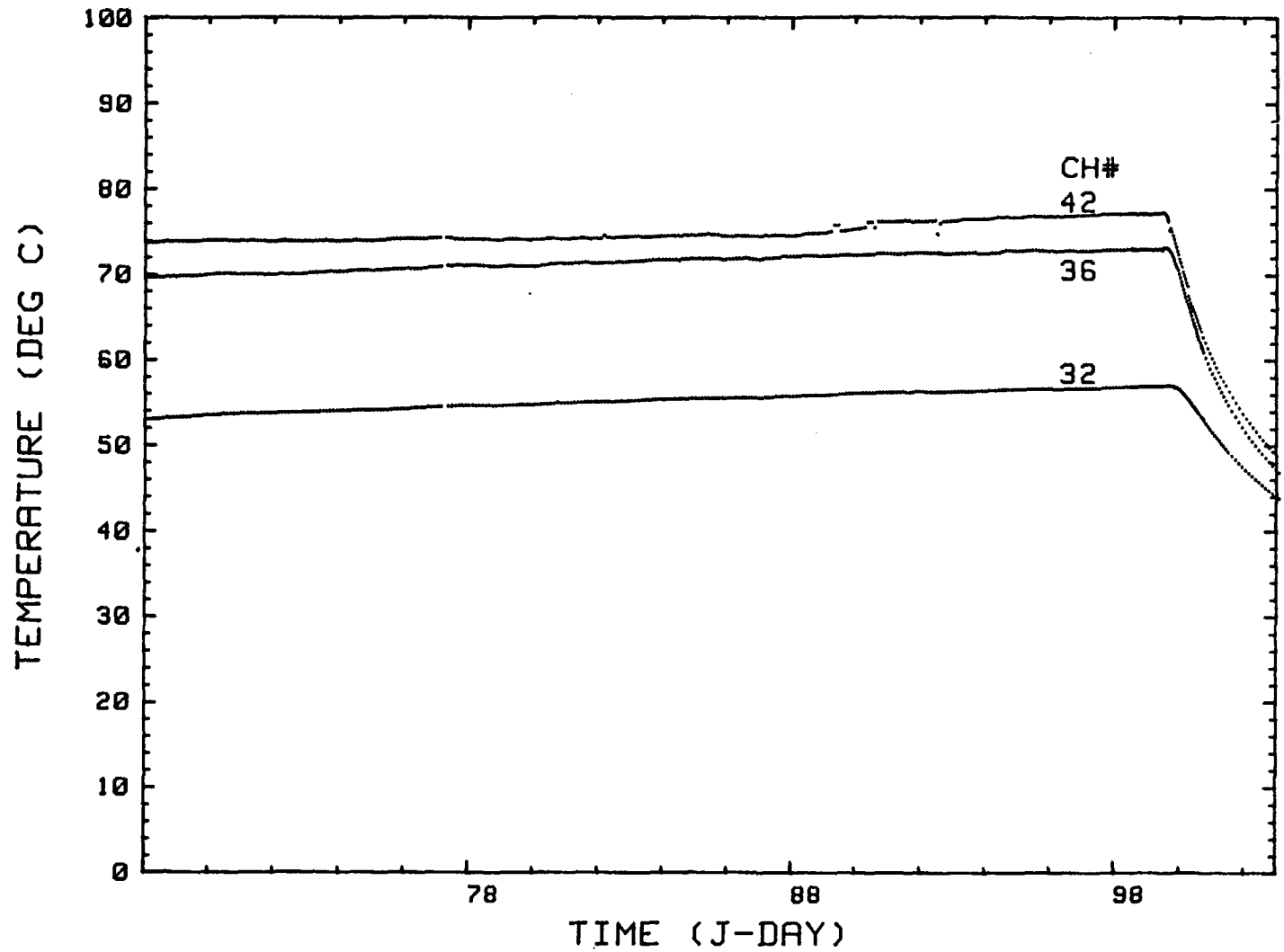


Figure 16 (Continued). Rock wall temperature profiles in the water migration holes. WM-1, Ch#32. WM-2, Ch#36. WM-3, Ch#42.

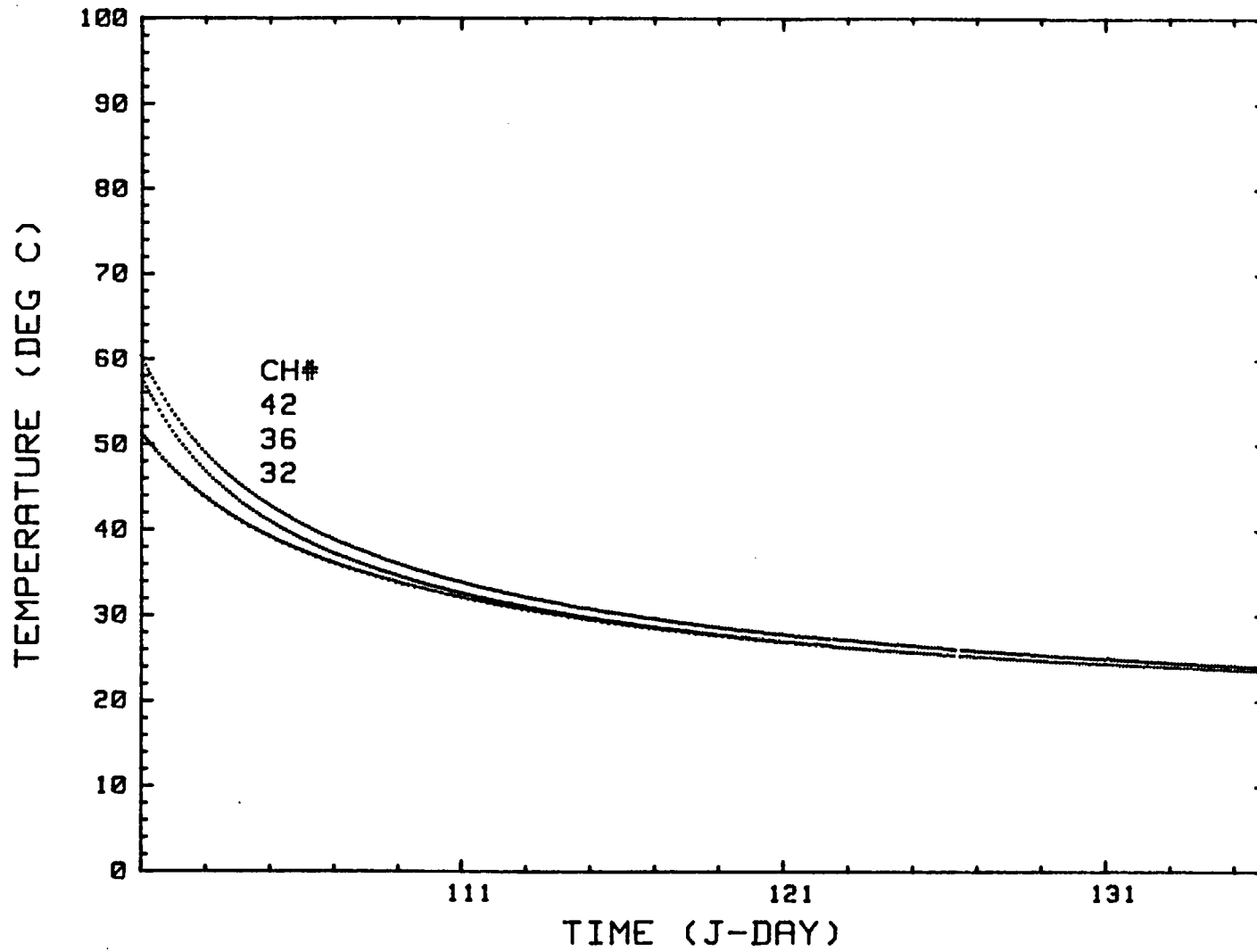


Figure 16 (Continued). Rock wall temperature profiles in the water migration holes. WM-1, Ch#32. WM-2, Ch#36. WM-3, Ch#42.

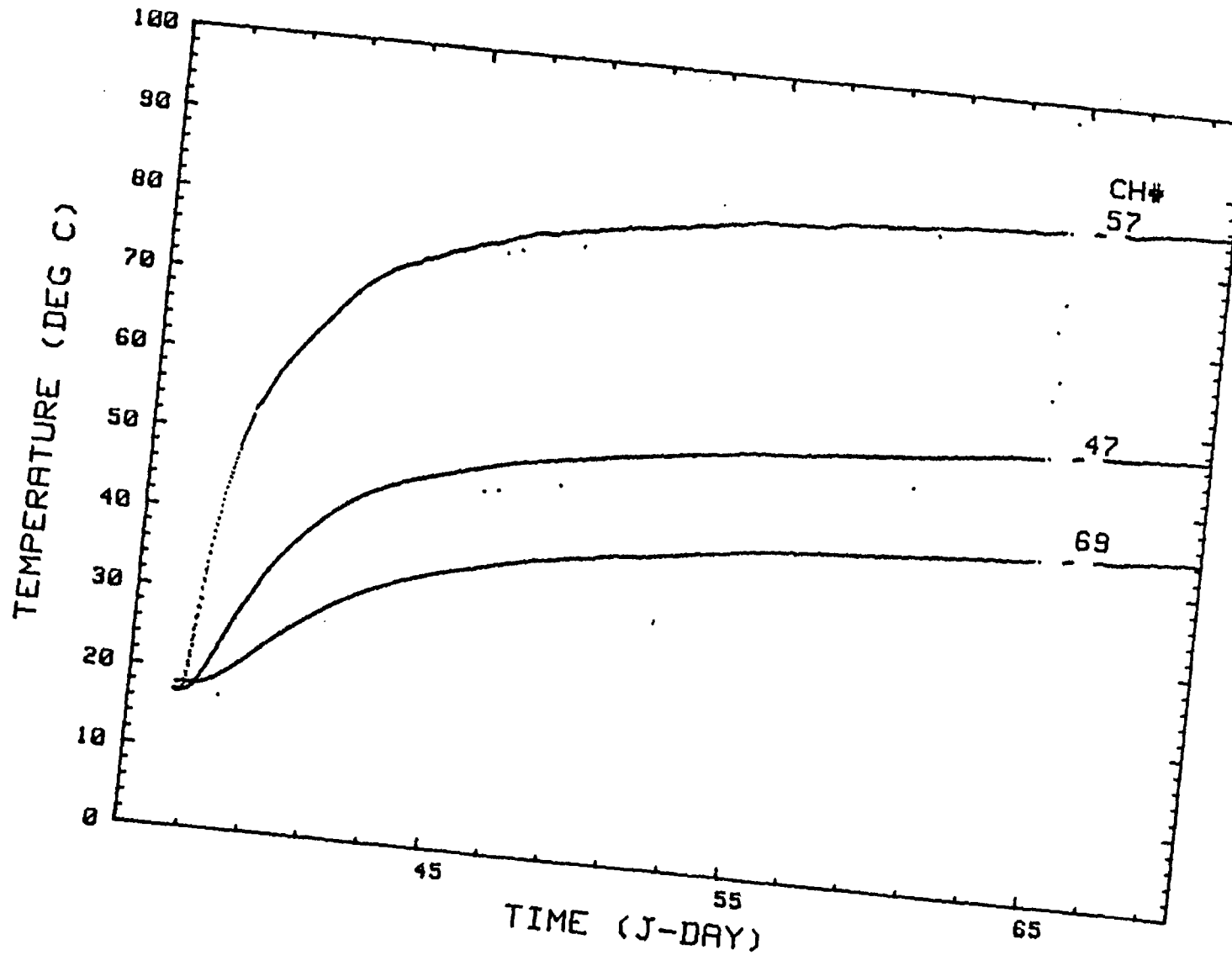


Figure 17. Representative temperature profiles from the two thermocouple holes and the stress hole. TH-1, Ch#47. TH-2, Ch#57. SH-1, Ch#69.

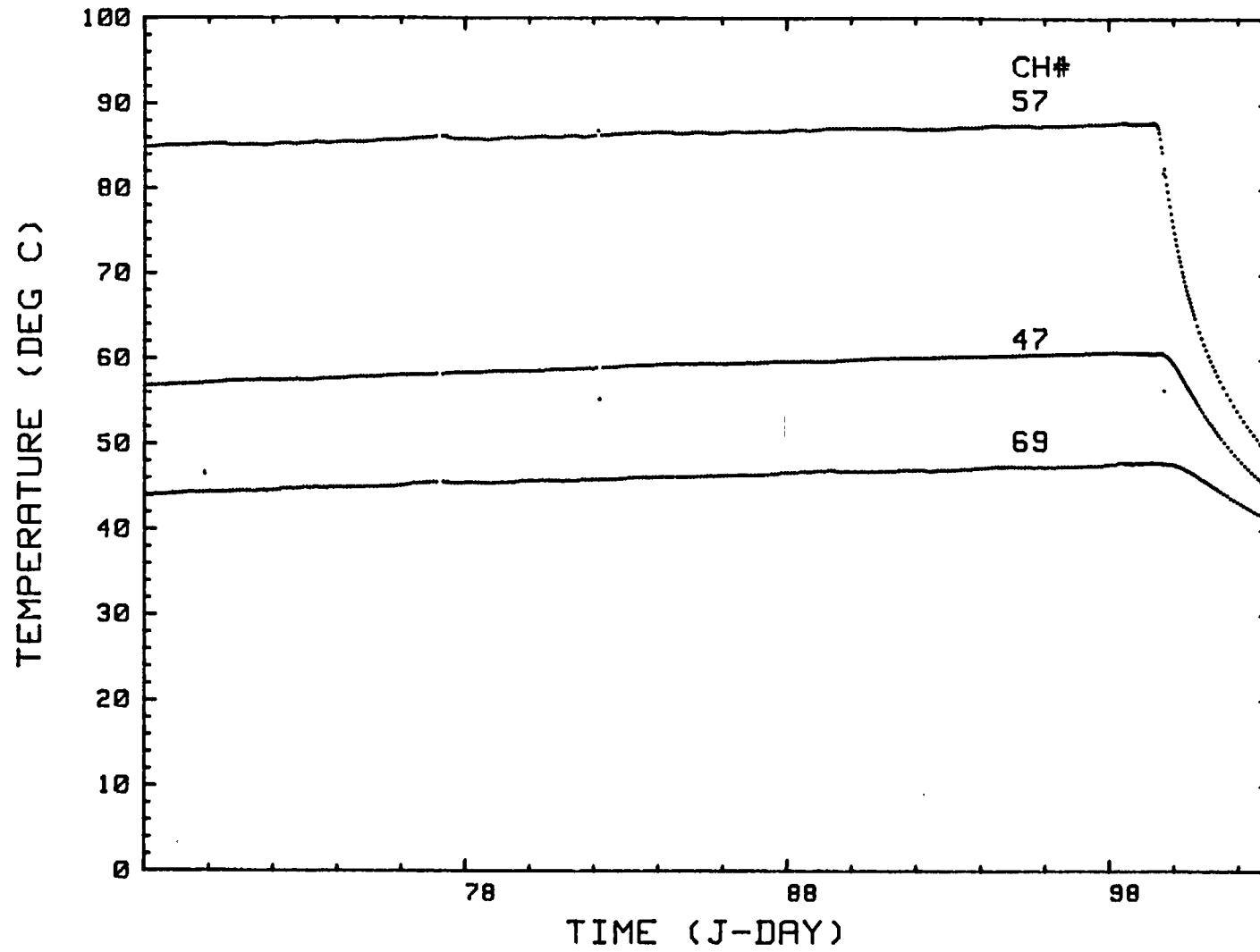


Figure 17 (Continued). Representative temperature profiles from the two thermocouple holes and the stress hole. TH-1, Ch#47. TH-2, Ch#57. SH-1, Ch#69.

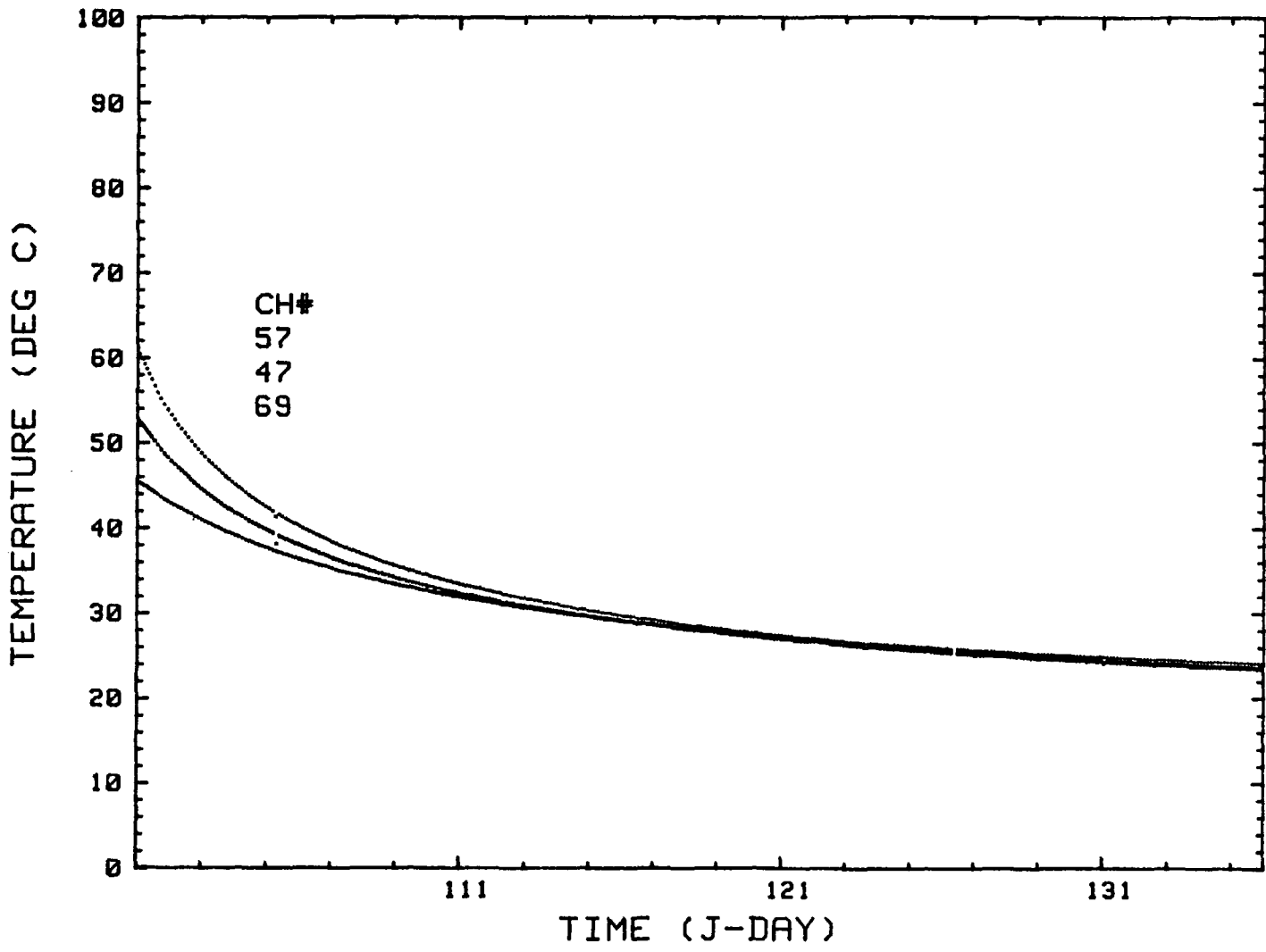


Figure 17 (Continued). Representative temperature profiles from the two thermocouple holes and the stress hole. TH-1, Ch#47. TH-2, Ch#57. SH-1, Ch#69.

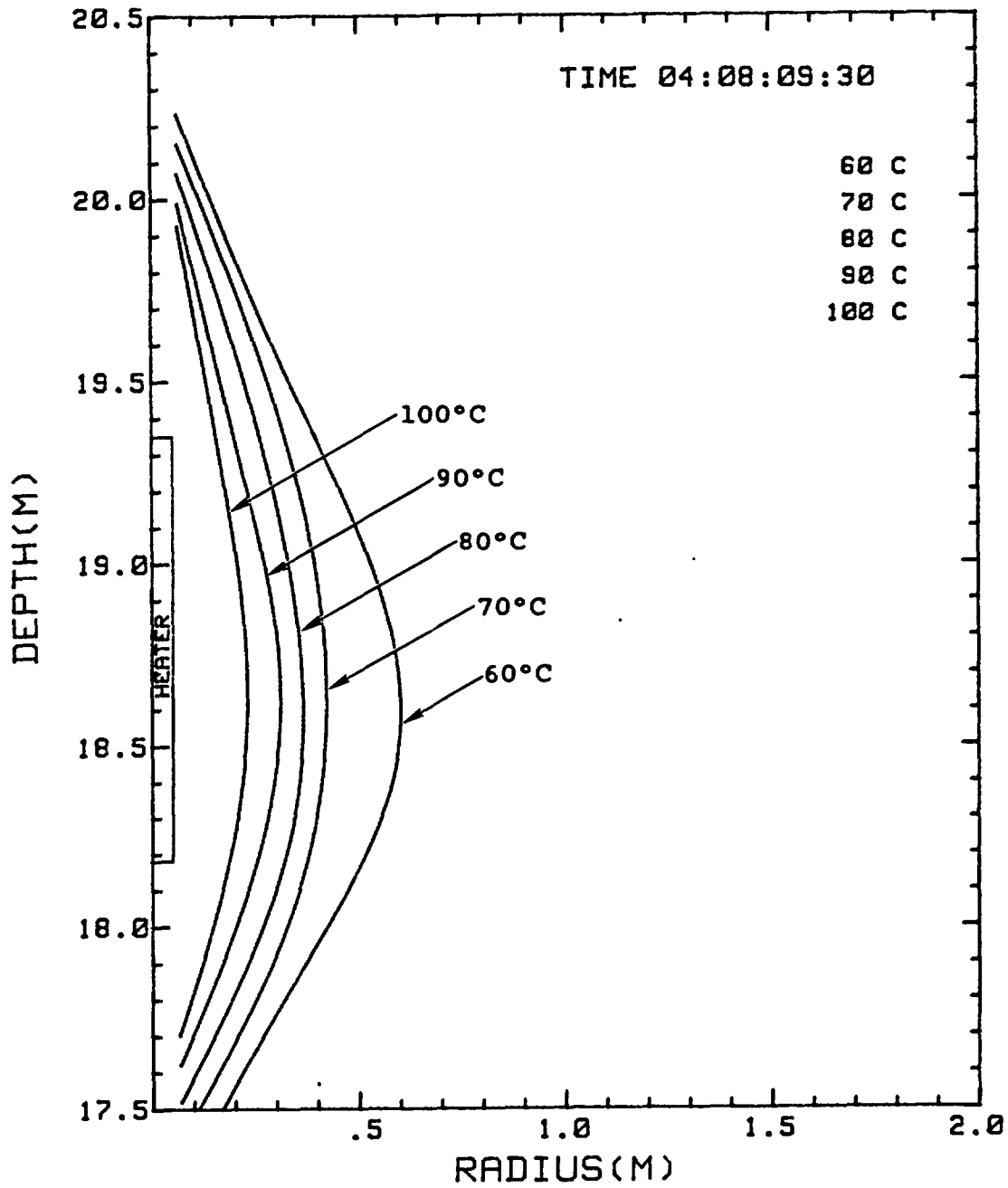


Figure 18. Experimentally determined temperature isotherms surrounding the heater just before turn-off.

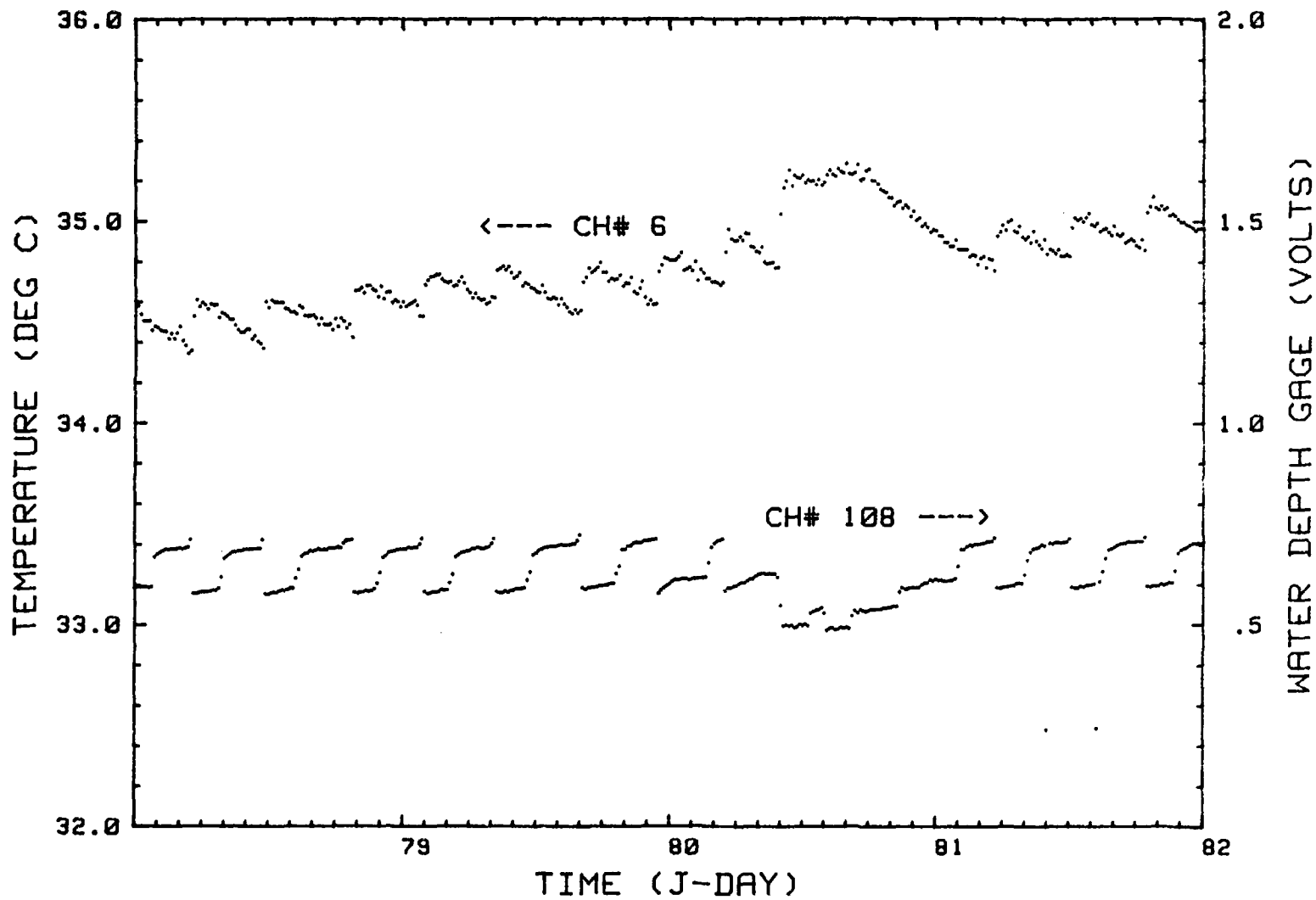


Figure 19. Comparison of air temperature response to water sample withdrawal from HHH-1.

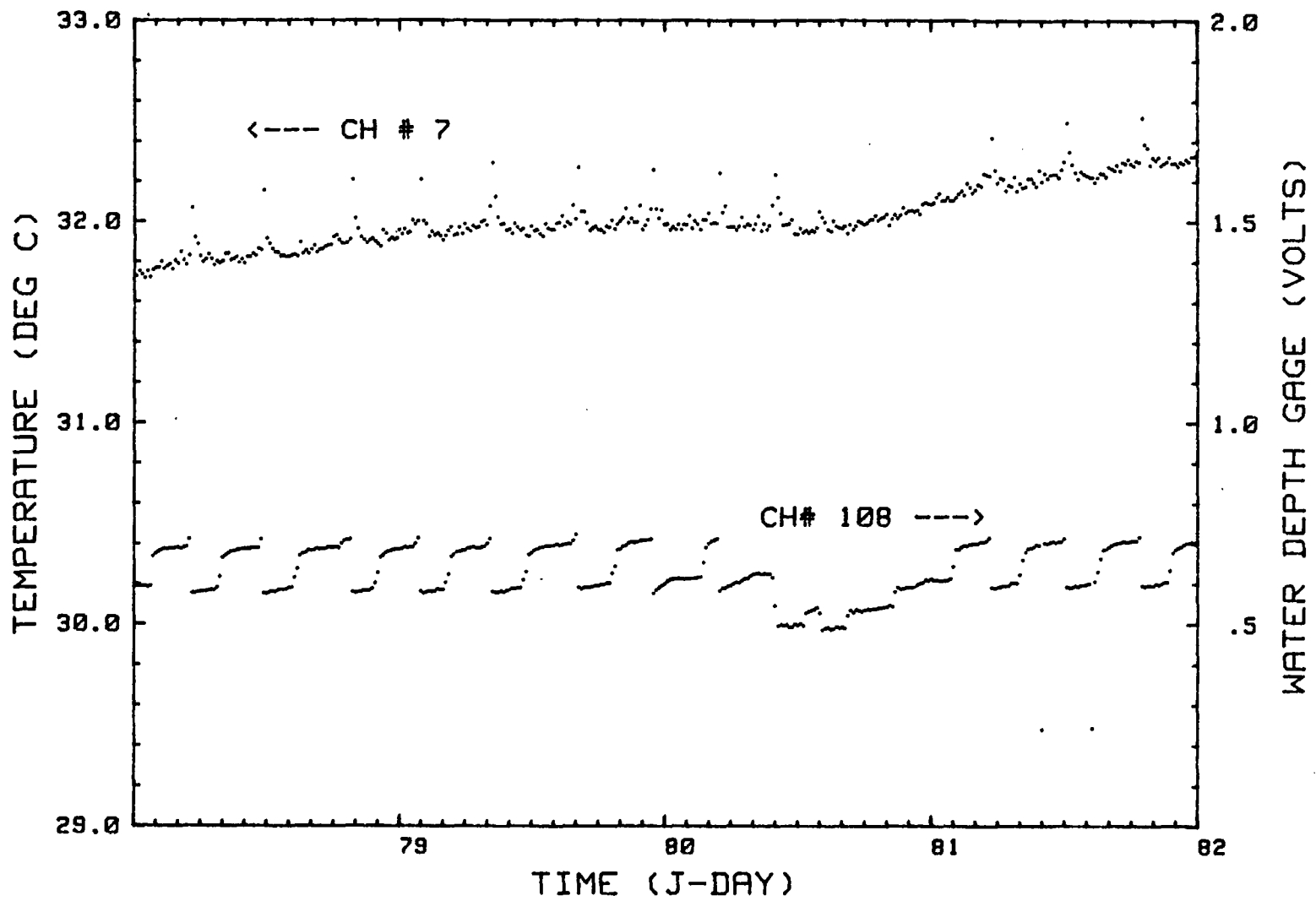


Figure 20. Comparison of water temperature response to water sample withdrawal from HH-1.

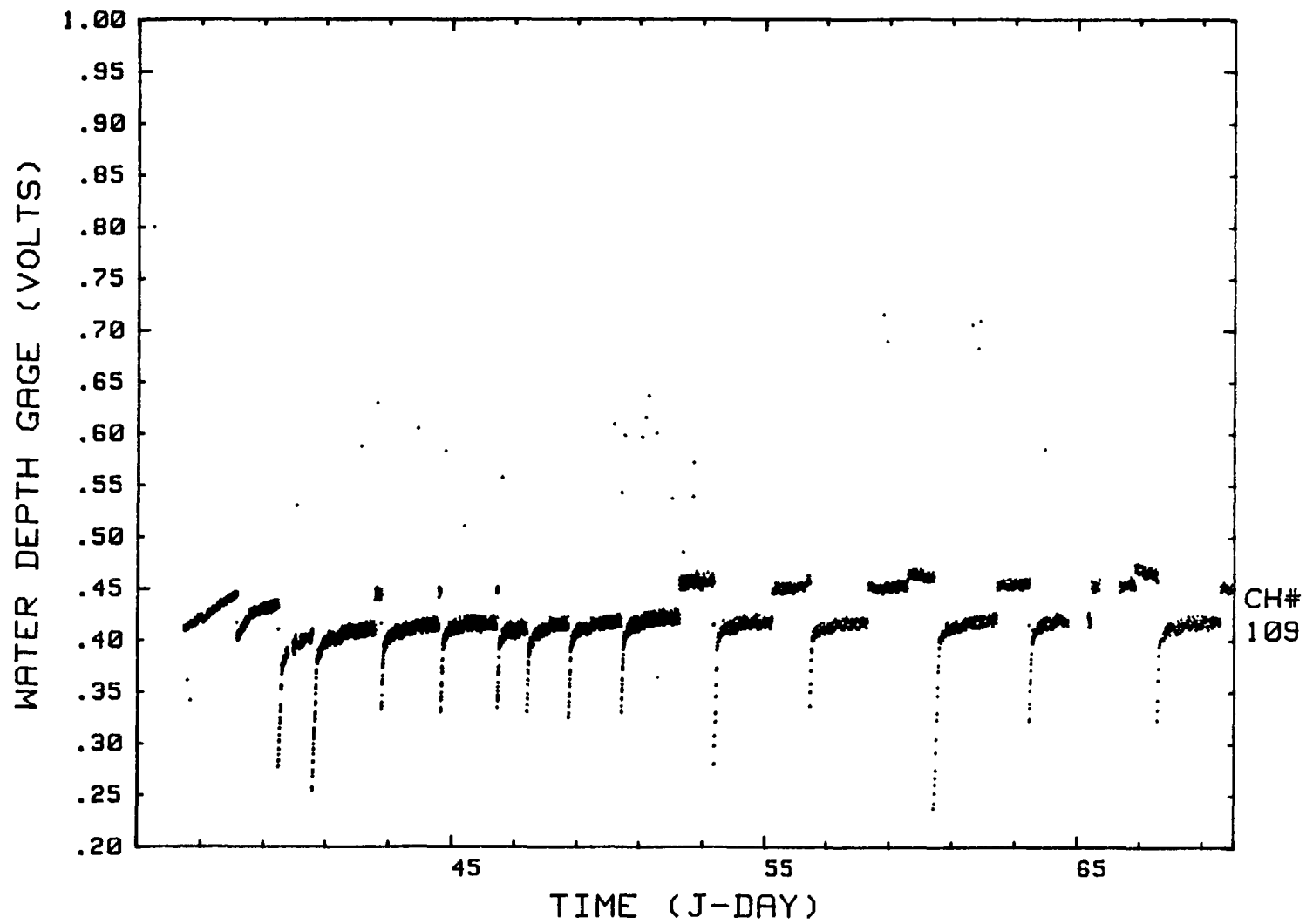


Figure 21. Depth gage data measured in WM-1.

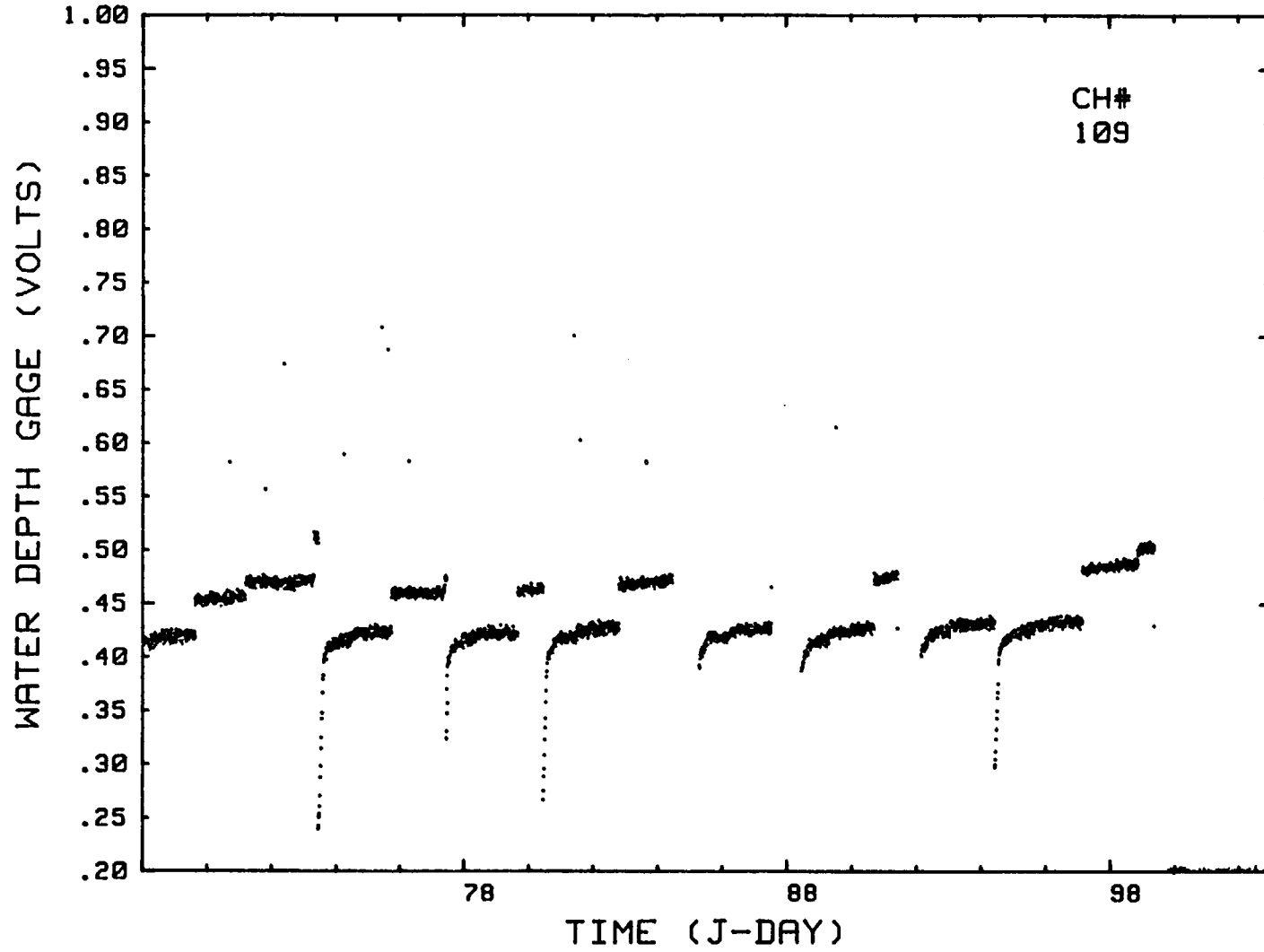


Figure 21 (Continued). Depth gage data measured in WM-1.

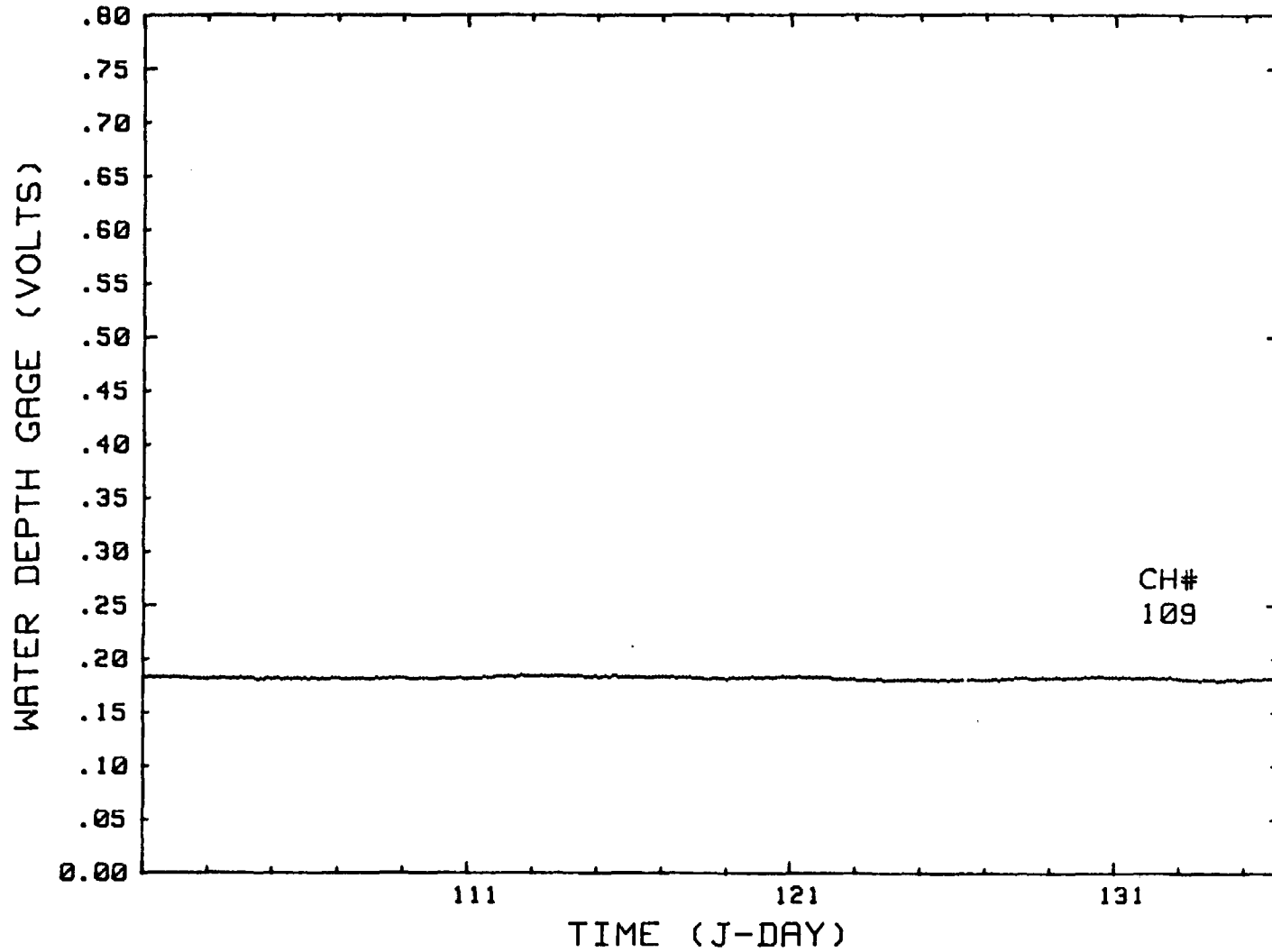


Figure 21 (Continued). Depth gage data measured in WM-1.

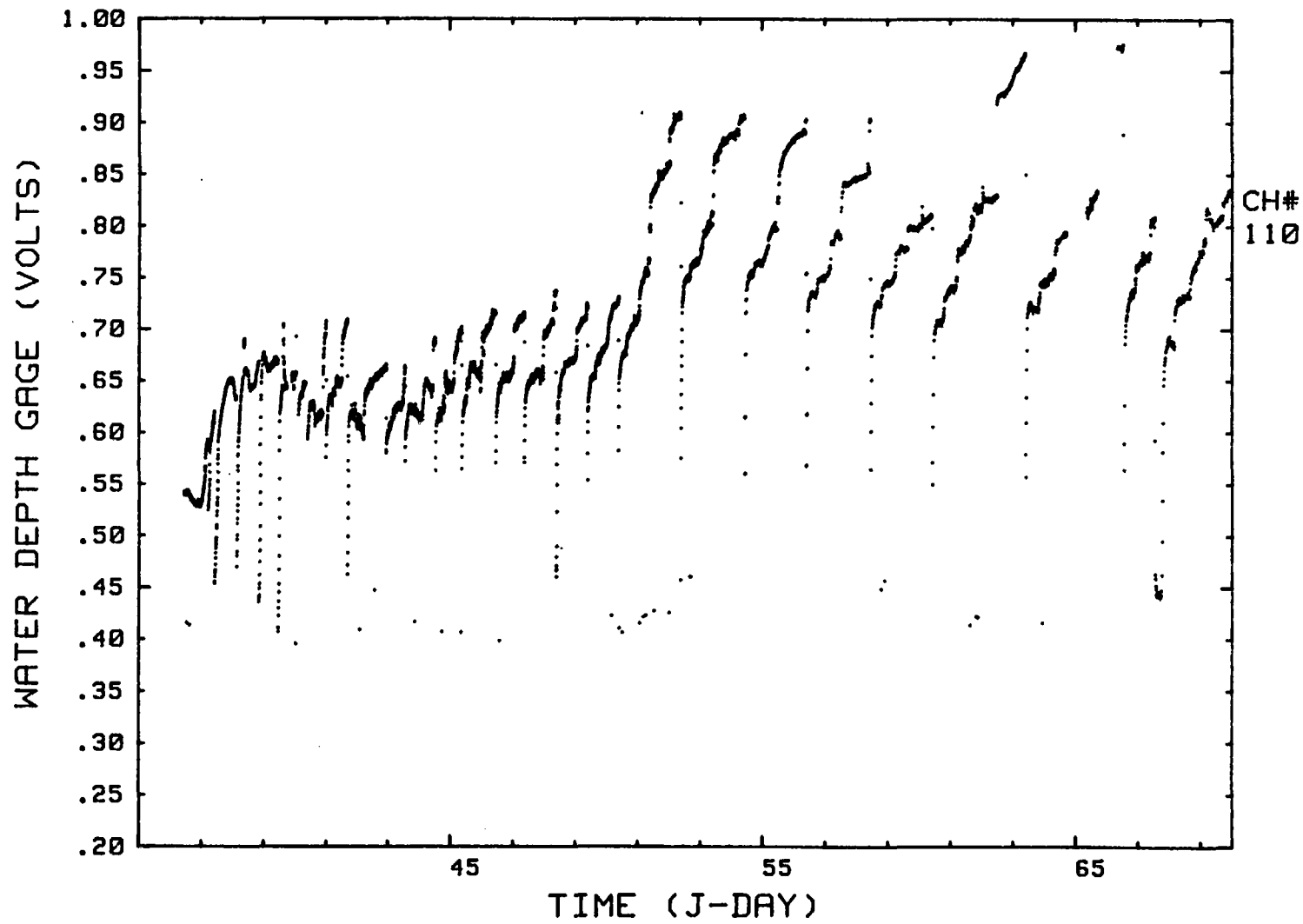


Figure 22. Depth gage data measured in WM-2.

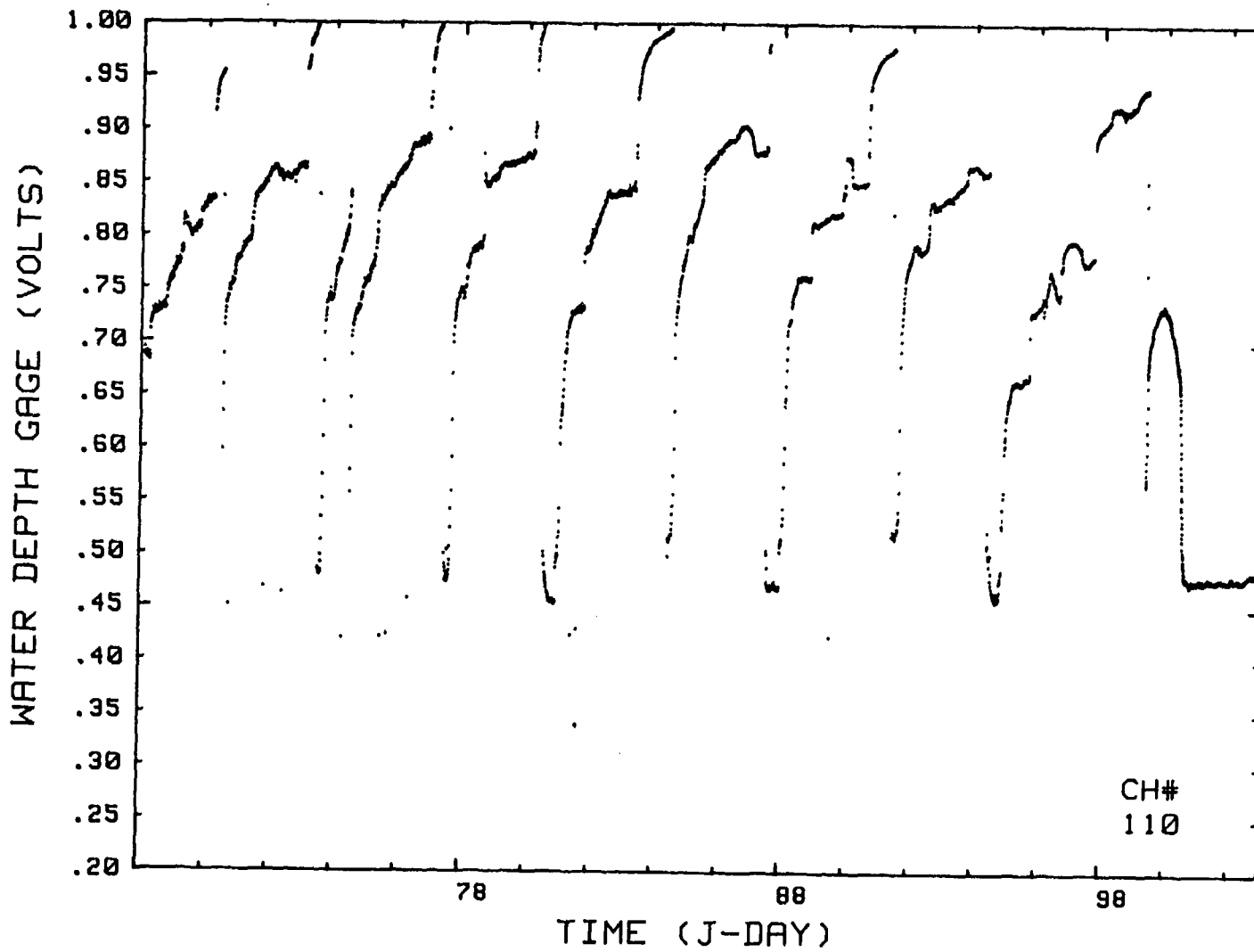


Figure 22 (Continued). Depth gage data measured in WM-2.

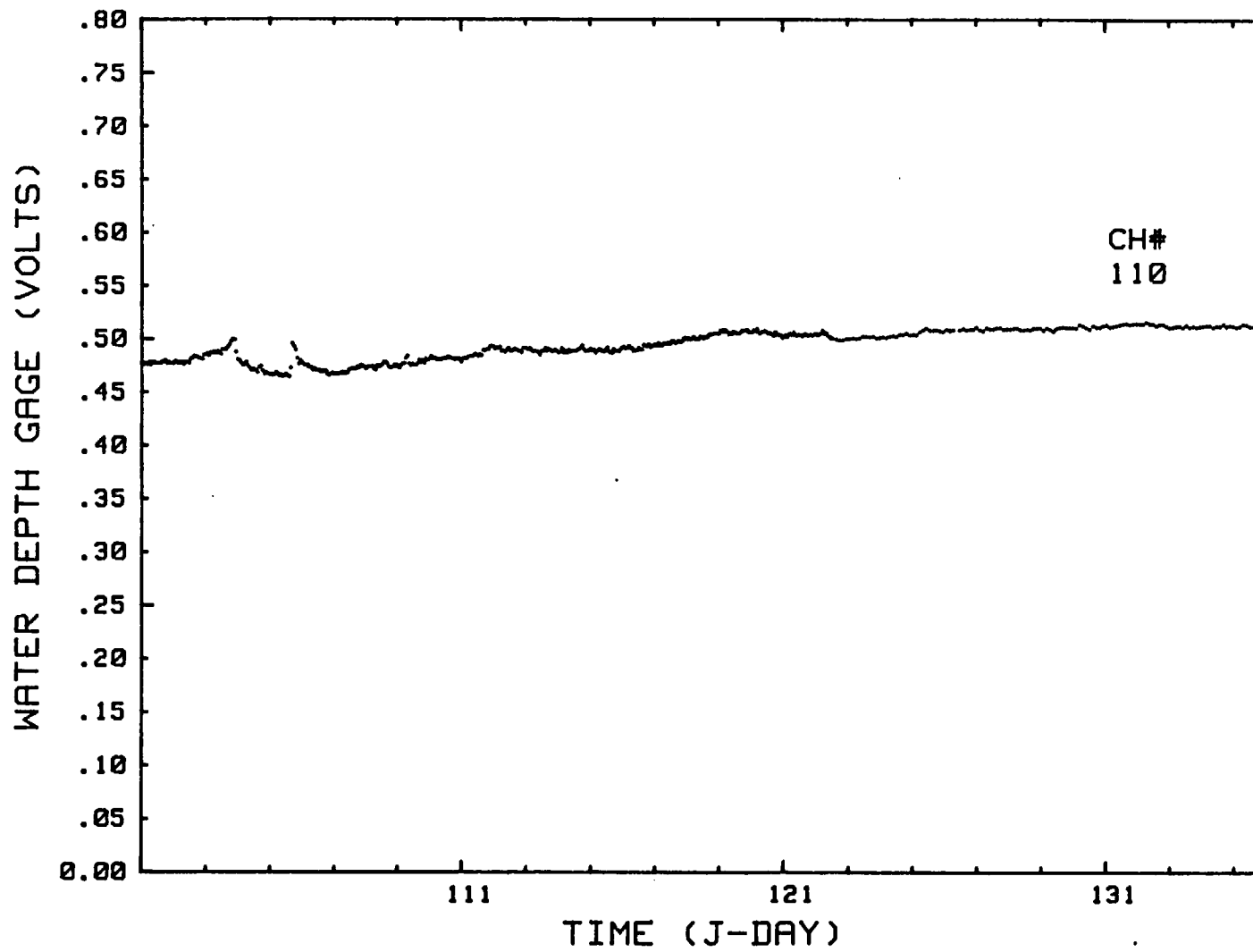


Figure 22 (Continued). Depth gage data measured in WM-2.

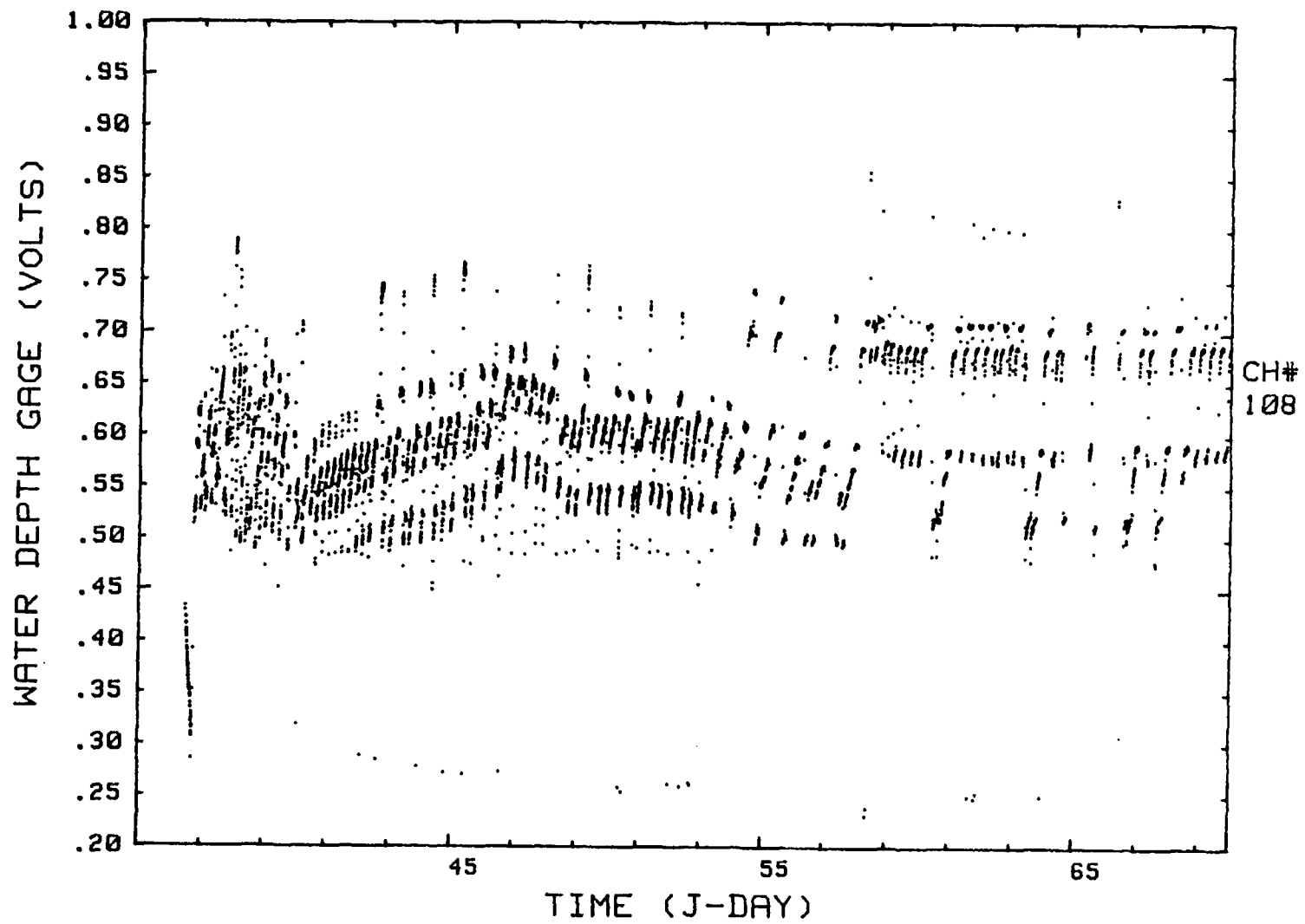


Figure 23. Depth gage data measured in the heater hole water collection cavity.

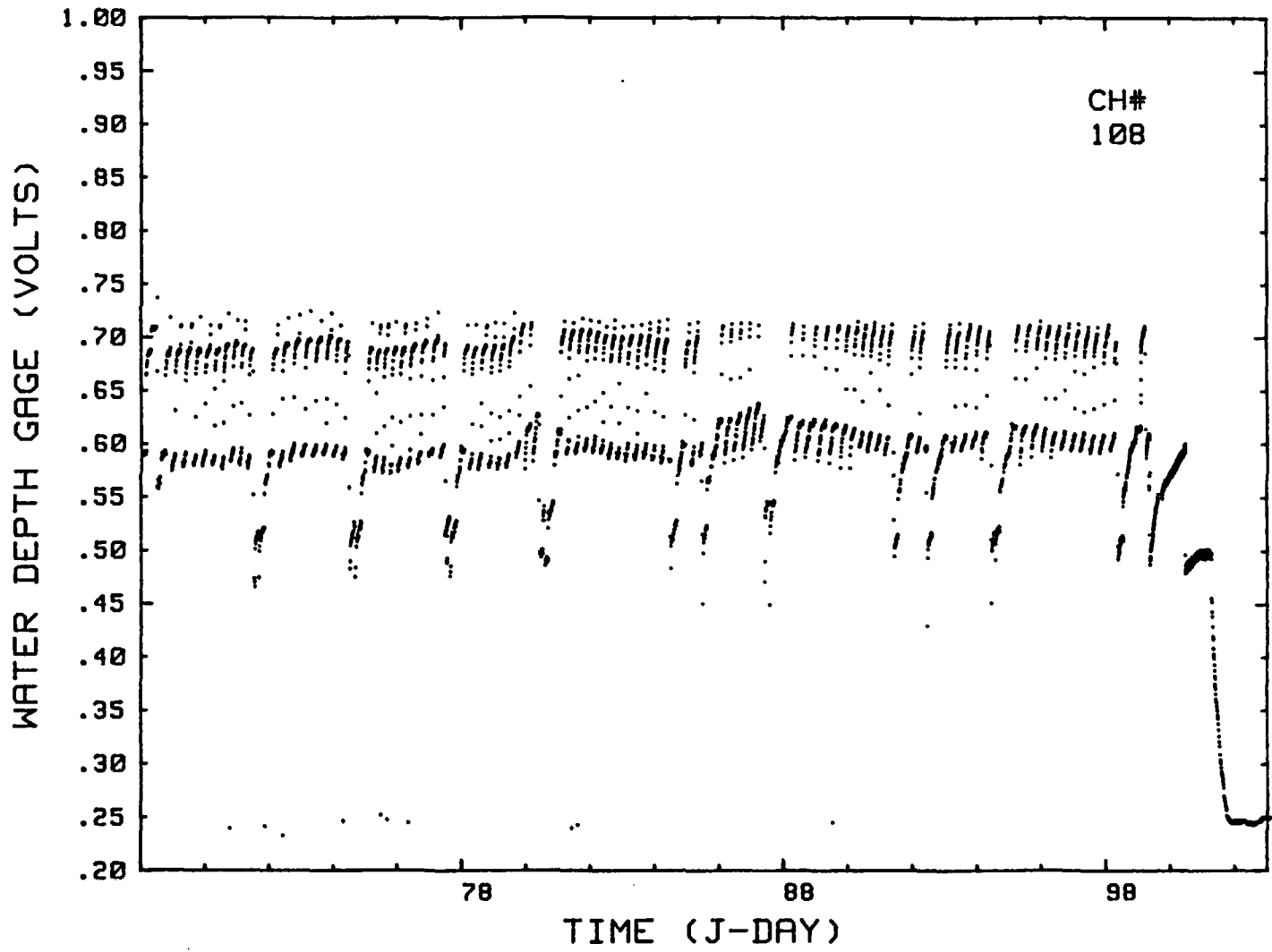


Figure 23 (Continued). Depth gage data measured in the heater hole water collection cavity.

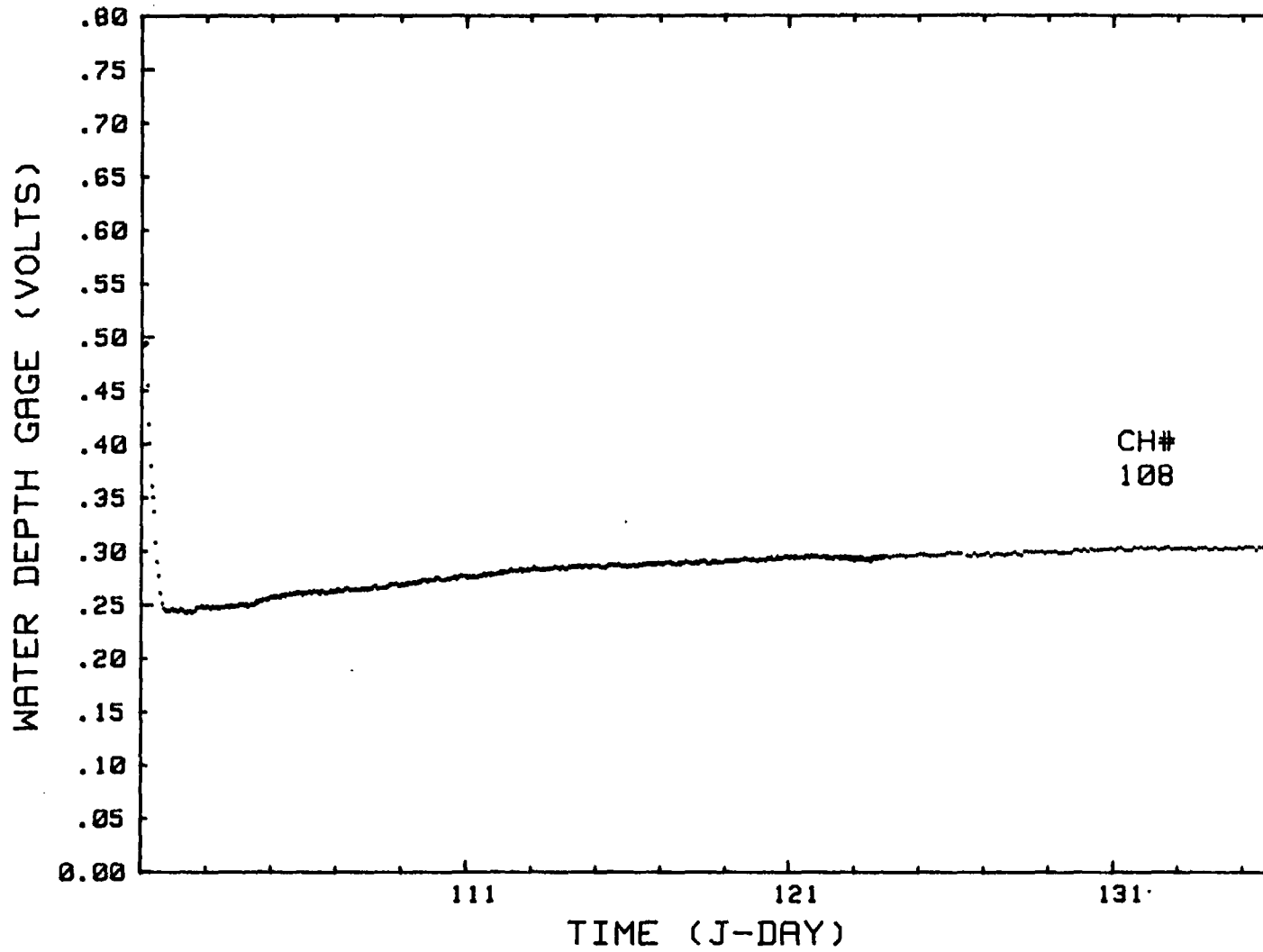


Figure 23 (Continued). Depth gage data measured in the heater hole water collection cavity.

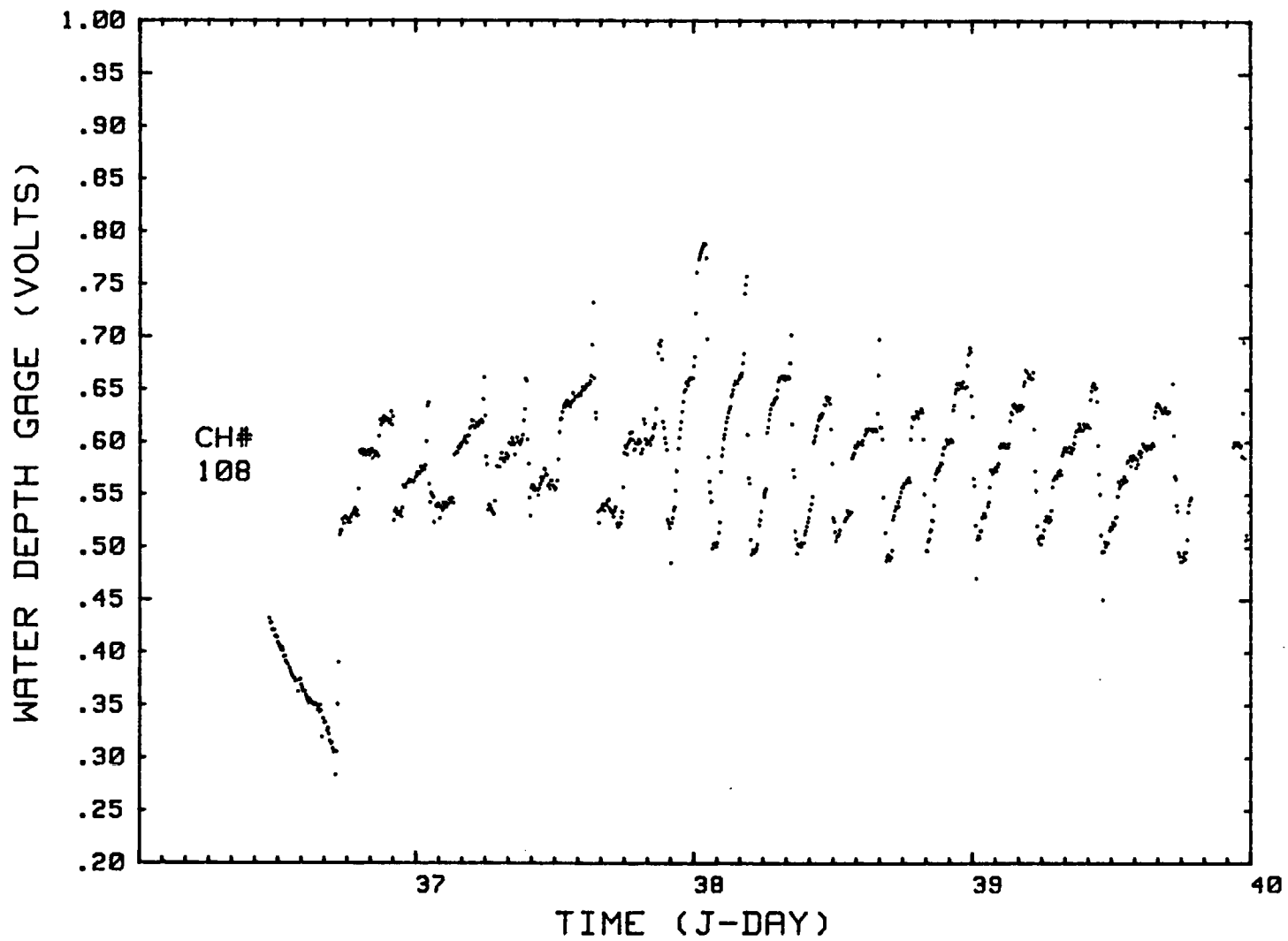


Figure 24. Depth gage data vs expanded time scale in HH-1 at heater turn-on.

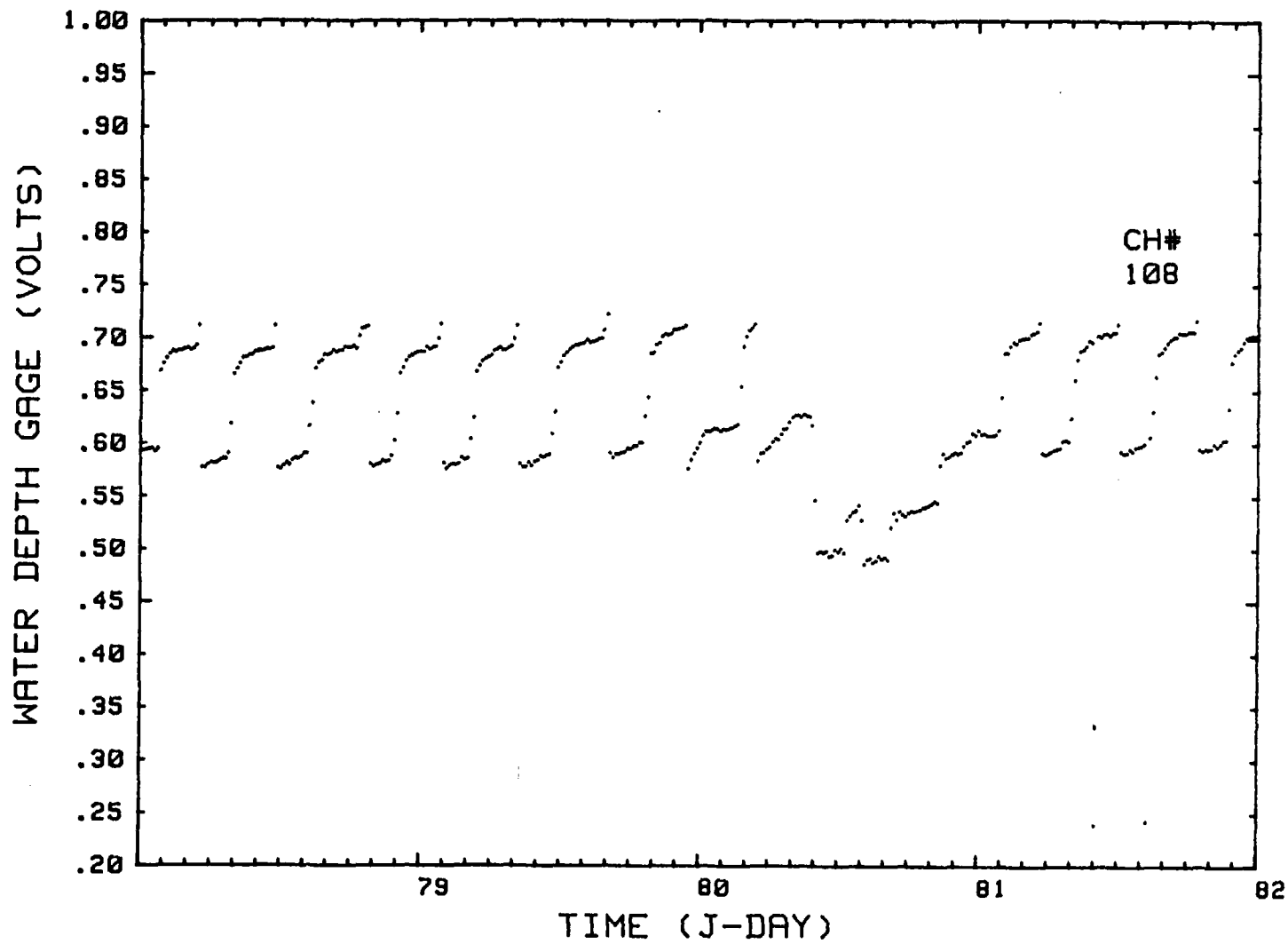


Figure 25. Depth gage data vs expanded time scale in HH-1, showing automatic and manual water sampling.

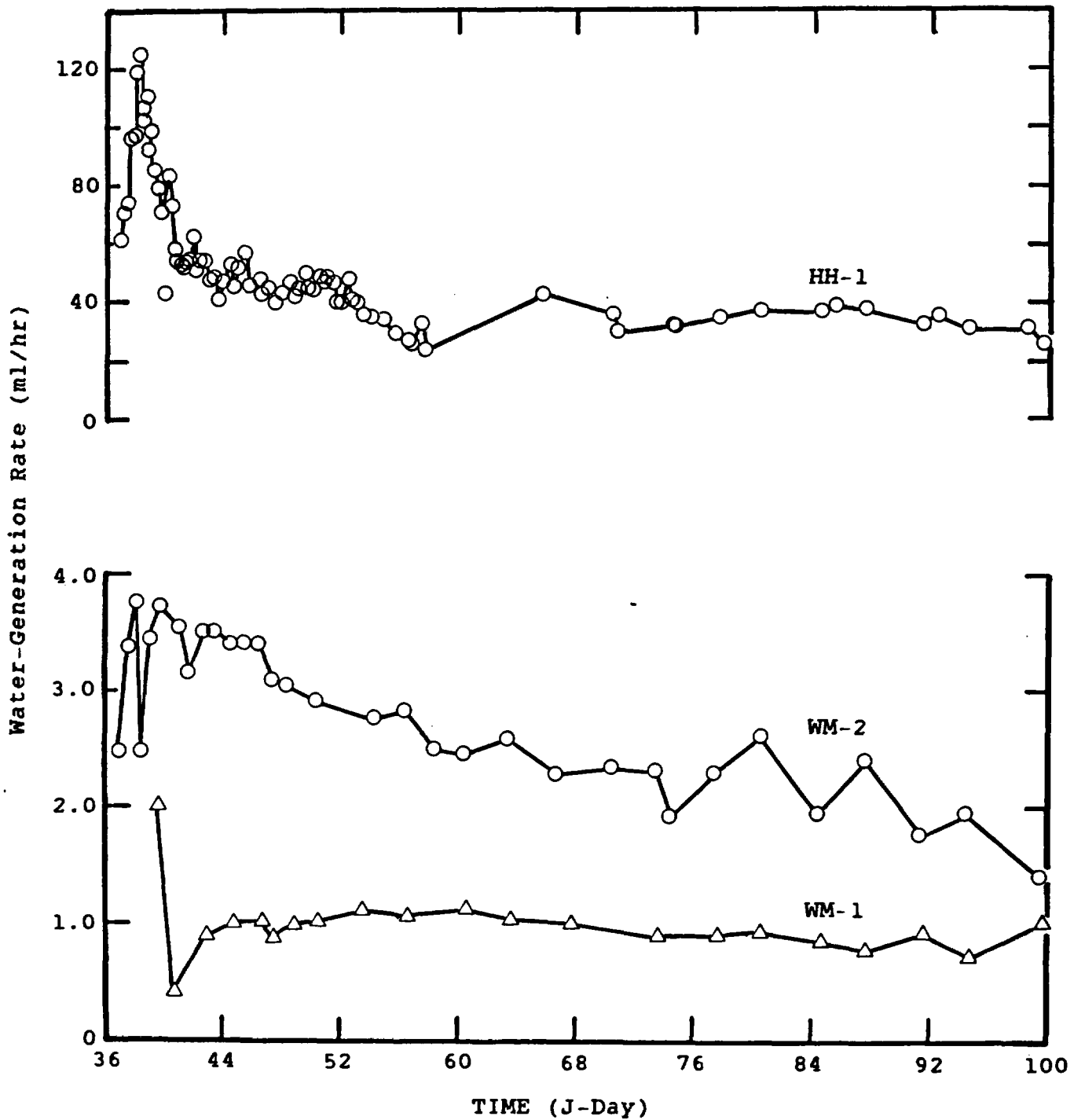


Figure 26. Water generation rates in HH-1, WM-1, and WM-2. Rates are not corrected for possible leakage past packer.

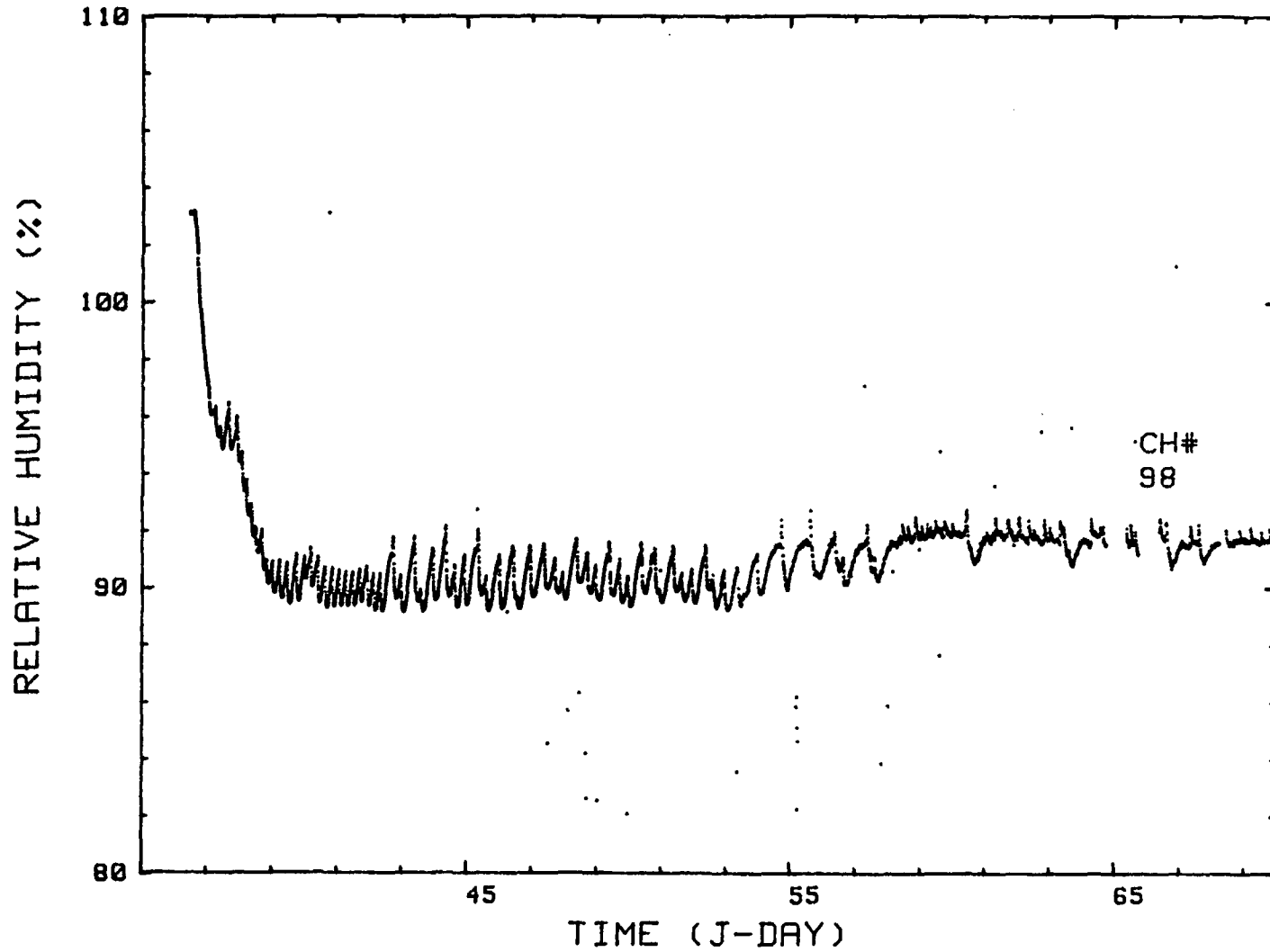


Figure 27. Relative humidity measured in HH-1 water collection cavity.

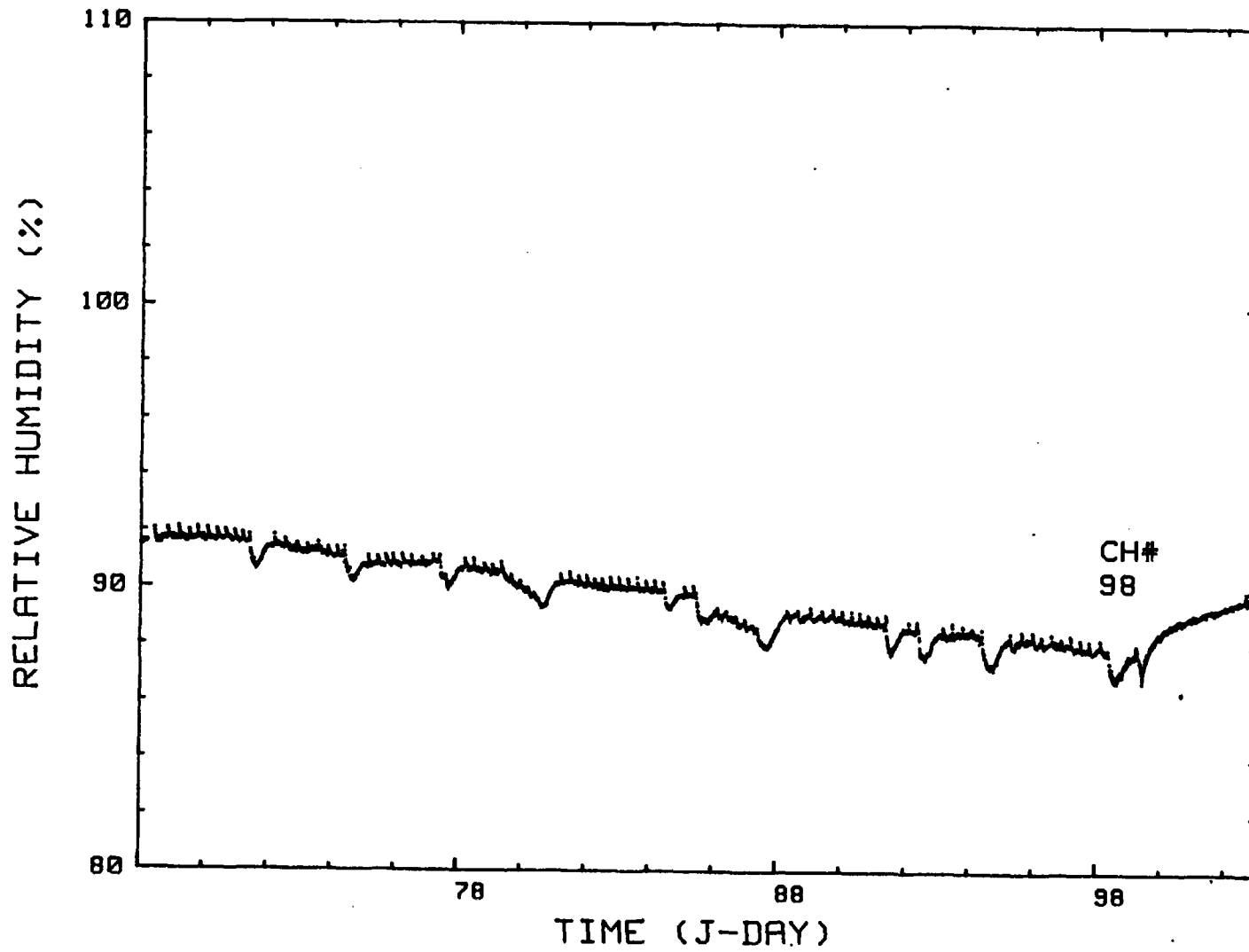


Figure 27 (Continued). Relative humidity measured in HH-1 water collection cavity.

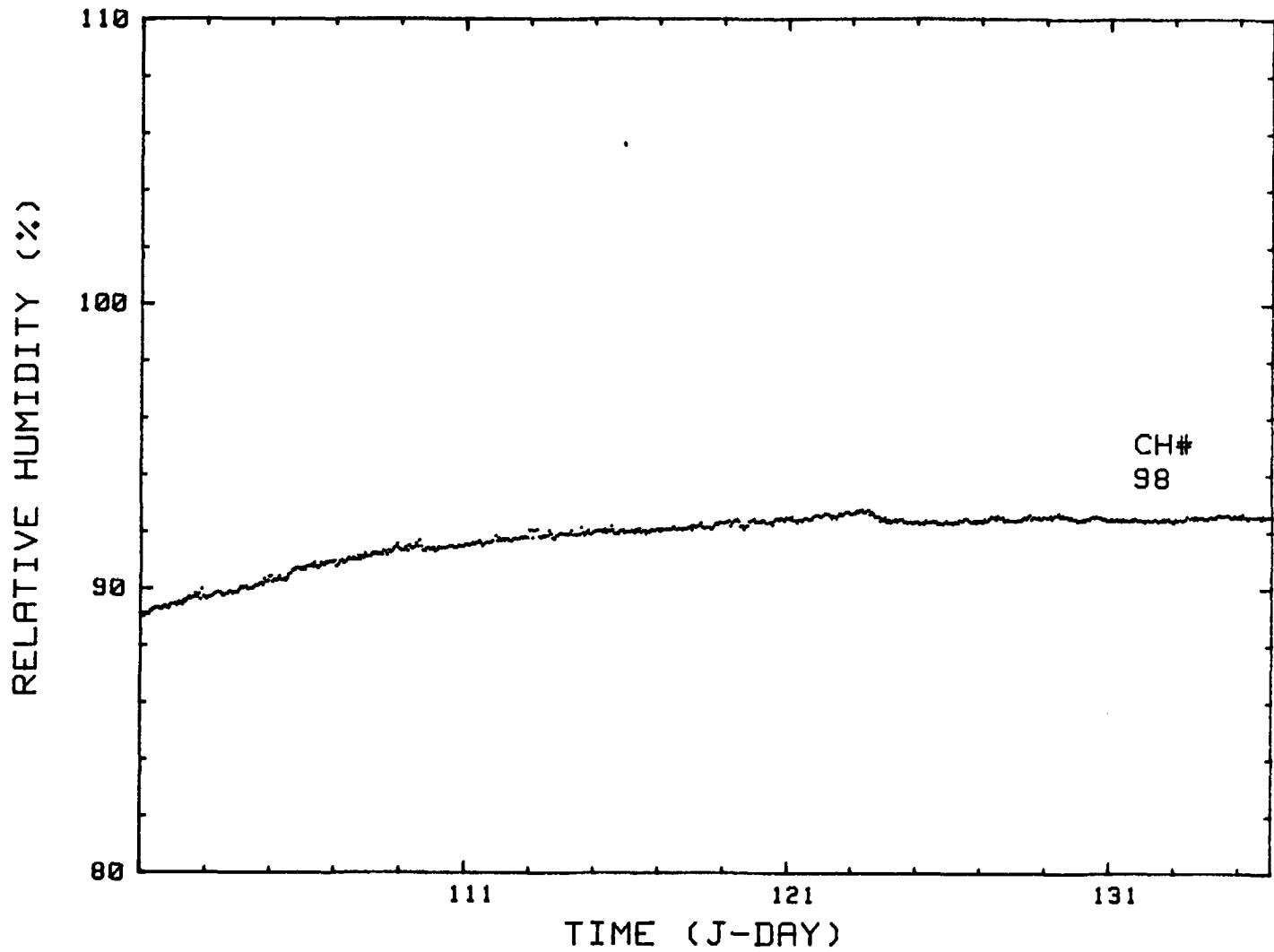


Figure 27 (Continued). Relative humidity measured in HH-1 water collection cavity.

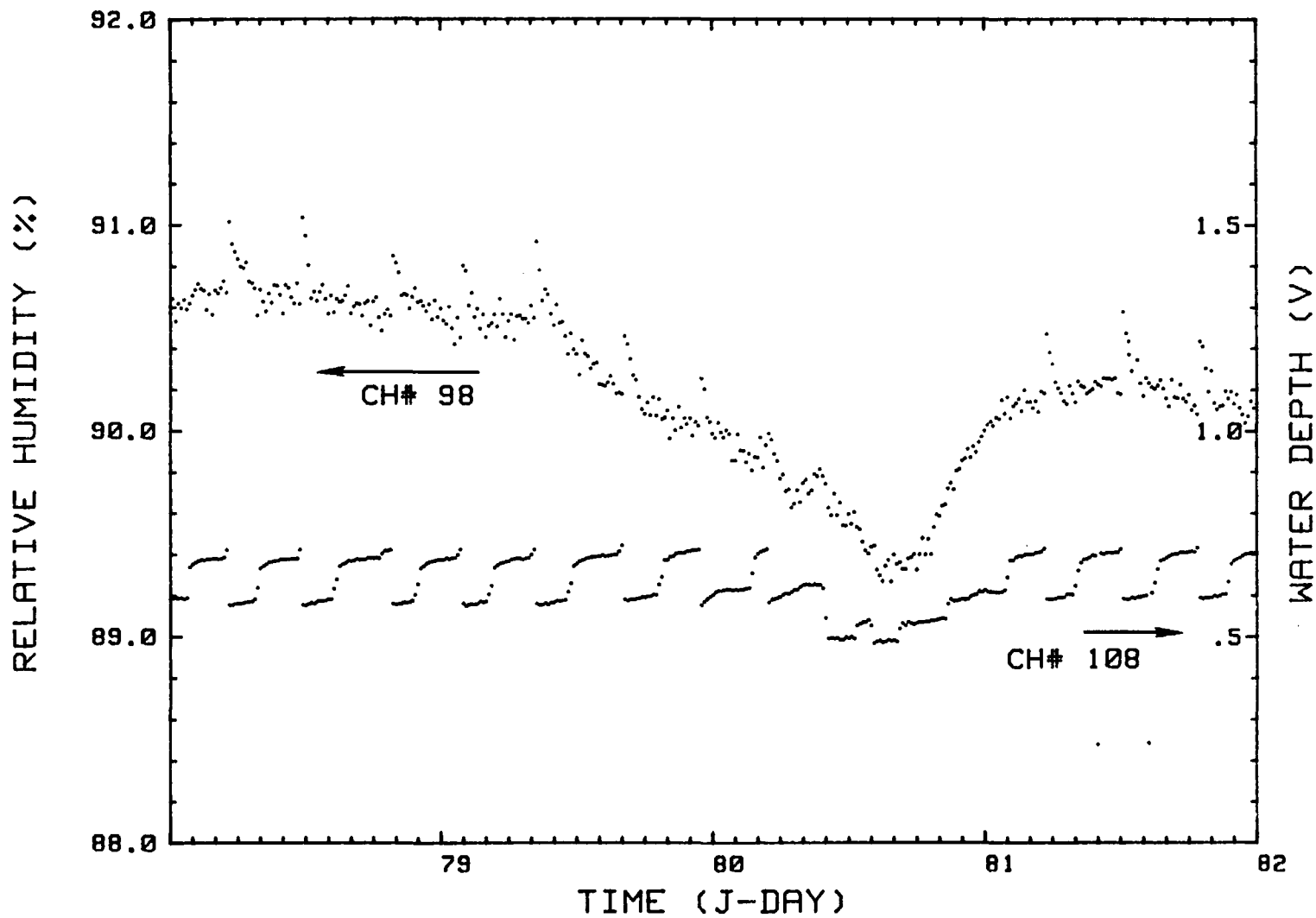


Figure 28. Comparison of the relative humidity gage response to water sample withdrawal in HH-1.

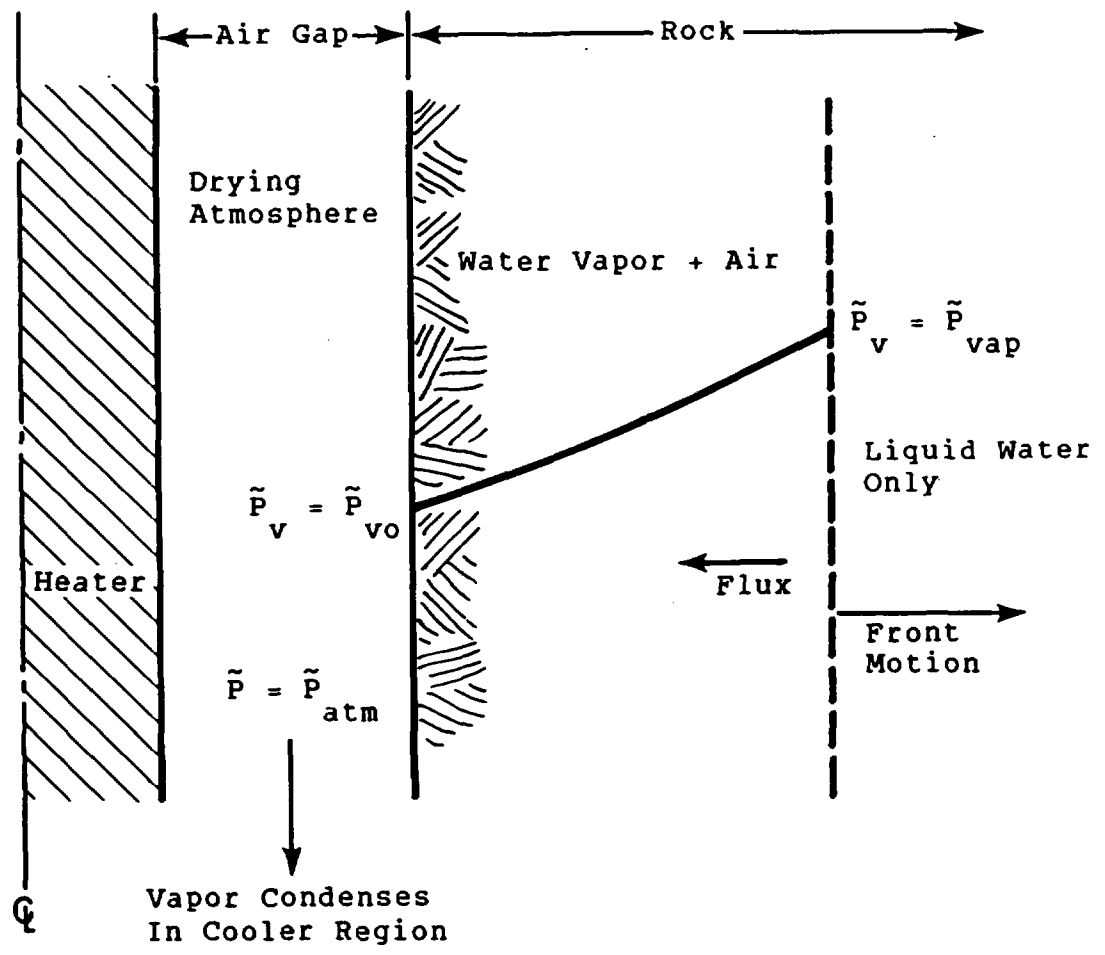


Figure 29. Schematic drawing of the evaporation front model in one-dimensional cylindrical geometry.

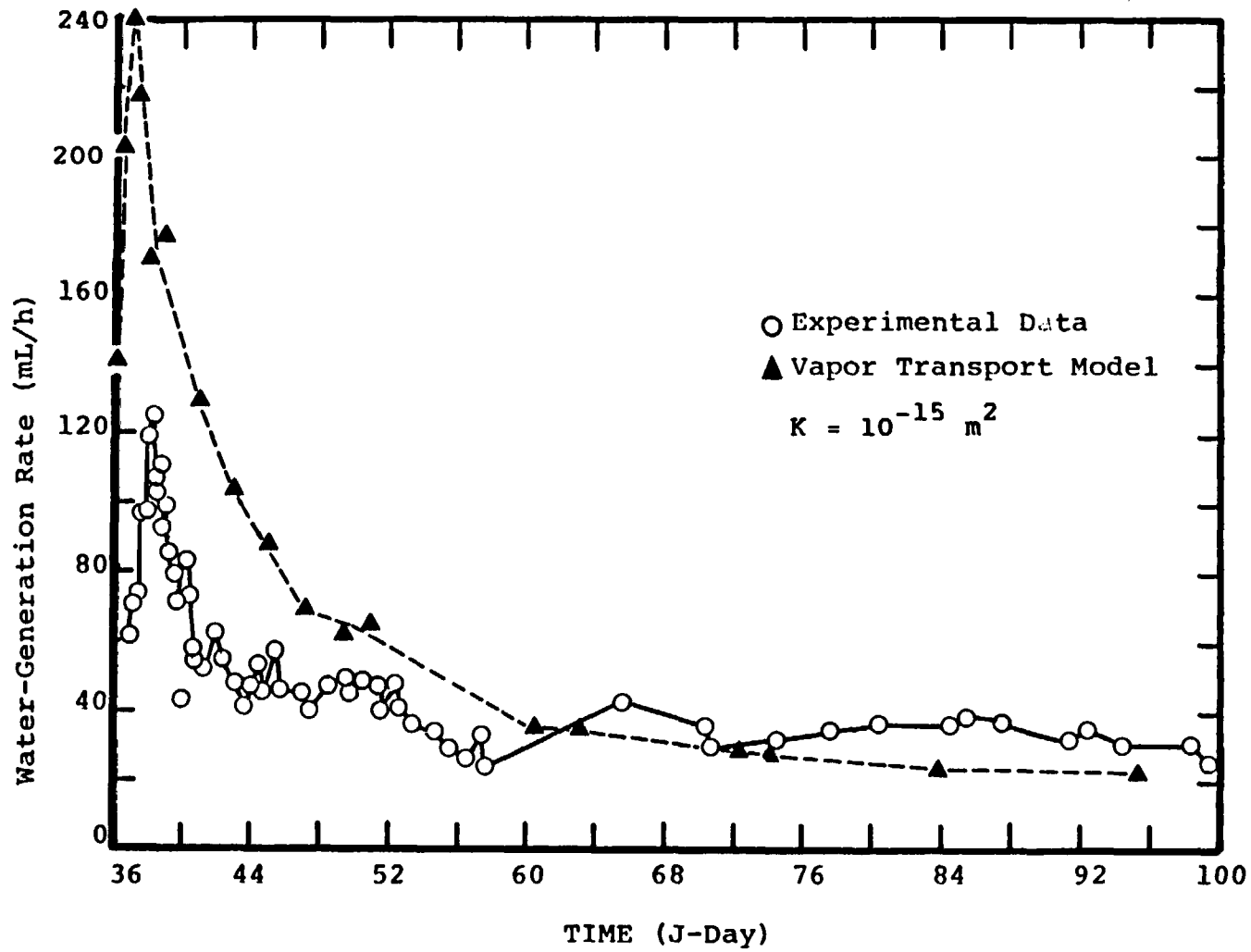


Figure 30. Comparison of evaporation front model results and experimental data from HH-1 for high humidity boundary condition and permeability =  $10^{-15} \text{ m}^2$ .

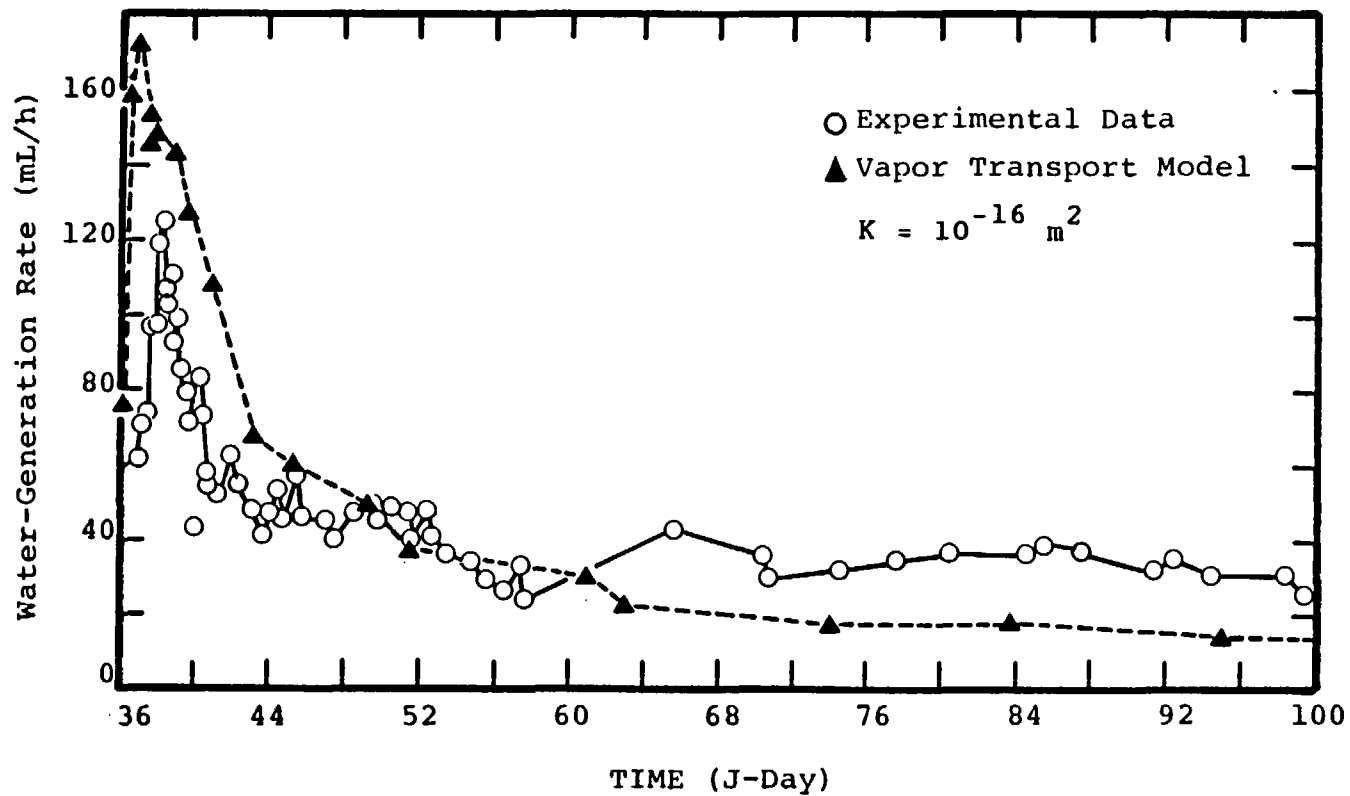


Figure 31. Comparison of evaporation front model results and experimental data from HH-1 for high humidity boundary condition and permeability =  $10^{-16} \text{ m}^2$ .

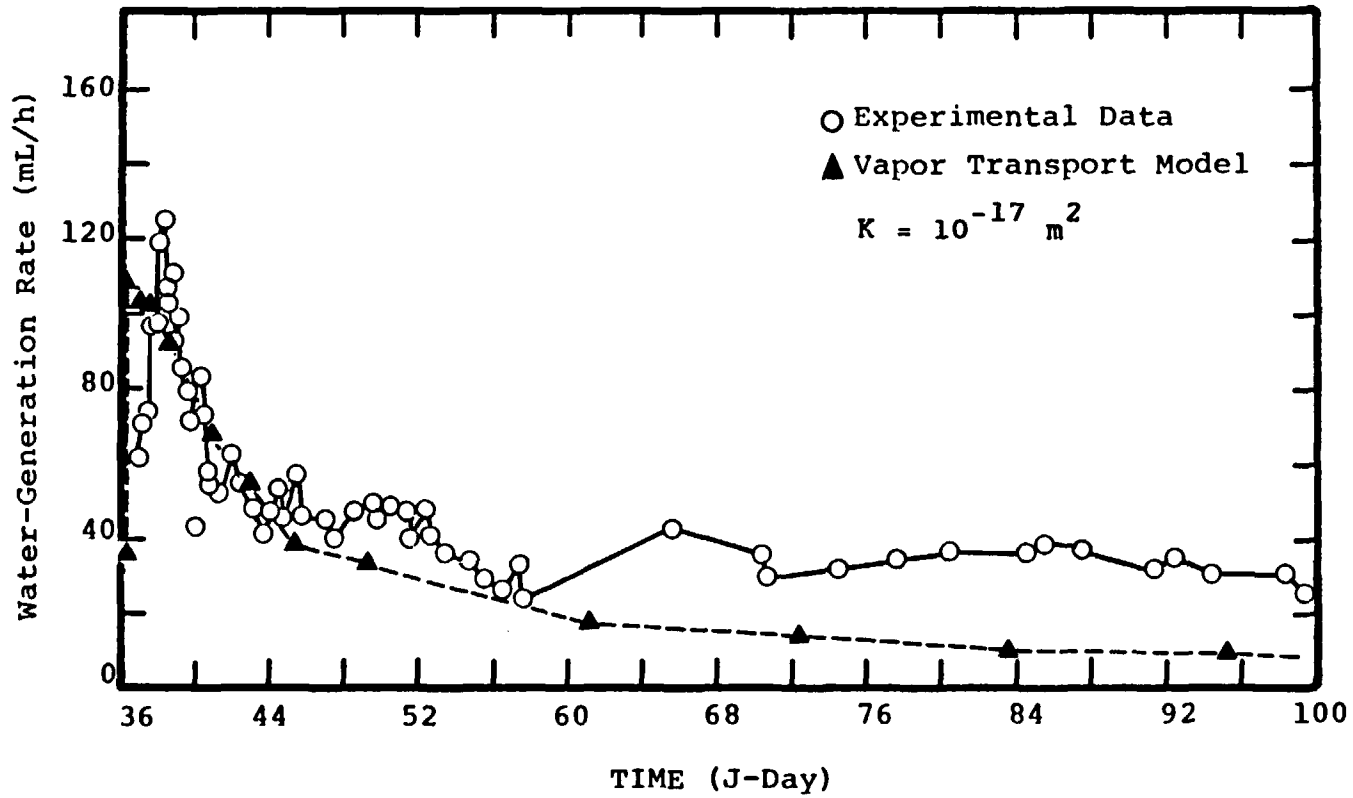


Figure 32. Comparison of evaporation front model results and experimental data from HH-1 for high humidity boundary condition and permeability =  $10^{-17} \text{ m}^2$ .

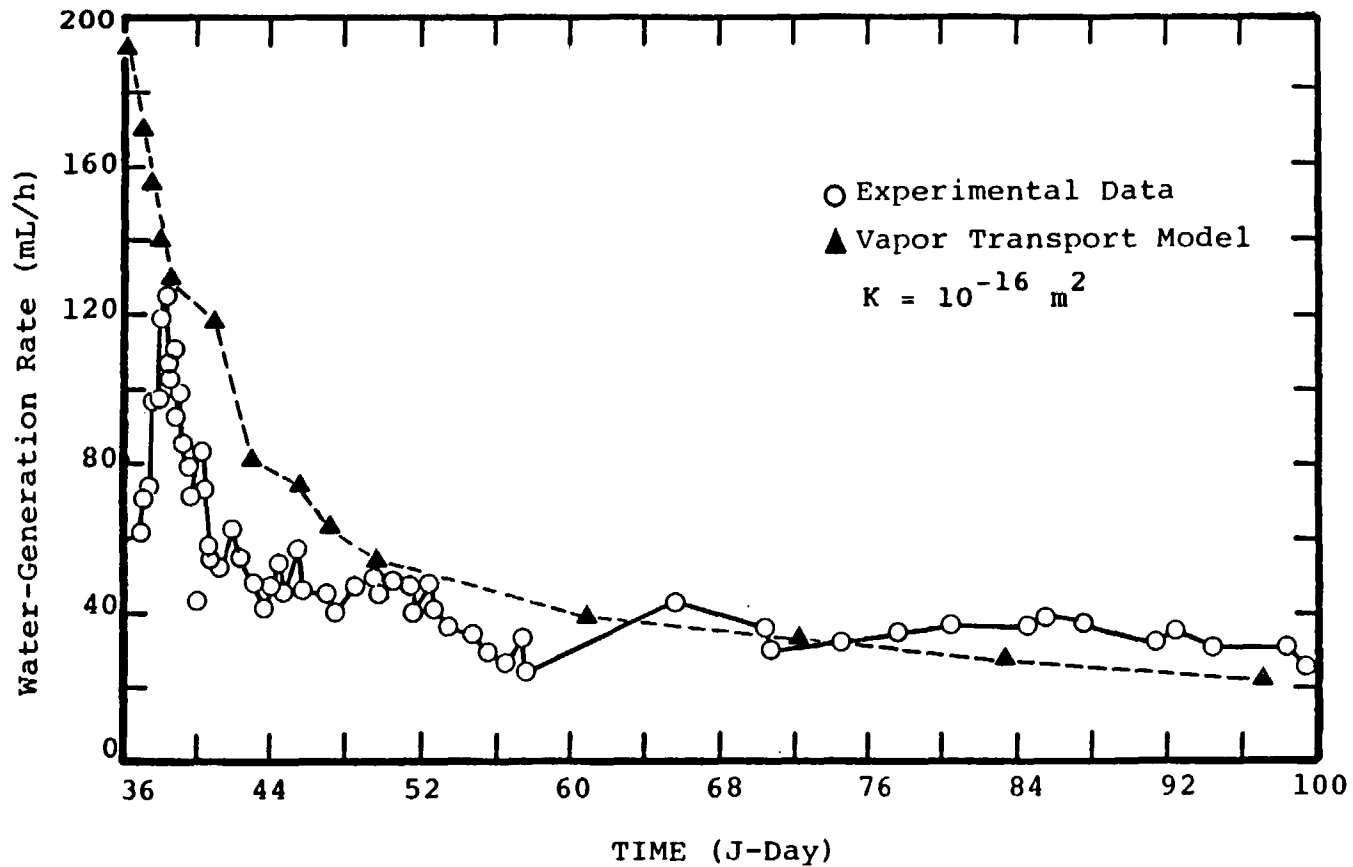


Figure 33. Comparison of evaporation front model results and experimental data from HH-1 for dry boundary condition and permeability =  $10^{-16} \text{ m}^2$ .

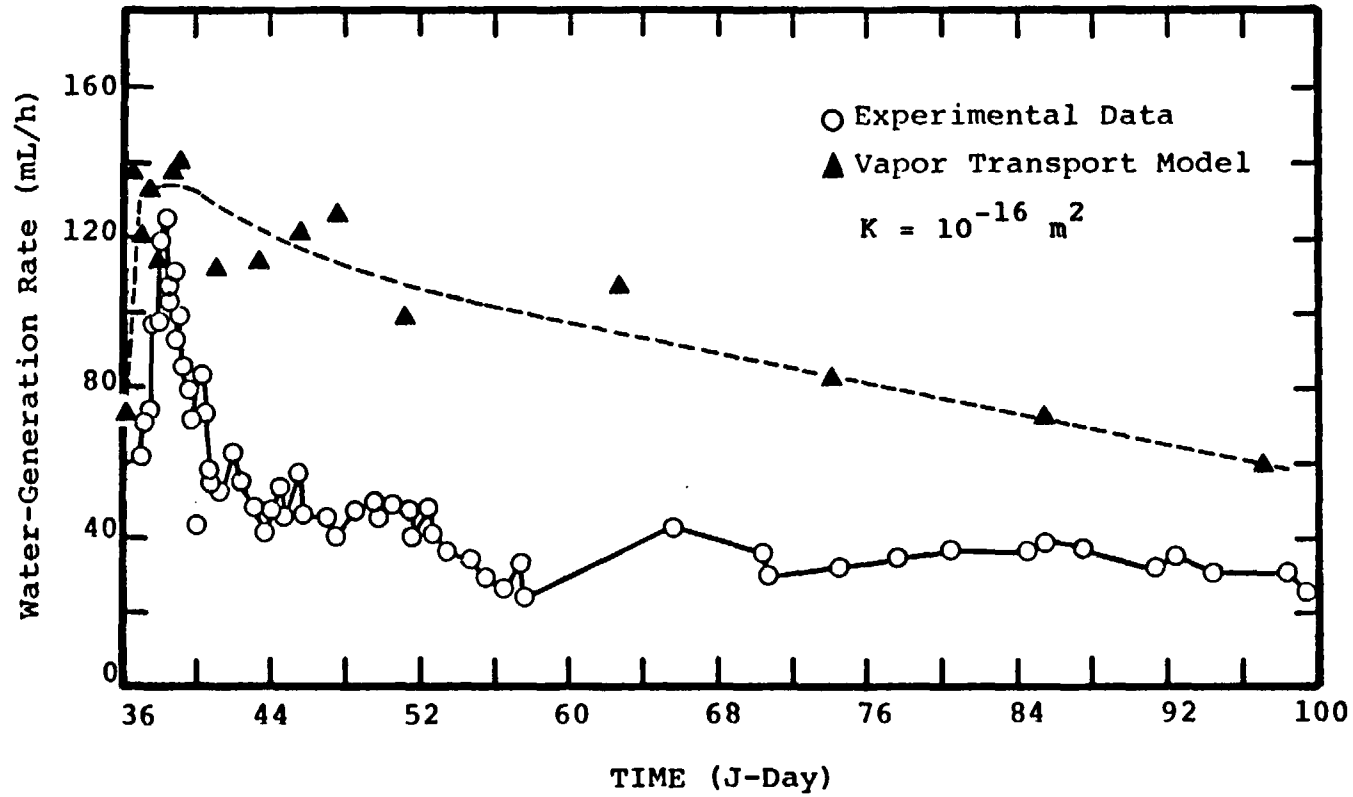


Figure 34. Effect of removing the isothermal boundary condition on the model results. Compare with Figure 31.

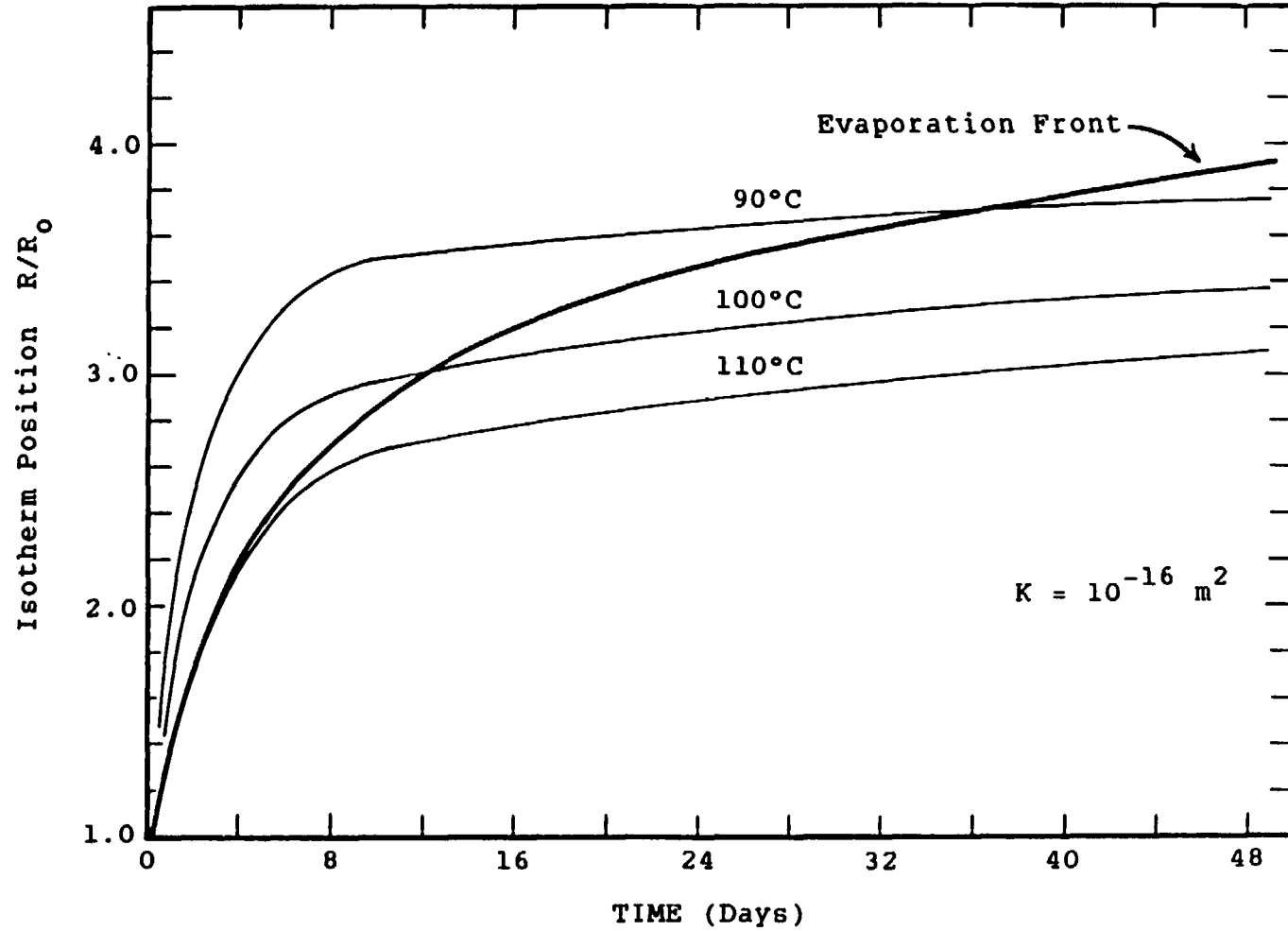


Figure 35. Evaporation front and isotherm position vs time.

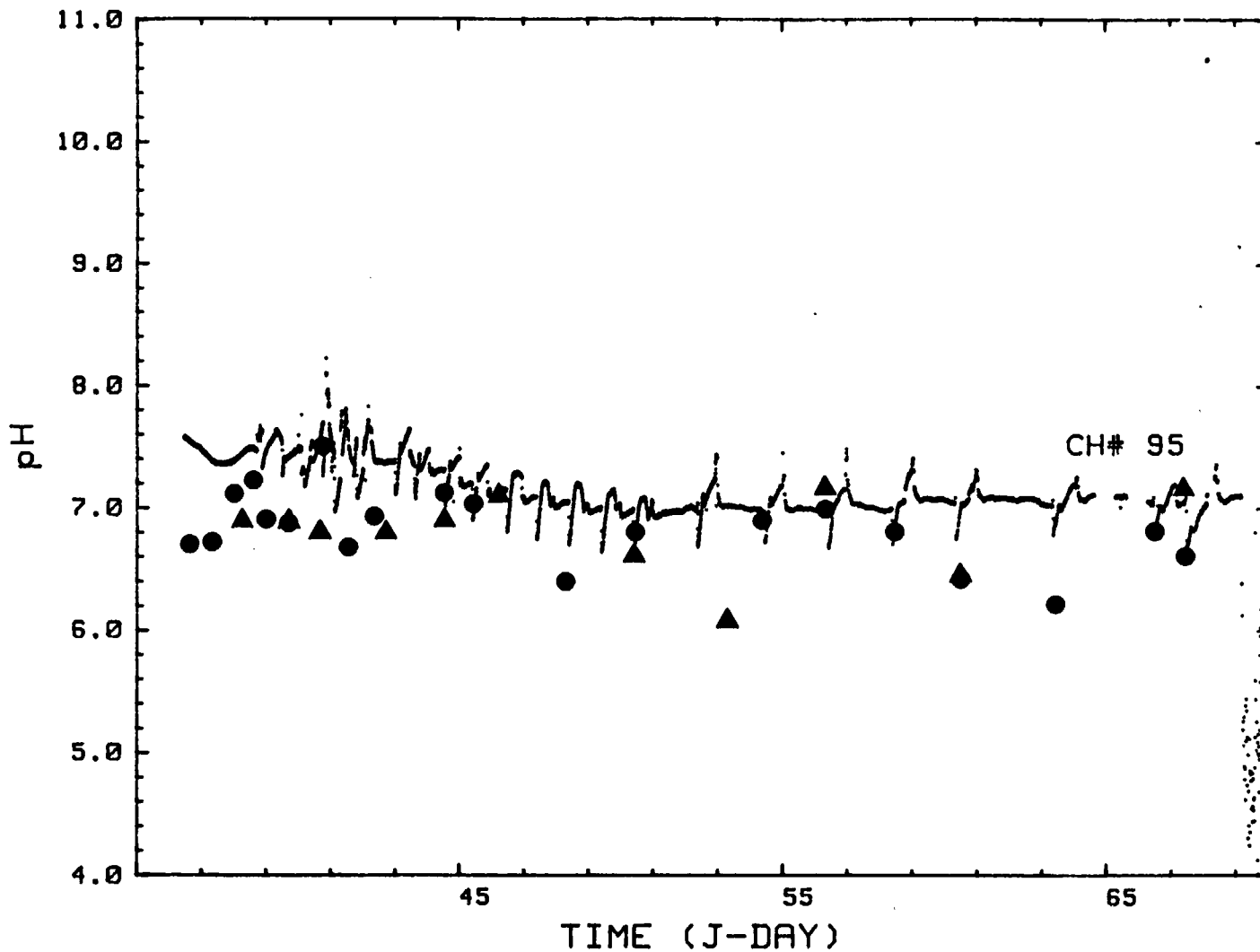


Figure 36. pH gage response in WM-2. Circles are pH values measured in the alcove in water samples collected from WM-2. Triangles are pH values measured in water samples collected from WM-1.

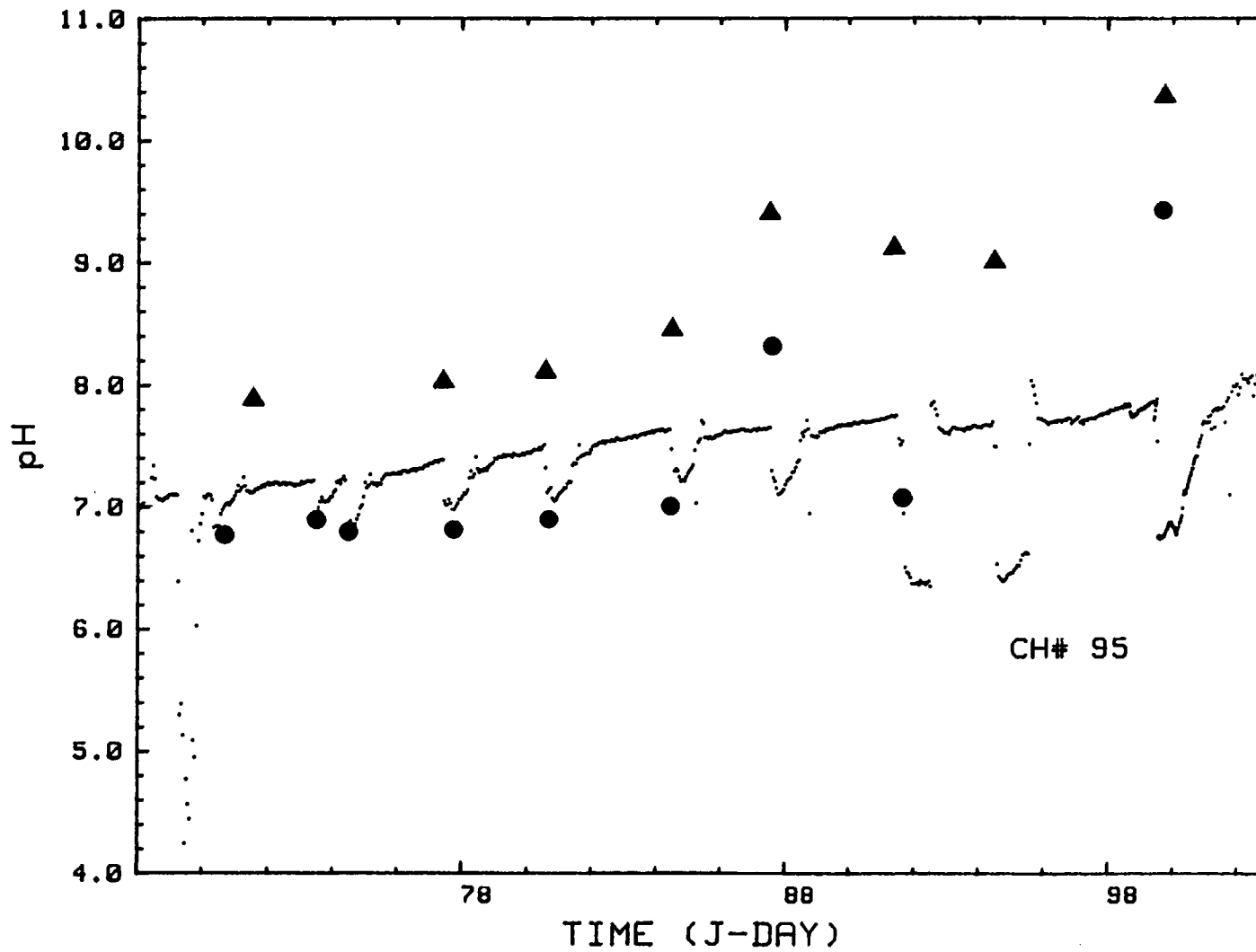


Figure 36 (Continued). pH gage response in WM-2. Circles are pH values measured in the alcove in water samples collected from WM-2. Triangles are pH values measured in water samples collected from WM-1.

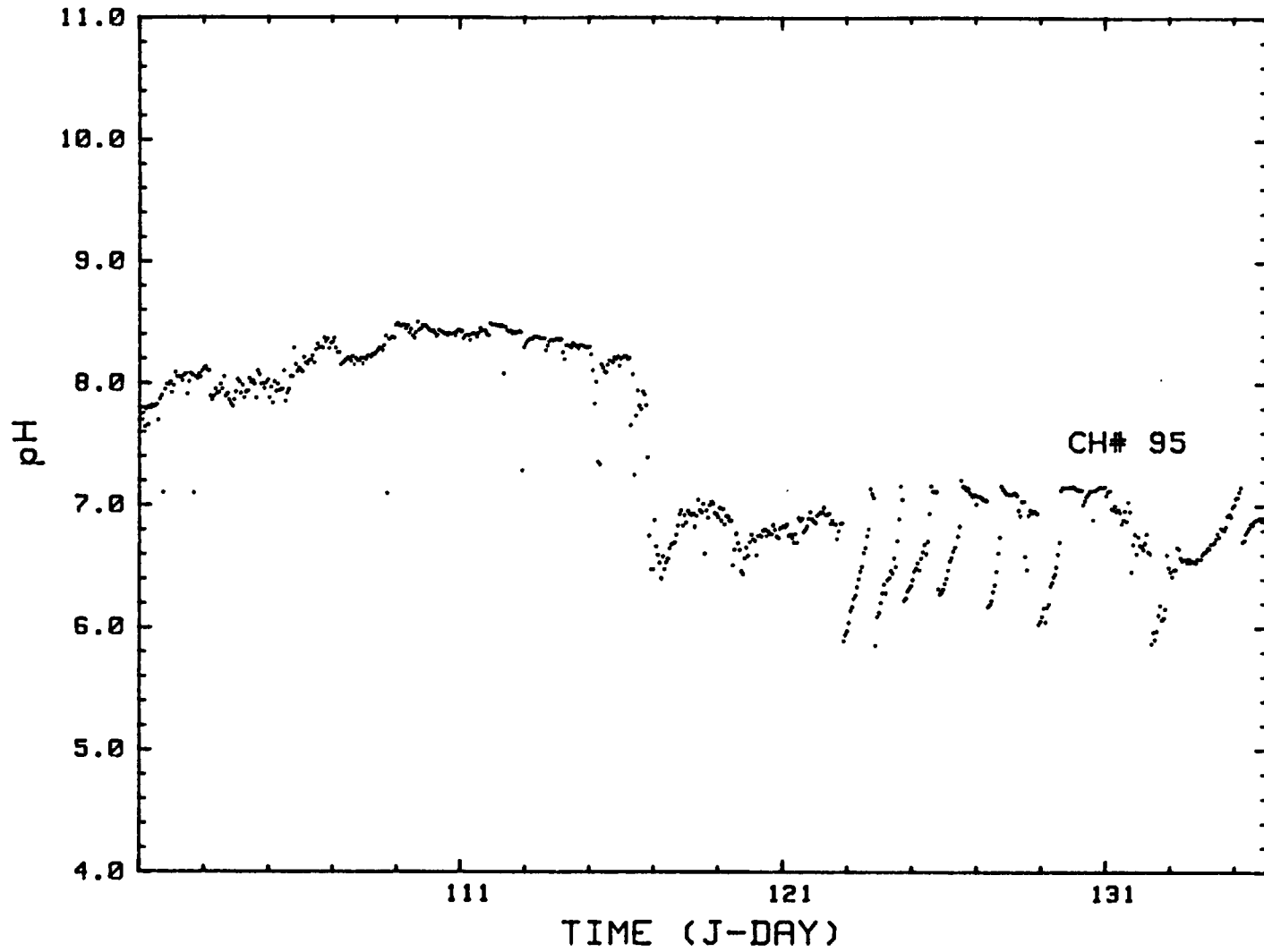


Figure 36 (Continued). pH gage response in WM-2. Circles are pH values measured in the alcove in water samples collected from WM-2. Triangles are pH values measured in water samples collected from WM-1.

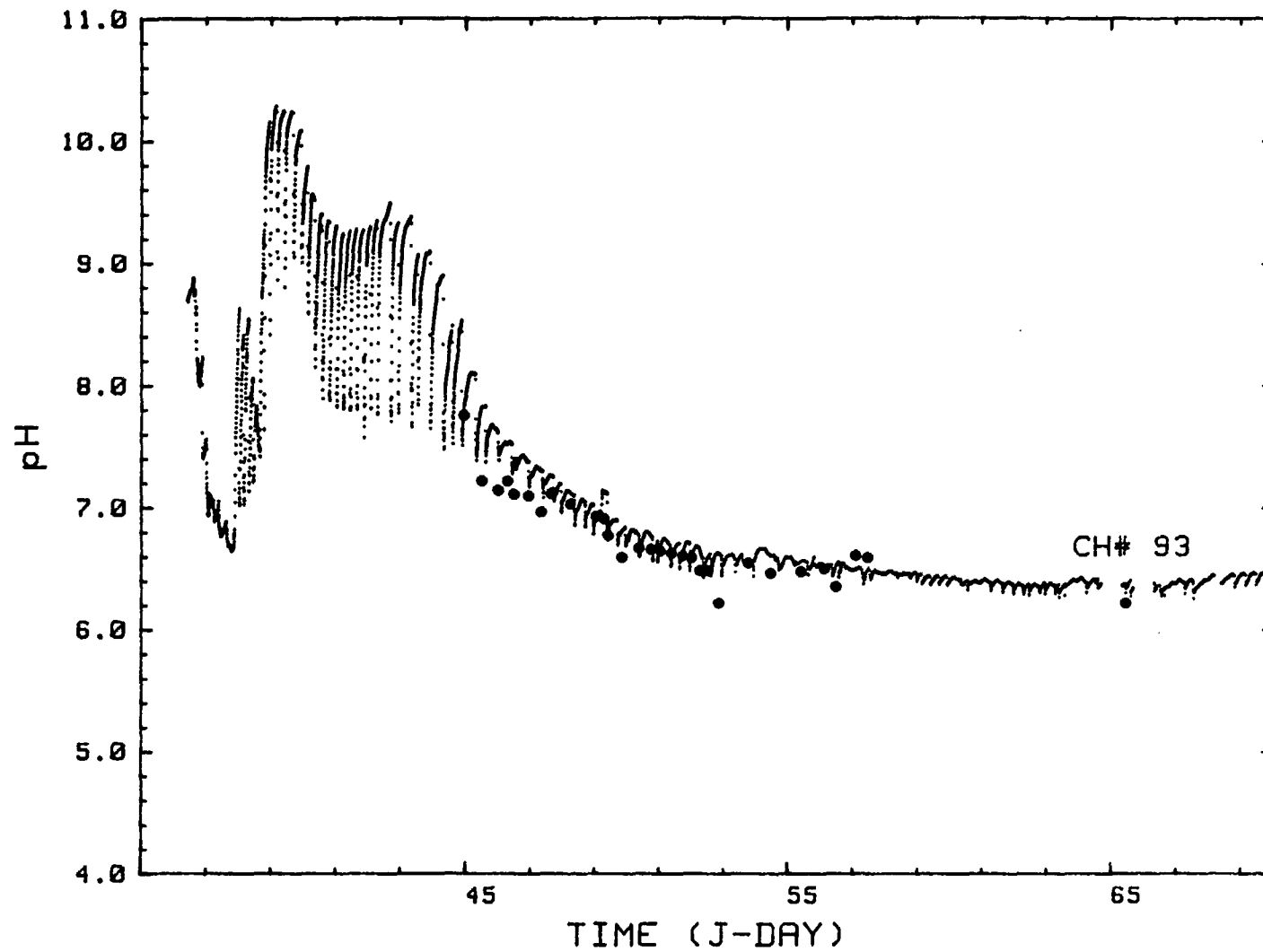


Figure 37. pH gage response in HH-1. Circles are pH values measured in the alcove in water samples collected from HH-1.

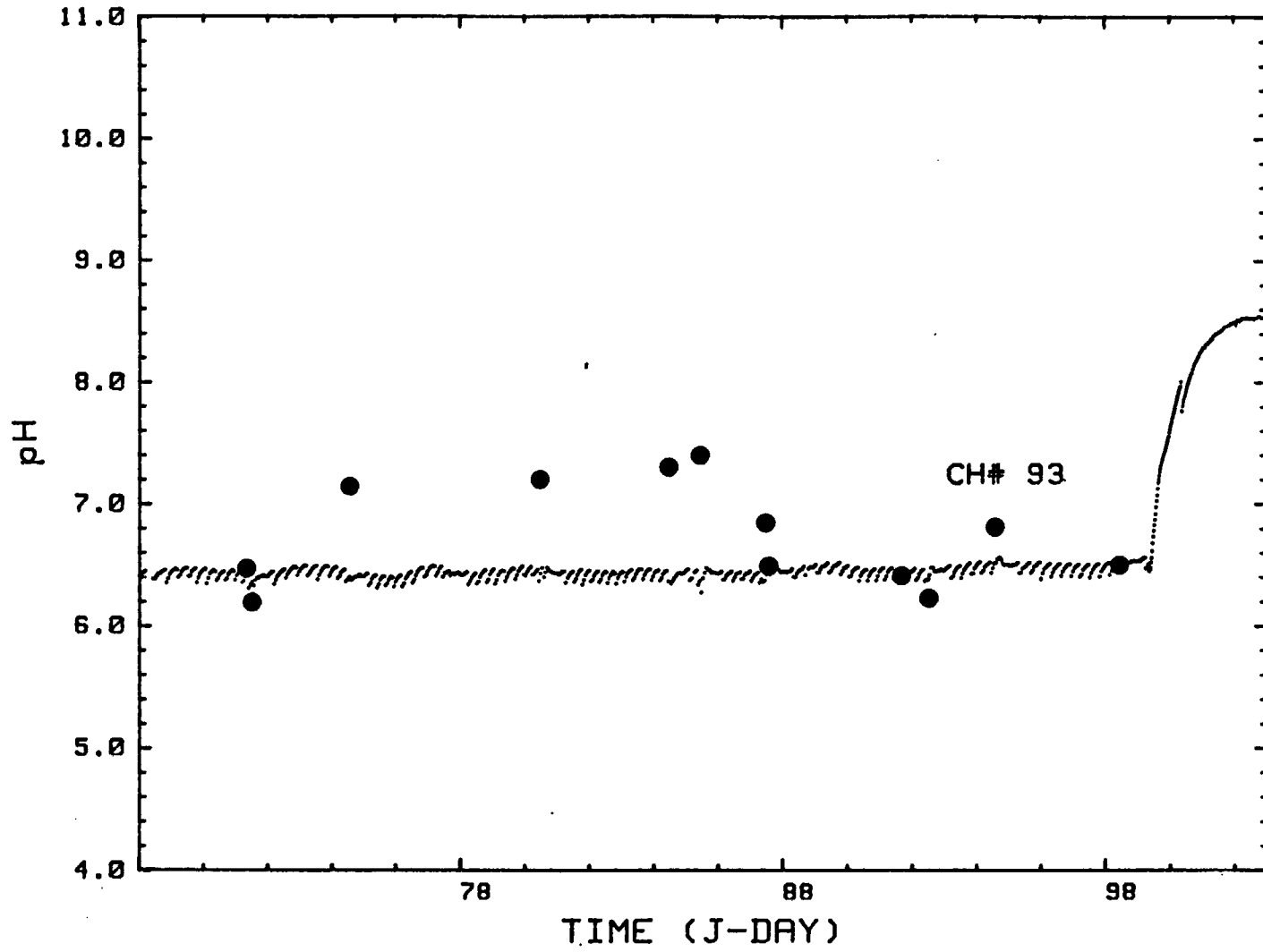


Figure 37 (Continued). pH gage response in HH-1. Circles are pH values measured in the alcove in water samples collected from HH-1.

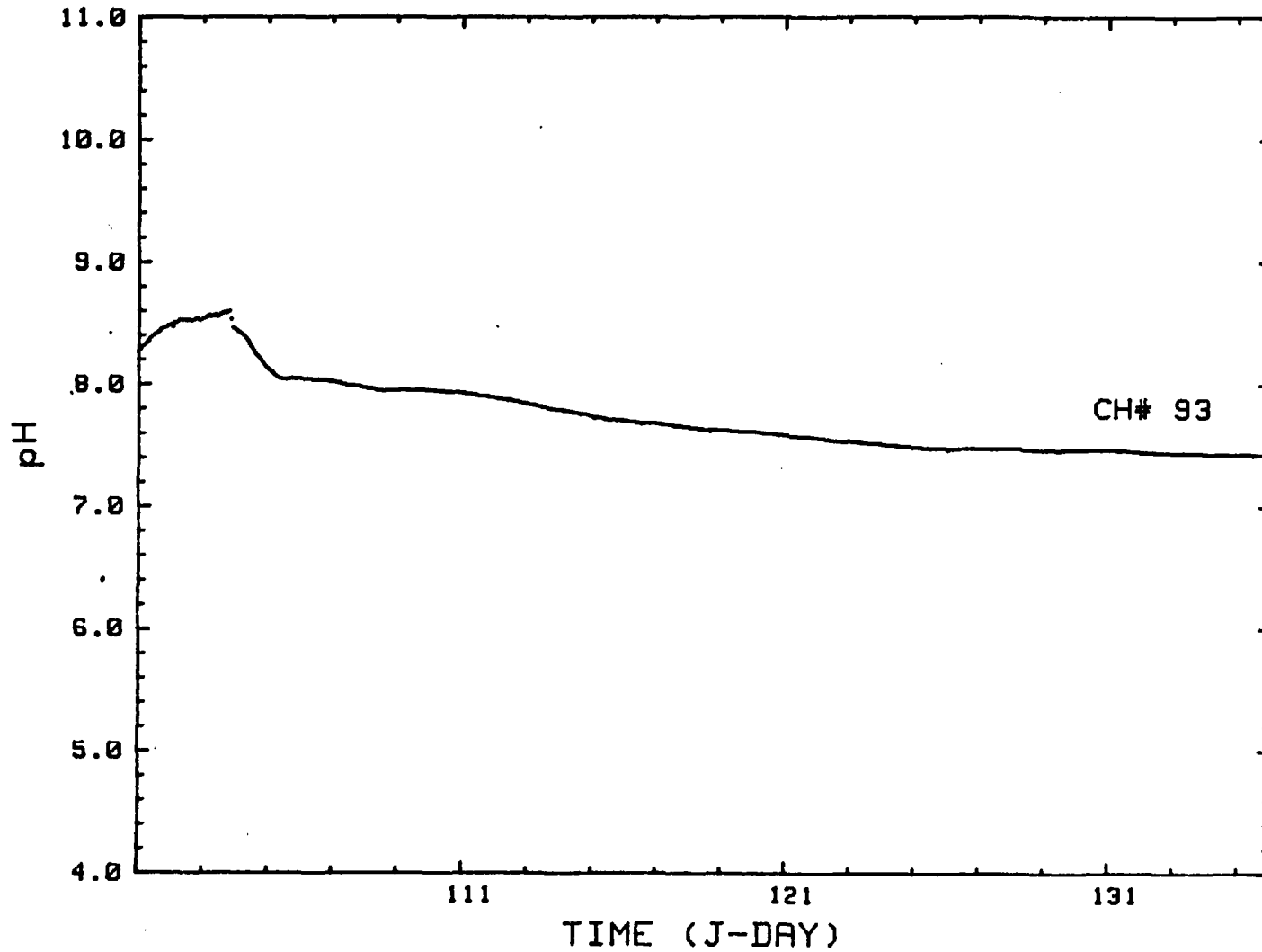


Figure 37 (Continued). pH gage response in HH-1. Circles are pH values measured in the alcove in water samples collected from HH-1.

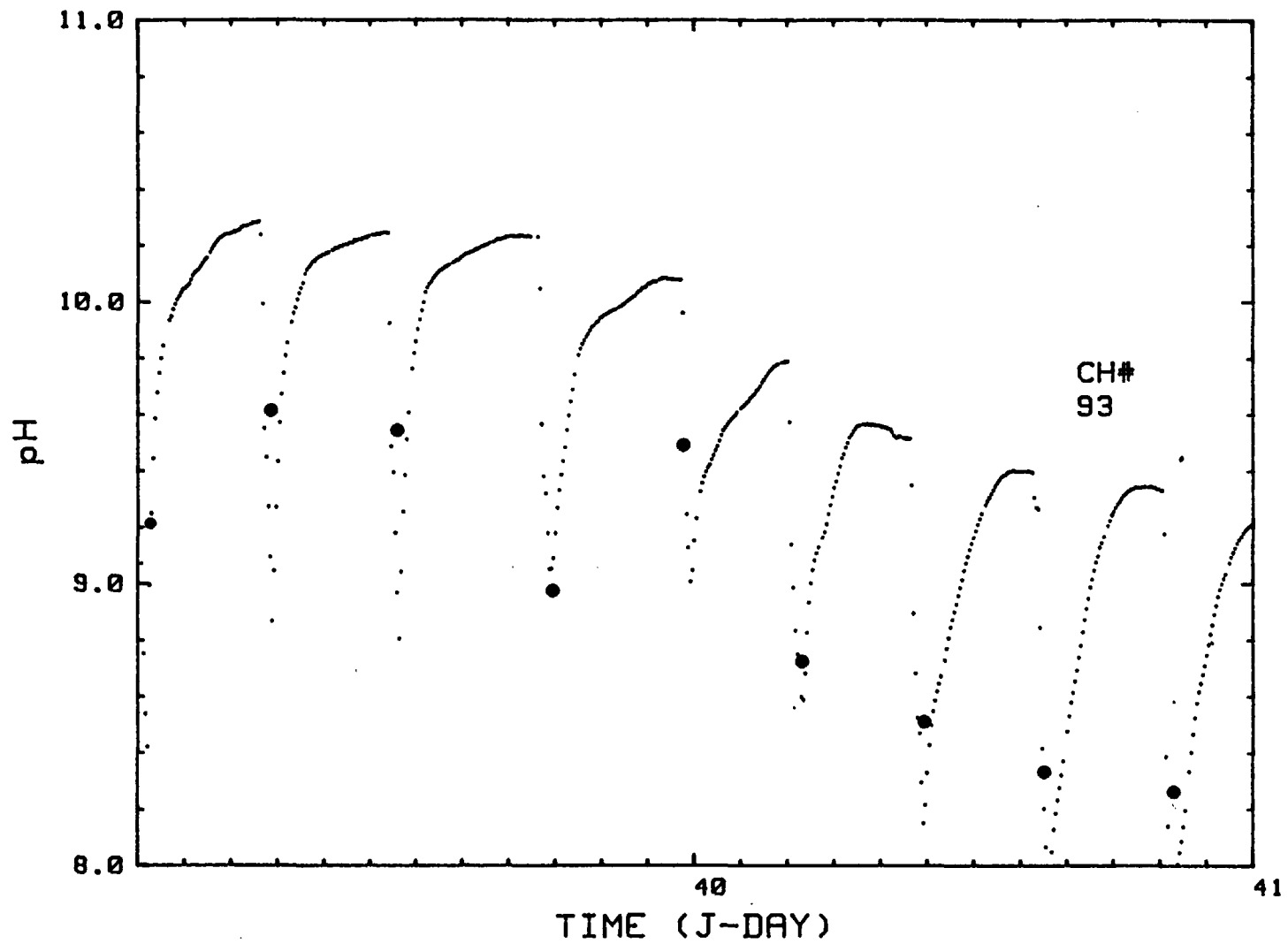


Figure 38. pH gage response to manual water sample removal from HH-1 vs expanded time scale. Circles are pH values measured in the alcove in the water samples collected.

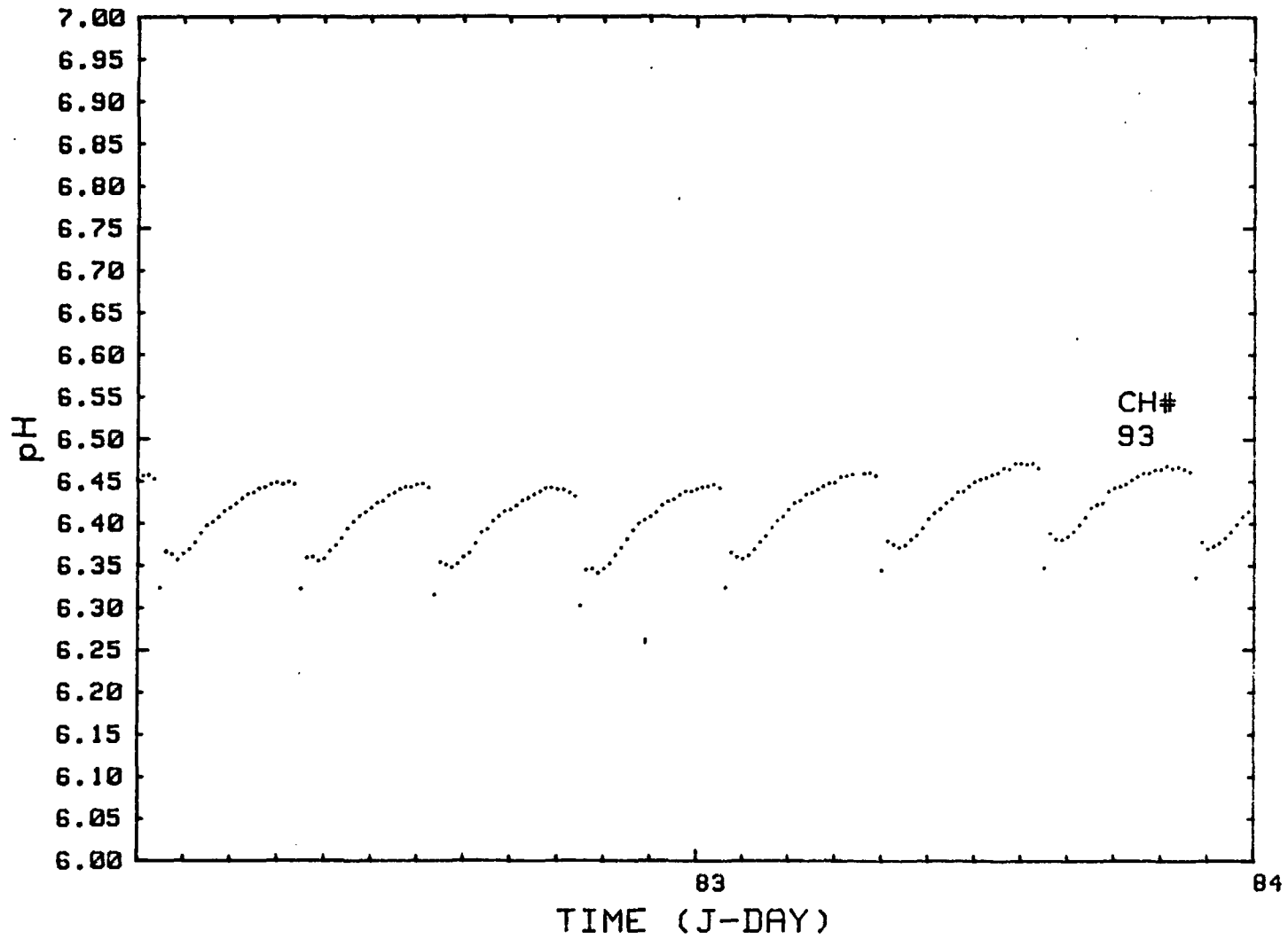


Figure 39. pH gage response to automatic collection of samples from HH-1 vs expanded time scale.

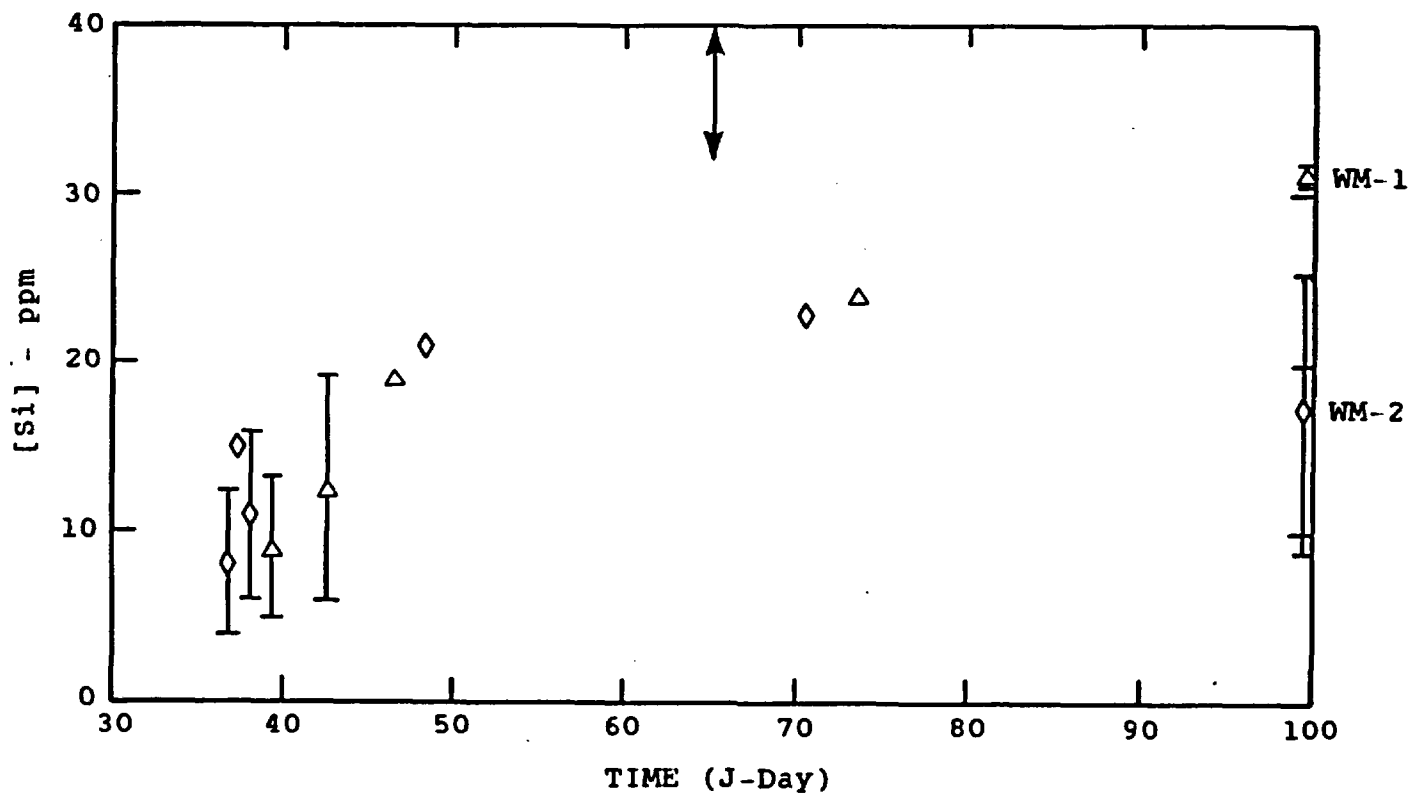
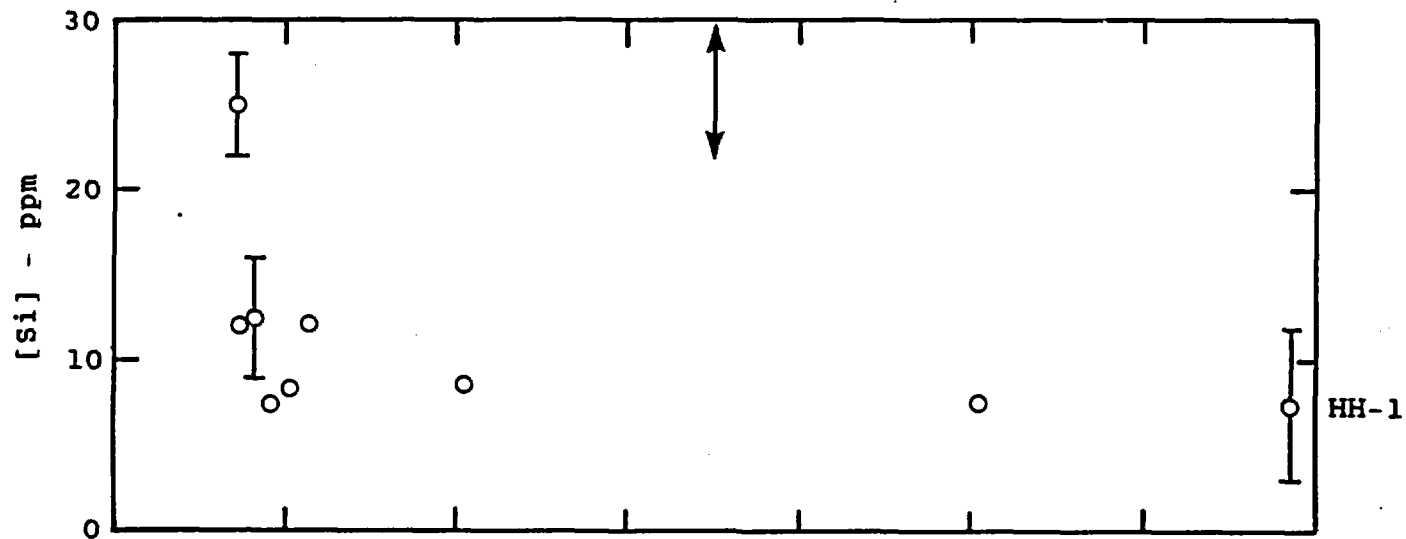


Figure 40. Silicon ion concentration in water samples collected from HH-1, WM-1, and WM-2 at different times.

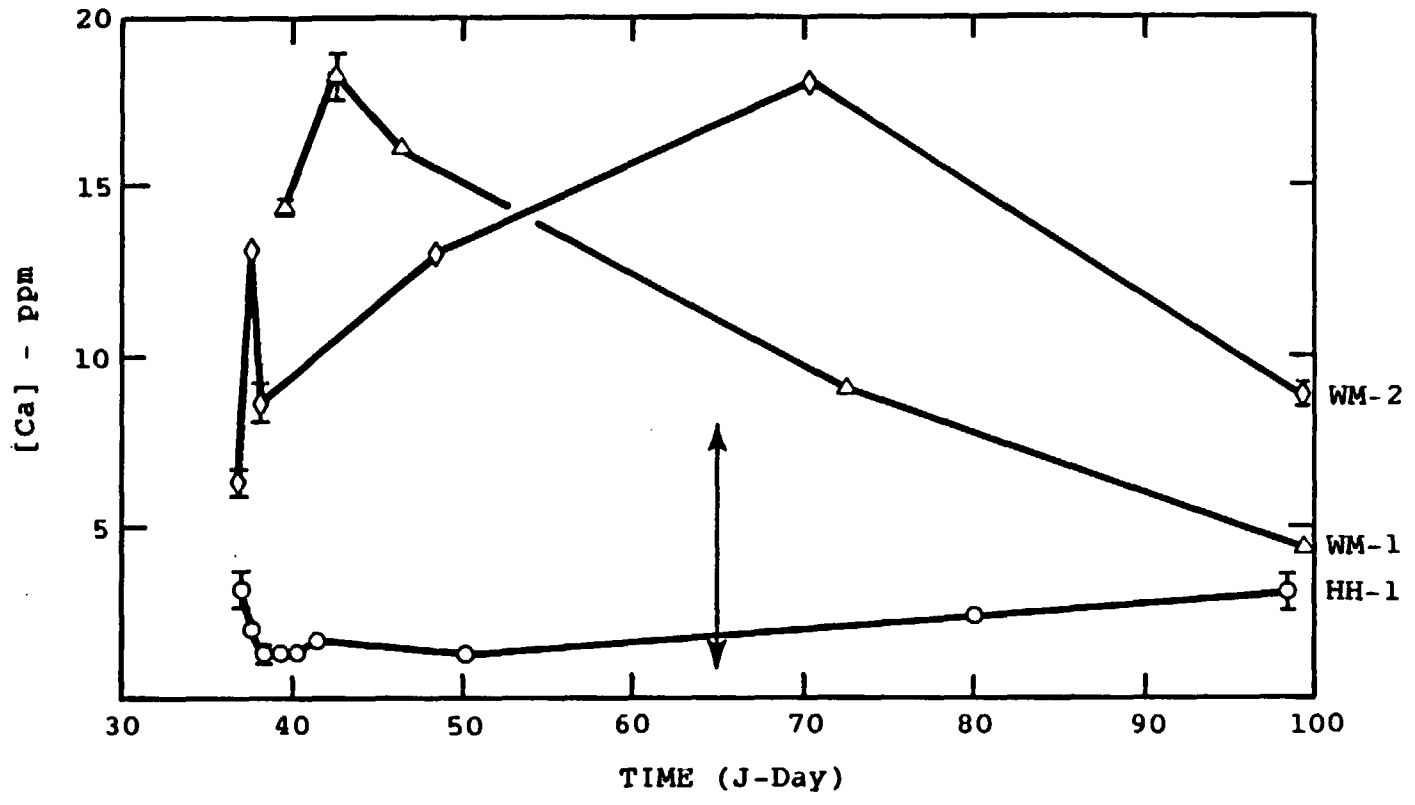


Figure 41. Calcium ion concentration in water samples collected from HH-1, WM-1, and WM-2 at different times.

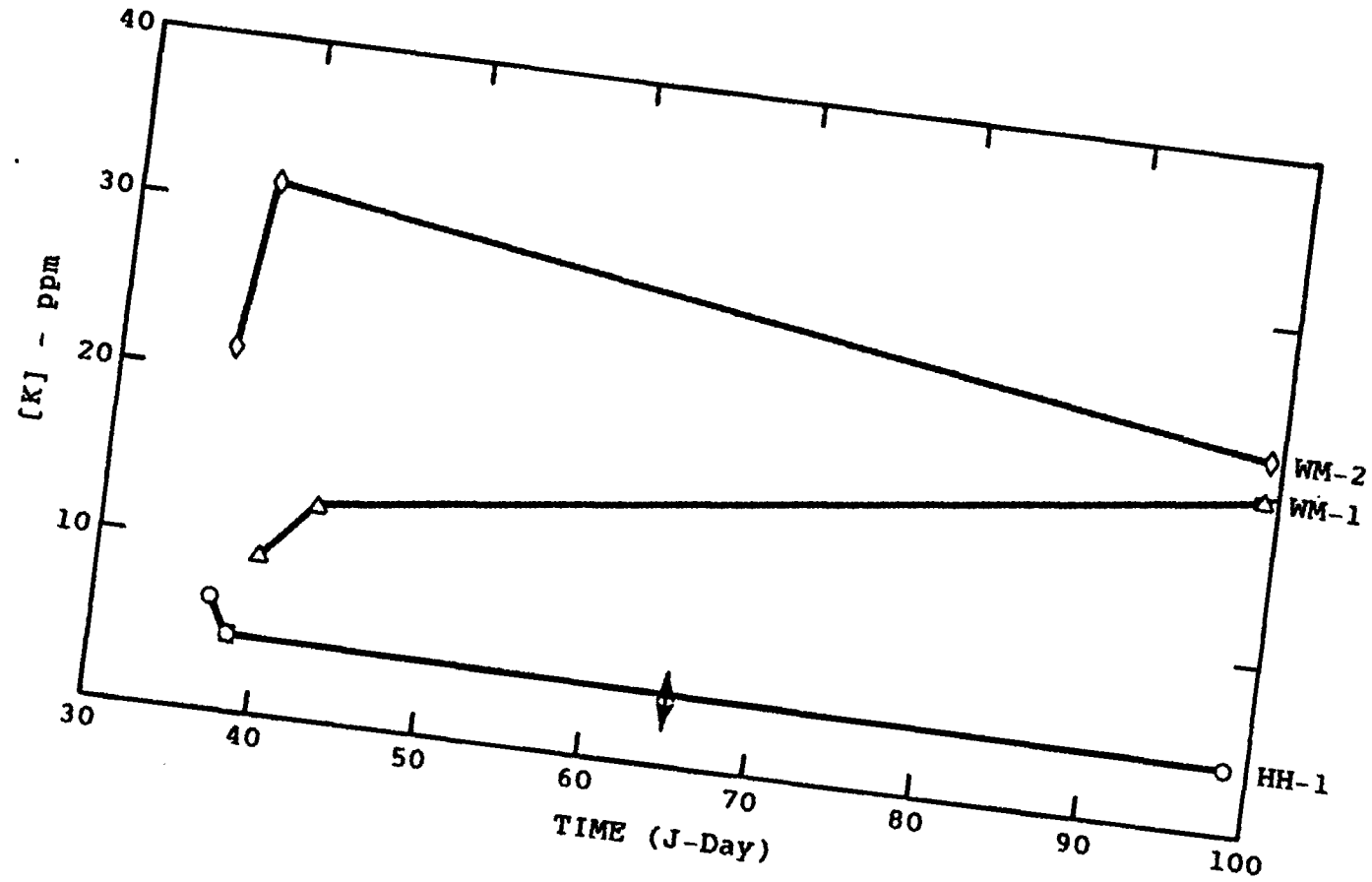


Figure 42. Potassium ion concentration in water samples collected from HH-1, WM-1, and WM-2 at different times.

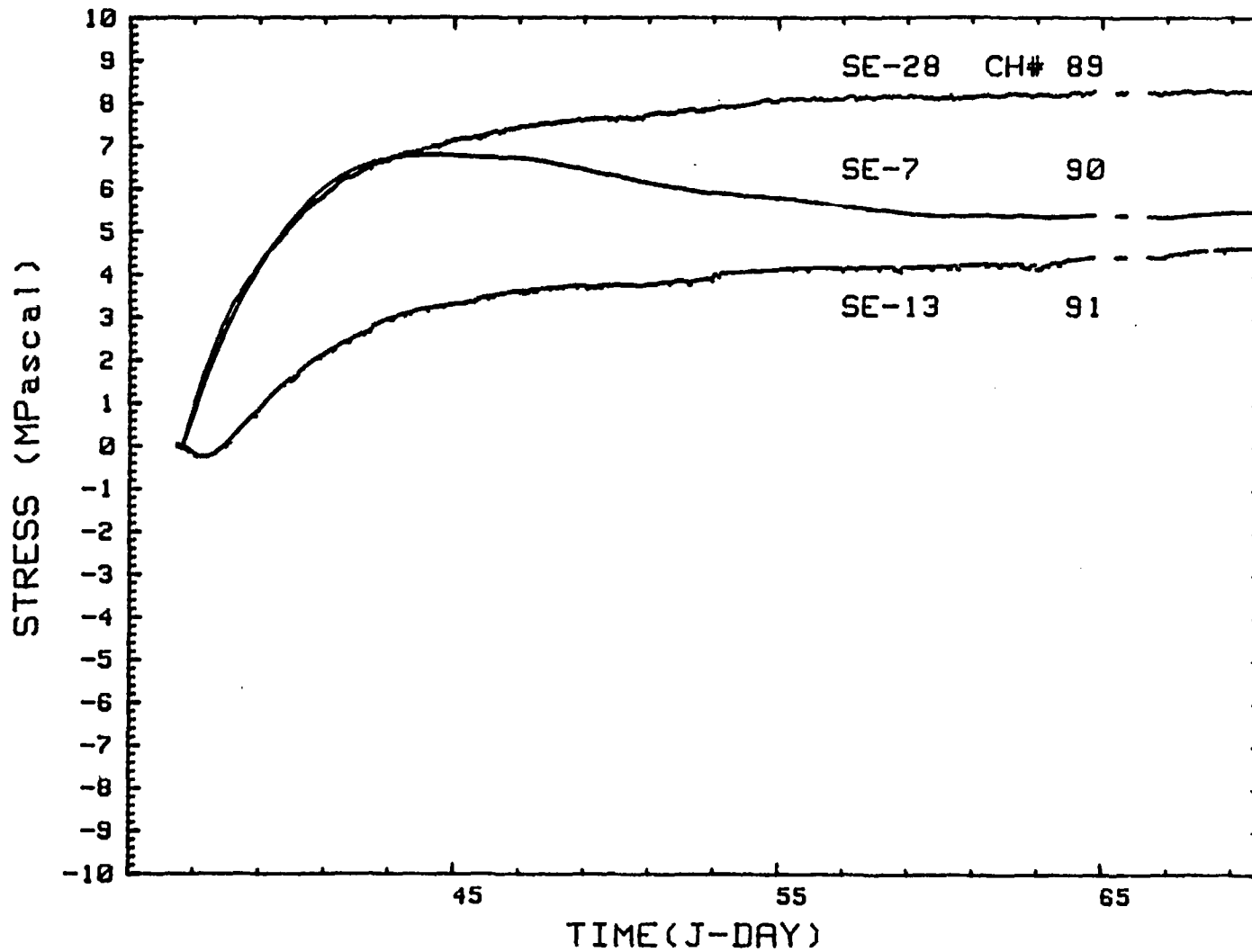


Figure 43. Stress meter data SE-28 and SE-7 oriented to measure thermal stresses radial to the heater. SE-13 oriented to measure circumferential thermal stresses.

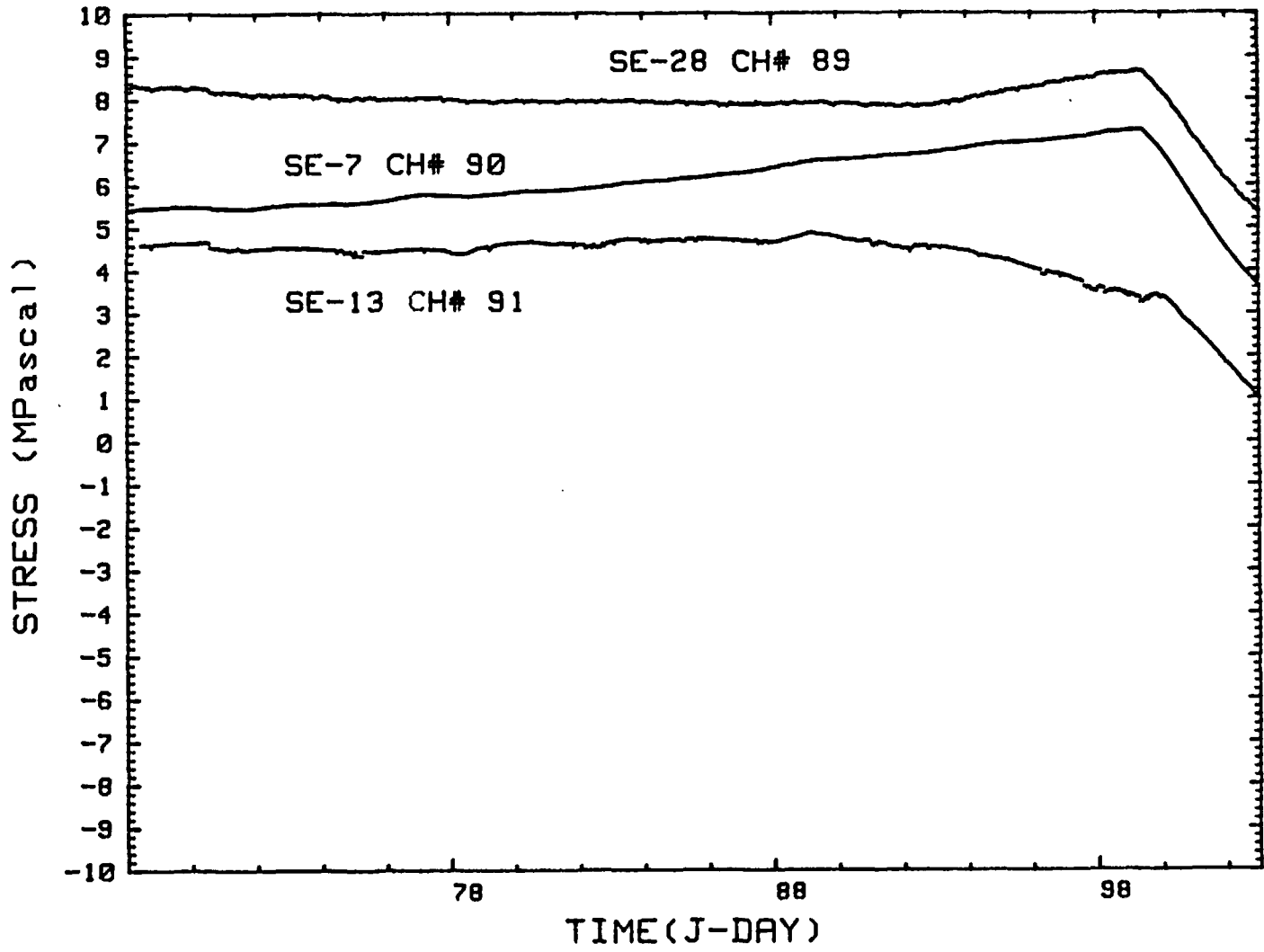


Figure 43 (Continued). Stress meter data SE-28 and SE-7 oriented to measure thermal stresses radial to the heater. SE-13 oriented to measure circumferential thermal stresses.

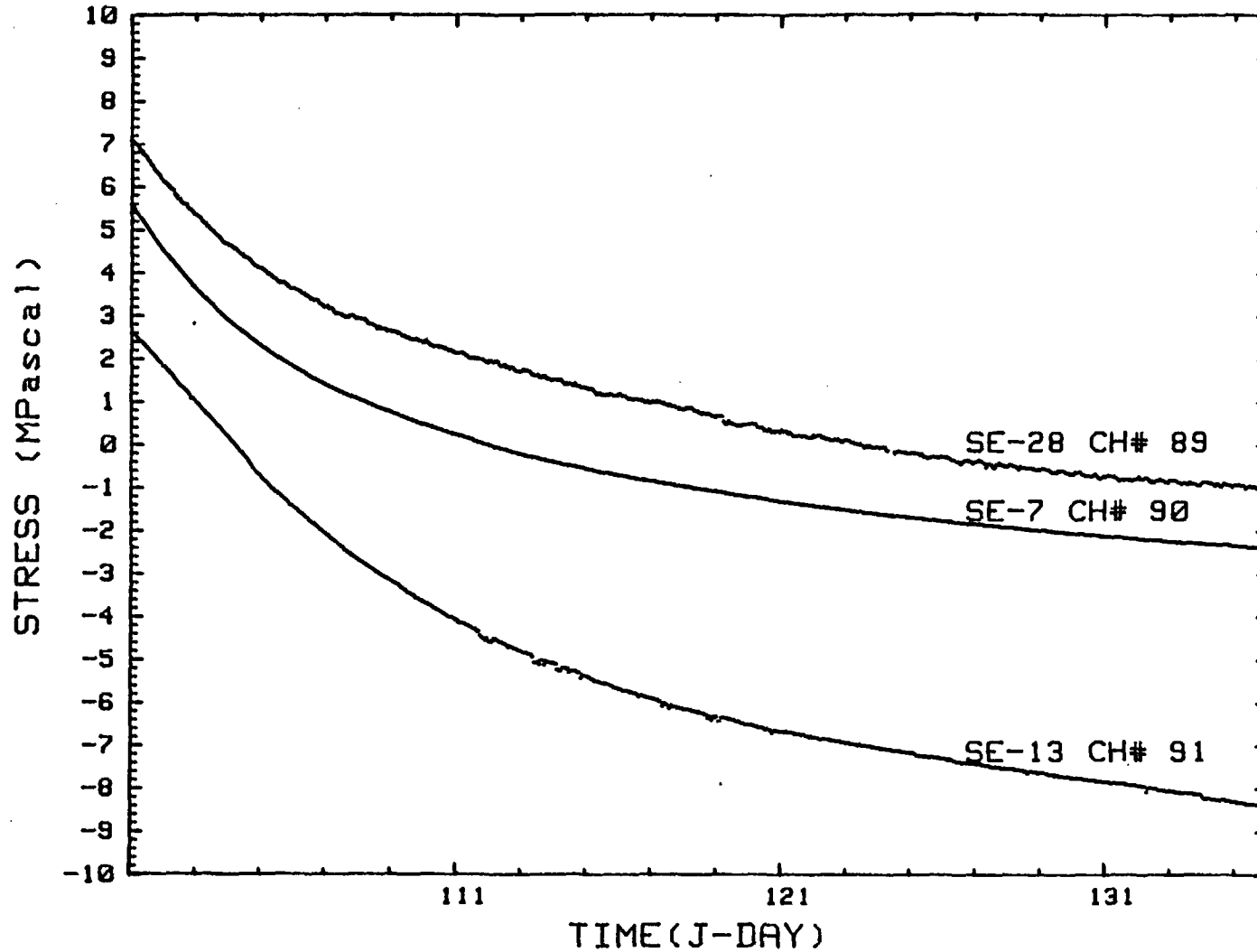


Figure 43 (Continued). Stress meter data SE-28 and SE-7 oriented to measure thermal stresses radial to the heater. SE-13 oriented to measure circumferential thermal stresses.

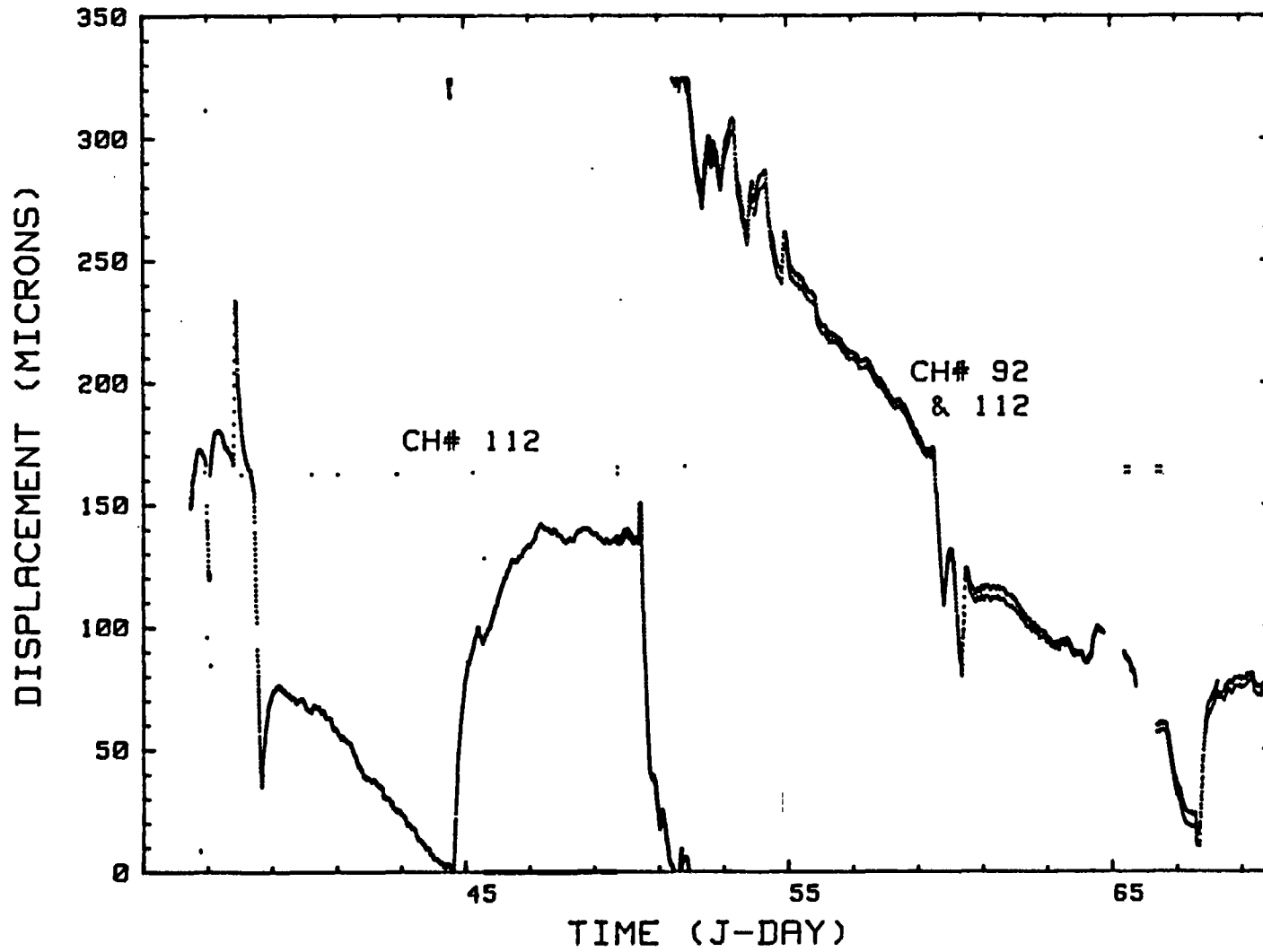


Figure 44. Laser interferometer data.

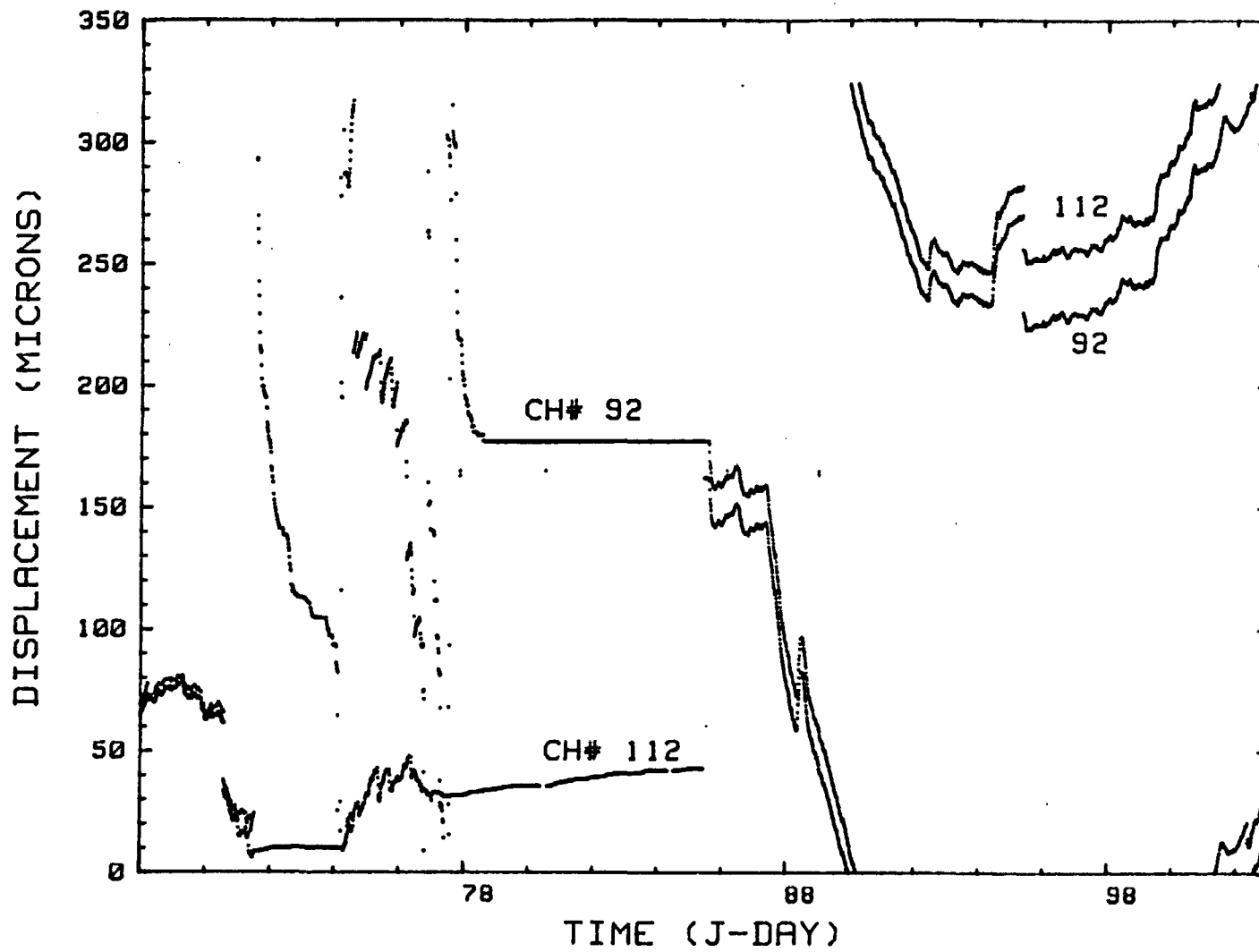


Figure 44 (Continued). Laser interferometer data.

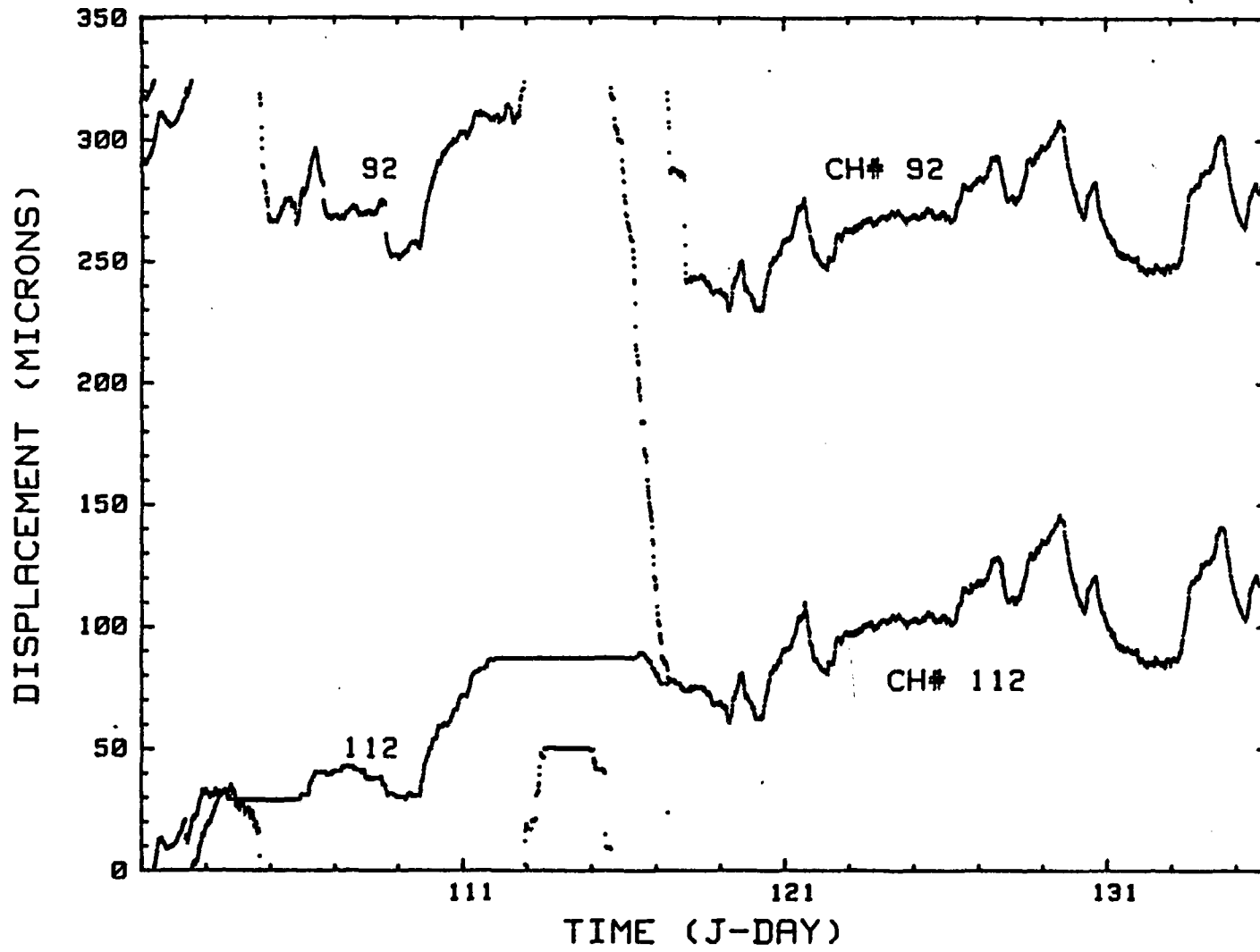


Figure 44 (Continued). Laser interferometer data.

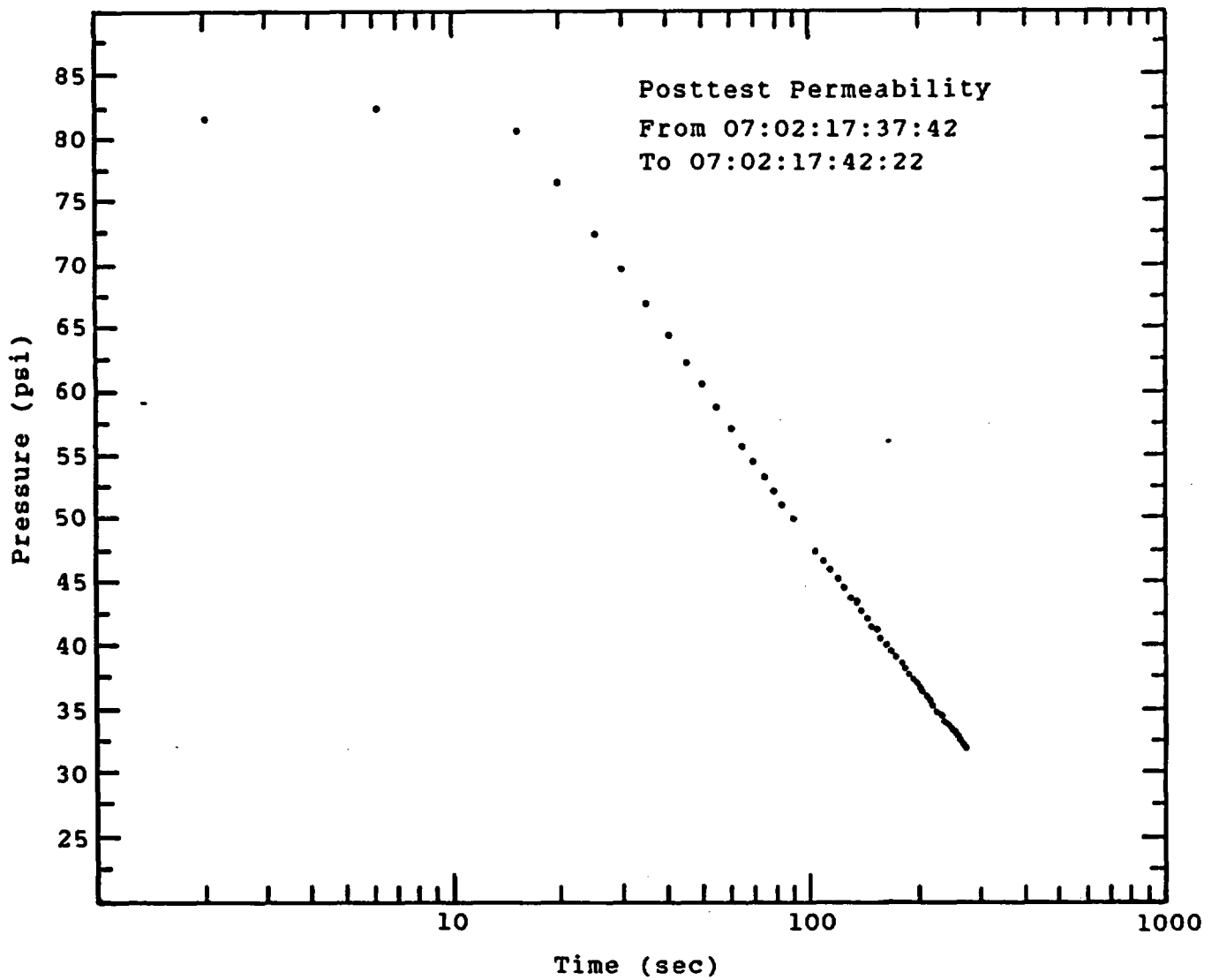


Figure 45. Example of the water pressure vs time data obtained during the posttest permeability testing in WM-1.

## DISTRIBUTION LIST

B. C. Rusche (RW-1)  
Director  
Office of Civilian Radioactive  
Waste Management  
U.S. Department of Energy  
Forrestal Building  
Washington, DC 20585

J. W. Bennett (RW-22)  
Office of Geologic Repositories  
U.S. Department of Energy  
Forrestal Building  
Washington, DC 20585

Ralph Stein (RW-23)  
Office of Geologic Repositories  
U.S. Department of Energy  
Forrestal Building  
Washington, DC 20585

J. J. Fiore, (RW-22)  
Program Management Division  
Office of Geologic Repositories  
U.S. Department of Energy  
Forrestal Building  
Washington, DC 20585

M. W. Frei (RW-23)  
Engineering & Licensing Division  
Office of Geologic Repositories  
U.S. Department of Energy  
Forrestal Building  
Washington, DC 20585

E. S. Burton (RW-25)  
Siting Division  
Office of Geologic Repositories  
U.S. Department of Energy  
Forrestal Building  
Washington, D.C. 20585

C. R. Cooley (RW-24)  
Geosciences & Technology Division  
Office of Geologic Repositories  
U.S. Department of Energy  
Forrestal Building  
Washington, DC 20585

T. P. Longo (RW-25)  
Program Management Division  
Office of Geologic Repositories  
U.S. Department of Energy  
Forrestal Building  
Washington, DC 20585

Cy Klingsberg (RW-24)  
Geosciences and Technology Division  
Office of Geologic Repositories  
U. S. Department of Energy  
Forrestal Building  
Washington, DC 20585

B. G. Gale (RW-25)  
Siting Division  
Office of Geologic Repositories  
U.S. Department of Energy  
Forrestal Building  
Washington, D.C. 20585

R. J. Blaney (RW-22)  
Program Management Division  
Office of Geologic Repositories  
U.S. Department of Energy  
Forrestal Building  
Washington, DC 20585

R. W. Gale (RW-40)  
Office of Policy, Integration, and  
Outreach  
U.S. Department of Energy  
Forrestal Building  
Washington, D.C. 20585

J. E. Shaheen (RW-44)  
Outreach Programs  
Office of Policy, Integration and  
Outreach  
U.S. Department of Energy  
Forrestal Building  
Washington, DC 20585

J. O. Neff  
Salt Repository Project Office  
U.S. Department of Energy  
505 King Avenue  
Columbus, OH 43201

D. C. Newton (RW-23)  
Engineering & Licensing Division  
Office of Geologic Repositories  
U.S. Department of Energy  
Forrestal Building  
Washington, DC 20585

O. L. Olson, Manager  
Basalt Waste Isolation Project Office  
U.S. Department of Energy  
Richland Operations Office  
Post Office Box 550  
Richland, WA 99352

D. L. Vieth, Director (4)  
Waste Management Project Office  
U.S. Department of Energy  
Post Office Box 14100  
Las Vegas, NV 89114

D. F. Miller, Director  
Office of Public Affairs  
U.S. Department of Energy  
Post Office Box 14100  
Las Vegas, NV 89114

D. A. Nowack (14)  
Office of Public Affairs  
U.S. Department of Energy  
Post Office Box 14100  
Las Vegas, NV 89114

B. W. Church, Director  
Health Physics Division  
U.S. Department of Energy  
Post Office Box 14100  
Las Vegas, NV 89114

Chief, Repository Projects Branch  
Division of Waste Management  
U.S. Nuclear Regulatory Commission  
Washington, D.C. 20555

Document Control Center  
Division of Waste Management  
U.S. Nuclear Regulatory Commission  
Washington, D.C. 20555

S. A. Mann, Manager  
Crystalline Rock Project Office  
U.S. Department of Energy  
9800 South Cass Avenue  
Argonne, IL 60439

K. Street, Jr.  
Lawrence Livermore National  
Laboratory  
Post Office Box 808  
Mail Stop L-209  
Livermore, CA 94550

L. D. Ramspott (3)  
Technical Project Officer for NNWSI  
Lawrence Livermore National  
Laboratory  
P.O. Box 808  
Mail Stop L-204  
Livermore, CA 94550

W. J. Purcell (RW-20)  
Office of Geologic Repositories  
U.S. Department of Energy  
Forrestal Building  
Washington, DC 20585

D. T. Oakley (3)  
Technical Project Officer for NNWSI  
Los Alamos National Laboratory  
P.O. Box 1663  
Mail Stop F-671  
Los Alamos, NM 87545

W. W. Dudley, Jr. (4)  
Technical Project Officer for NNWSI  
U.S. Geological Survey  
Post Office Box 25046  
418 Federal Center  
Denver, CO 80225

NTS Section Leader  
Repository Project Branch  
Division of Waste Management  
U.S. Nuclear Regulatory Commission  
Washington, D.C. 20555

V. M. Glanzman  
U.S. Geological Survey  
Post Office Box 25046  
913 Federal Center  
Denver, CO 80225

P. T. Prestholt  
NRC Site Representative  
1050 East Flamingo Road  
Suite 319  
Las Vegas, NV 89119

M. E. Spaeth  
Technical Project Officer for NNWSI  
Science Applications  
International, Corp.  
2769 South Highland Drive  
Las Vegas, NV 89109

SAIC-T&MSS Library (2)  
Science Applications  
International, Corp.  
2950 South Highland Drive  
Las Vegas, NV 89109

W. S. Twenhofel, Consultant  
Science Applications  
International, Corp.  
820 Estes Street  
Lakewood, CO 80215

A. E. Gurrola  
General Manager  
Energy Support Division  
Holmes & Narver, Inc.  
Post Office Box 14340  
Las Vegas, NV 89114

J. A. Cross, Manager  
Las Vegas Branch  
Fenix & Scisson, Inc.  
Post Office Box 15408  
Las Vegas, NV 89114

N. E. Carter  
Battelle Columbus Laboratory  
Office of Nuclear Waste Isolation  
505 King Avenue  
Columbus, OH 43201

John Fordham  
Desert Research Institute  
Water Resources Center  
Post Office Box 60220  
Reno, NV 89506

J. B. Wright  
Technical Project Officer for NNWSI  
Westinghouse Electric Corporation  
Waste Technology Services Division  
Nevada Operations  
Post Office Box 708  
Mail Stop 703  
Mercury, NV 89023

ONWI Library (2)  
Battelle Columbus Laboratory  
Office of Nuclear Waste Isolation  
505 King Avenue  
Columbus, OH 43201

W. M. Hewitt, Program Manager  
Roy F. Weston, Inc.  
2301 Research Blvd., 3rd Floor  
Rockville, MD 20850

H. D. Cunningham  
General Manager  
Reynolds Electrical &  
Engineering Co., Inc.  
Post Office Box 14400  
Mail Stop 555  
Las Vegas, NV 89114

T. Hay, Executive Assistant  
Office of the Governor  
State of Nevada  
Capitol Complex  
Carson City, NV 89710

R. R. Loux, Jr., Director (8)  
Nuclear Waste Project Office  
State of Nevada  
Capitol Complex  
Carson City, NV 89710

C. H. Johnson, Technical  
Program Manager  
Nuclear Waste Project Office  
State of Nevada  
Capitol Complex  
Carson City, NV 89710

Dr. Martin Mifflin  
Desert Research Institute  
Water Resources Center  
Suite 201  
1500 East Tropicana Avenue  
Las Vegas, NV 89109

Department of Comprehensive  
Planning  
Clark County  
225 Bridger Avenue, 7th Floor  
Las Vegas, NV 89155

Lincoln County Commission  
Lincoln County  
Post Office Box 90  
Pioche, NV 89043

Community Planning and  
Development  
City of North Las Vegas  
Post Office Box 4086  
North Las Vegas, NV 89030

0331 J. K. Johnstone (5)  
0315 J. P. Brannen  
1500 W. Herrmann  
1510 J. W. Nunziato  
1512 J. C. Cummings  
1512 G. R. Hadley (5)  
1520 T. B. Lane  
1524 R. L. Johnson  
1524 W. N. Sullivan  
1524 R. K. Thomas  
2530 D. B. Hayes  
6300 R. W. Lynch  
6310 T. O. Hunter  
6310 NNWSICF  
6311 L. W. Scully  
6311 B. Brasier  
6311 A. W. Dennis  
6311 T. W. Eglinton  
6311 J. T. Neal  
6311 P. D. O'Brien  
6311 L. Perrine (2)  
6311 C. G. Shirley  
6311 K. D. Young  
6312 F. W. Bingham  
6312 N. K. Hayden  
6312 B. S. Langkopf  
6312 R. R. Peters  
6312 J. G. Yeager  
6313 F. B. Nimick  
6313 R. M. Zimmerman  
6314 J. R. Tillerson  
6314 J. A. Fernandez

Planning Department  
Nye County  
Post Office Box 153  
Tonopah, NV 89049

Economic Development  
Department  
City of Las Vegas  
400 East Stewart Avenue  
Las Vegas, NV 89101

Flo Butler  
Los Alamos Technical Associates  
P.O. Box 410  
Los Alamos, NM 87544

6314 A. J. Mansure  
6315 Y. T. Lin  
6315 S. Sinnock  
6332 WMT Library  
6430 N. R. Ortiz  
3141 C. M. Ostrander (5)  
3151 W. L. Garner (3)  
7112 C. R. Mehl  
7112 D. R. Waymire (5)  
8024 M. A. Pound  
DOE/TIC (28)  
(3154-3, C. H. Dalin)

